PNL-4003
UC-62c

Evaluation of Solar Air Heating Central Receiver Concepts

June 1982

Prepared for the U.S. Department of Energy
under Contract DE-AC06-76RLO 1830

Pacific Northwest Laboratory
Operated for the U.S. Department of Energy
by Battelle Memorial Institute

Battelle

PNL-4003

PACIFIC NORTHWEST LABORATORY
operated by
BATTELLE
for the
UNITED STATES DEPARTMENT OF ENERGY
under Contract DE-AC06-76RLO 1830

Printed in the United States of America
Available from
National Technical Information Service
United States Department of Commerce
5285 Port Royal Road
Springfield, Virginia 22151

NTIS Price Codes
Microfiche A01

Printed Copy

Pages	Price Codes
001-025	A02
026-050	A03
051-075	A04
076-100	A05
101-125	A06
126-150	A07
151-175	A08
176-200	A09
201-225	A010
226-250	A011
251-275	A012
276-300	A013

PNL-4003
UC-62c

EVALUATION OF SOLAR AIR-HEATING CENTRAL RECEIVER CONCEPTS

S. P. Bird
M. K. Drost
T. A. Williams
D. R. Brown
J. A. Fort
B. A. Garrett-Price
S. G. Hauser
M. A. McLean
A. M. Paluszek
J. K. Young

June 1982

Prepared for
the U.S. Department of Energy
under Contract DE-AC06-76RLO 1830

Pacific Northwest Laboratory
Richland, Washington 99352

SUMMARY

Under the sponsorship of Sandia National Laboratories, as part of the U.S. Department of Energy Solar Thermal Energy Systems Program, the Pacific Northwest Laboratory performed a comparative analysis of solar thermal air-heating receivers suitable for producing high temperature air for either process heat or power generation applications. Seven air-heating receiver concepts were considered. The concepts are listed below with their proponents.

Concept	Proponent
Metal Tube Receiver	Boeing
Ceramic Tube Receiver	Black and Veatch
Sodium Heat Pipe Receiver	Foster Wheeler/Dynatherm
Ceramic Matrix Receiver	Sanders
Ceramic Dome Receiver	Massachusetts Institute of Technology-Lincoln laboratory
Small Particle Receiver	Lawrence Berkeley Laboratory
Volumetric Receiver	Pacific Northwest Laboratory

An assessment of each of the concepts was completed over a range of operating conditions. Product temperatures of 1000°F (538°C), 1500°F (816°C), and 2000°F (1093°C) were considered. Product pressures included 1 atm, 5 atm, and 10 atm. In order to give a comparison over a range of plant sizes, three power levels were considered: 1 MWt, 50 MWt, and 300 MWt. Several conceptual designs were developed for each receiver concept, covering the applicable ranges of pressure, temperature, and size. Based on these conceptual designs, engineering and economic analyses were conducted to estimate the performance and cost of the receiver over the range of operating conditions.

Conceptual designs developed for the seven receivers were based on the common assumption of available materials and technology in the time frame from 1990 to 2000. No attempt was made to optimize each conceptual receiver design in detail. Rather, designs were based on proponent-supplied information, where possible. The concepts that have not been the subject of a detailed design study lacked information on optimum receiver designs; therefore the conceptual designs developed in this study were not necessarily optimum. Performance was

estimated using a consistent performance model for all designs. Costs were estimated on the basis of consistent assumptions, ground rules, methodologies, and unit costs of materials and labor applied uniformly to all of the concepts.

The principal results and conclusions of the analysis include:

- For near-term application the metal tube receiver gives reasonable performance and cost. The ceramic tube receiver also gives reasonable performance and represents the nearest-term technology for a 2000°F (1093°C) receiver.
- The sodium heat pipe receiver is a good performer but appears to have a high cost.
- The ceramic matrix, ceramic dome, and small particle receivers all have interesting features, but each concept as now formulated has a major weakness which would probably limit any application. The ceramic matrix receiver and small particle receiver both experience excessive spillage losses, while the ceramic dome receiver has both high spillage and high thermal losses.
- The volumetric concept has excellent performance and reasonable cost, but the concept is not well developed, and major technical questions must be answered before the concept can be considered technically feasible. With those reservations the volumetric concept appears to have the greatest potential for a substantial improvement in the performance of high temperature air-heating receivers.
- This report documents an evaluation of air-heating receivers. The study has not considered complete solar industrial process heat systems. Factors such as heliostat field configuration and cost, storage, energy transport, and user interfacing have not been considered. The results of this study are intended to provide inputs to a more comprehensive systems study. While the results of this study are significant for a comparision of receivers, ultimately the comparison must be based on complete systems rather than just receivers.

ACKNOWLEDGMENTS

This work was supported by Sandia National Laboratories as part of the U.S. Department of Energy's Solar Thermal Energy Systems Program. The authors would like to acknowledge the special assistance of D. Atwood of Sandia in preparing the numerous DELSOL computer simulations. Appreciation is also extended to Dr. A. Hunt, Dr. P. T. Jarvinen, and staff members at Boeing, Black and Veatch, Dynatherm, and Sanders for assistance in characterizing the conceptual designs. Finally, the authors would like to thank S. W. Matsumoto and the graphics and technical publications sections of PNL for assistance in preparation of the final report.

NOMENCLATURE

A	-	exterior receiver area (m^2)
A_a	-	aperture area (m^2)
A_n	-	volumetric receiver zone in frontal area (m^2)
D	-	hydraulic diameter (m)
$F_{n-\infty}$	-	volumetric receiver zone n view factor to ambient
g	-	acceleration due to gravity (m/s^2)
Gr	-	Grashof number (dimensionless)
h_{fc}	-	forced convection component of convective heat transfer coefficient ($kWt/m^2 \cdot K$)
h_{nc}	-	natural convection component ($kWt/m^2 \cdot k$)
K	-	thermal conductivity ($kWt/m \cdot K$)
L	-	insulation thickness (m)
L_n	-	volumetric receiver absorber zone n depth (m)
Nu	-	Nusselt number (dimensionless)
Pr	-	Prandtl number (dimensionless)
$Q_{aperture}$	-	power incident on aperture (kWt)
$Q_{reflection}$	-	reflection loss heat transfer rate (kWt)
$Q_{reradiation}$	-	reradiation loss heat transfer rate (kWt)
Q_r	-	reradiation loss heat transfer rate for calculation of effective emissivity (kWt)
R_e	-	Reynolds number (dimensionless)
T_c	-	small particle receiver cover temperature (K)
T_n	-	volumetric receiver zone n temperature (K)
T_w	-	cavity temperature of cavity receivers (K)
T_∞	-	temperature of environment (K)

Greek Letters

α	-	material absorptivity
α_n	-	volumetric receiver zone n absorptivity
ε	-	material emissivity
ε_{eff}	-	effective cavity emissivity

ε_n	-	volumetric receiver zone n emissivity
ρ	-	material reflectivity
ρ_n	-	volumetric receiver zone n reflectivity
τ	-	material transmissivity
τ_n	-	volumetric receiver zone in transmissivity
σ	-	Stefan-Baltzmann constant (5.729×10^{-12} w/(cm^2$\cdot$K^4)

CONTENTS

FIGURES

TABLES

EVALUATION OF SOLAR AIR-HEATING CENTRAL RECEIVER CONCEPTS

1.0 INTRODUCTION

The central receiver concept provides a promising means of generating electricity or industrial process heat using solar energy. In this concept a field of tracking mirrors (heliostats) focus solar radiation onto a heat exchanger, called the receiver, located at the top of a tower. An example of one central receiver design appears in Figure 1.1. It is possible to use air as the working fluid in the receiver. After being heated the air can be used directly in an industrial process heat application or expanded in a gas turbine to generate electricity.

1.1 PURPOSE OF STUDY

Numerous organizations have proposed innovative concepts for air-heating central receivers. The purpose of this study was to evaluate the potential of seven proposed concepts based on an independent, uniform assessment of each concept's performance and cost. A list of the seven concepts and their proponents appears in Table 1.1.

An assessment of the cost and performance of each concept was desired for a range of operating conditions: pressure from 1 to 10 atmospheres, temperatures from 1000 (538°C) to 2000°F (1093°C), and sizes from 1 to 300 MWt. Several conceptual designs were developed for each receiver concept, covering the applicable ranges of pressure, temperature, and size. Based on these conceptual designs, engineering and economic analyses were conducted to estimate the performance and cost of the receiver over the range of operating conditions.

The study was limited to a comparison of the air-heating receivers and did not include complete air-heating process heat systems. Other factors affecting system cost and performance (such as heliostat field cost and performance, tower design, storage, energy transport and the user interface) were not considered. The results were to be used as input to a more comprehensive system study.

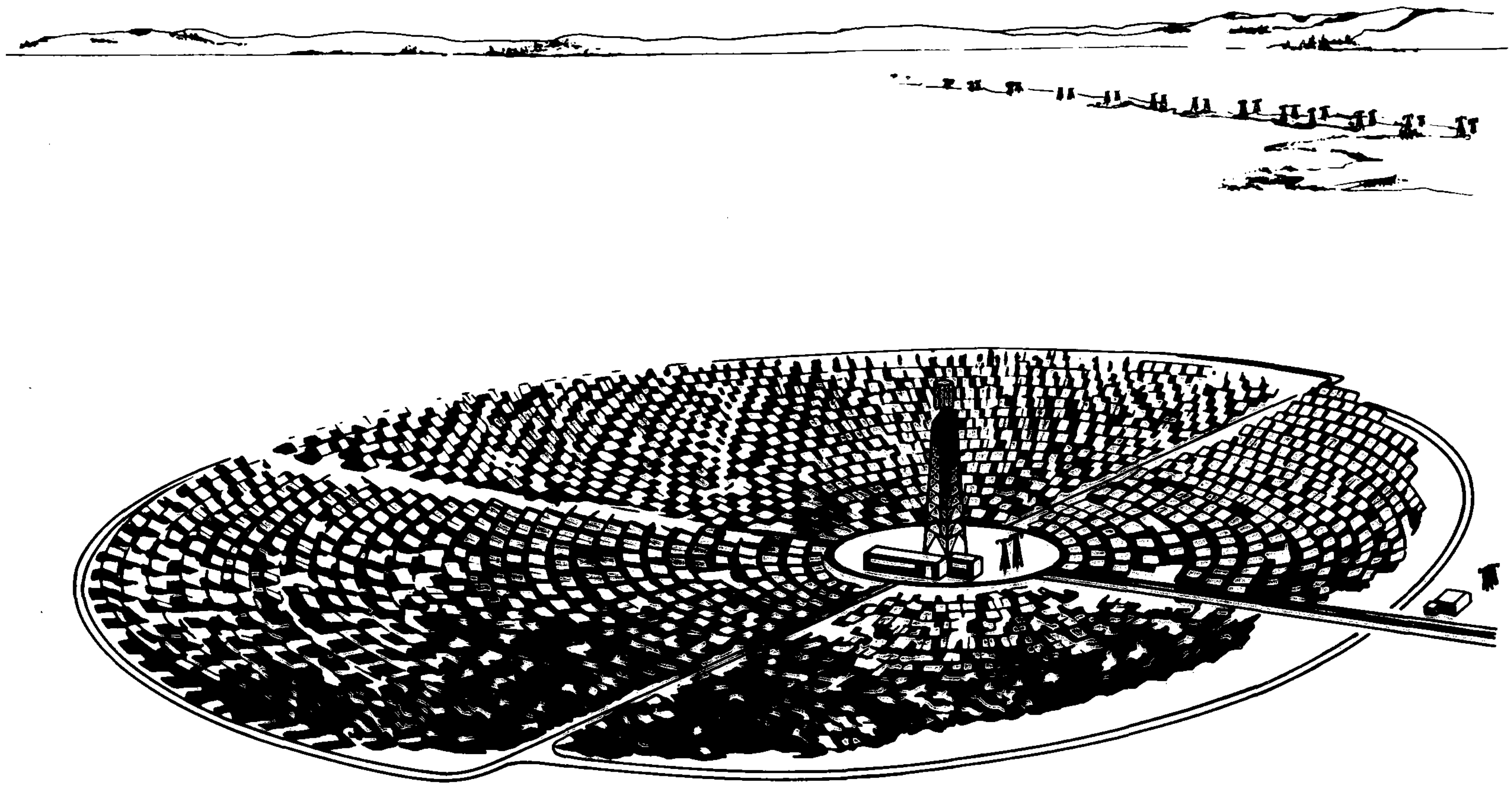

FIGURE 1.1. Central Receiver Concept - Example

TABLE 1.1 Receiver Design Concepts Evaluated

Heat Exchanger Concept	Proponent
Metal tubes	Boeing
Ceramic tubes	Black and Veatch
Sodium heat pipes	Foster Wheeler/Dynatherm
Ceramic matrix	Sanders
Ceramic domes	Massachussetts Institute of Technology-Lincoln Laboratory
Small particles	Lawrence Berkeley Laboratory
Volumetric	Pacific Northwest Laboratory

1.2 PROJECT ORGANIZATION

The air-heating receiver analysis was performed by the Pacific Northwest Laboratory (PNL) for Sandia National Laboratories as part of the U.S. Department of Energy's Solar Thermal Energy Systems Program. The project consists of four tasks:

Task I - Design Review
Task II - Conceptual Design
Task III - Performance Analysis
Task IV - Cost Analysis

The Task I Design Review was used to identify the concepts selected for analysis. The conceptual design task is described in Section 2 of this report. Sections 3 and 4 discuss the performance and costs analyses, respectively. Results of these analyses and a qualitative assessment of each receiver appear in Section 5. Section 6 presents conclusions from the study.

2.0 CONCEPTUAL DESIGNS

The seven receiver concepts considered in the study are at various stages of development. Some have had detailed preliminary designs prepared; others are merely conceptual ideas. In order to perform uniform analyses of each receiver's performance and cost, it was necessary to prepare conceptual designs for each receiver over a range of operating conditions. This section discusses the selection of design points considered in the analysis, the method and ground rules used in formulating the conceptual designs, and a brief description of the designs produced for each concept.

2.1 SELECTION OF DESIGN POINTS

An assessment of each receiver concept was desired for a range of operating conditions. Ranges of pressure (1 to 10 atm), temperature (1000 (538°C) to 2000°F (1093°C)), and size (1 to 300 MWt) were selected at the outset of the study as representative of the scope of operating conditions for which air-heating central receivers have been proposed. Within each range three specific points were selected for analysis:

- Pressure - 1, 5, and 10 atm
- Temperature - 1000 (538), 1500 (816), and 2000°F (1093°C)
- Size - 1, 50, and 300 MWt.

The selection of specific analysis points within each range was arbitrary. However, the temperatures selected nearly coincide with the appropriate operating temperatures generally quoted for three classes of materials: stainless steel (1000°F (538°C)), super alloys (1500°F (816°C), and ceramics (2000°F (1093°C)).

Any combination of the above operating conditions (for example, 5 atm, 1500°F (816°C), and 50 MWt) is referred to as a design point. The limited scope of the study precluded the analysis of each receiver concept at all 27 design points. Therefore, a method was derived to select a tractable number of design points for each receiver and still cover the desired operating range. First, a base line design point was selected to correspond most closely to the operating conditions suggested by the design proponent. Second, with two of the three variables constant, two additional design points were selected by varying the third variable over its range. This step was repeated three times, once for each variable. Third, any impracticable design points that were derived by the method were eliminated.

The method is illustrated in Figure 2.1 for the metal tube receiver. Boeing's proposal was for a 3-atm, 1335°F (724°C), 12-MWt receiver. This is closest to a base line design point of 5 atmospheres, 1500°F (816°C), and 50 MWt. Starting from this point, six other design points were added as shown. However, one of the design points, the 2000°F (1093°C) case, was impossible because of the material limitation of the metal tube. It was therefore eliminated.

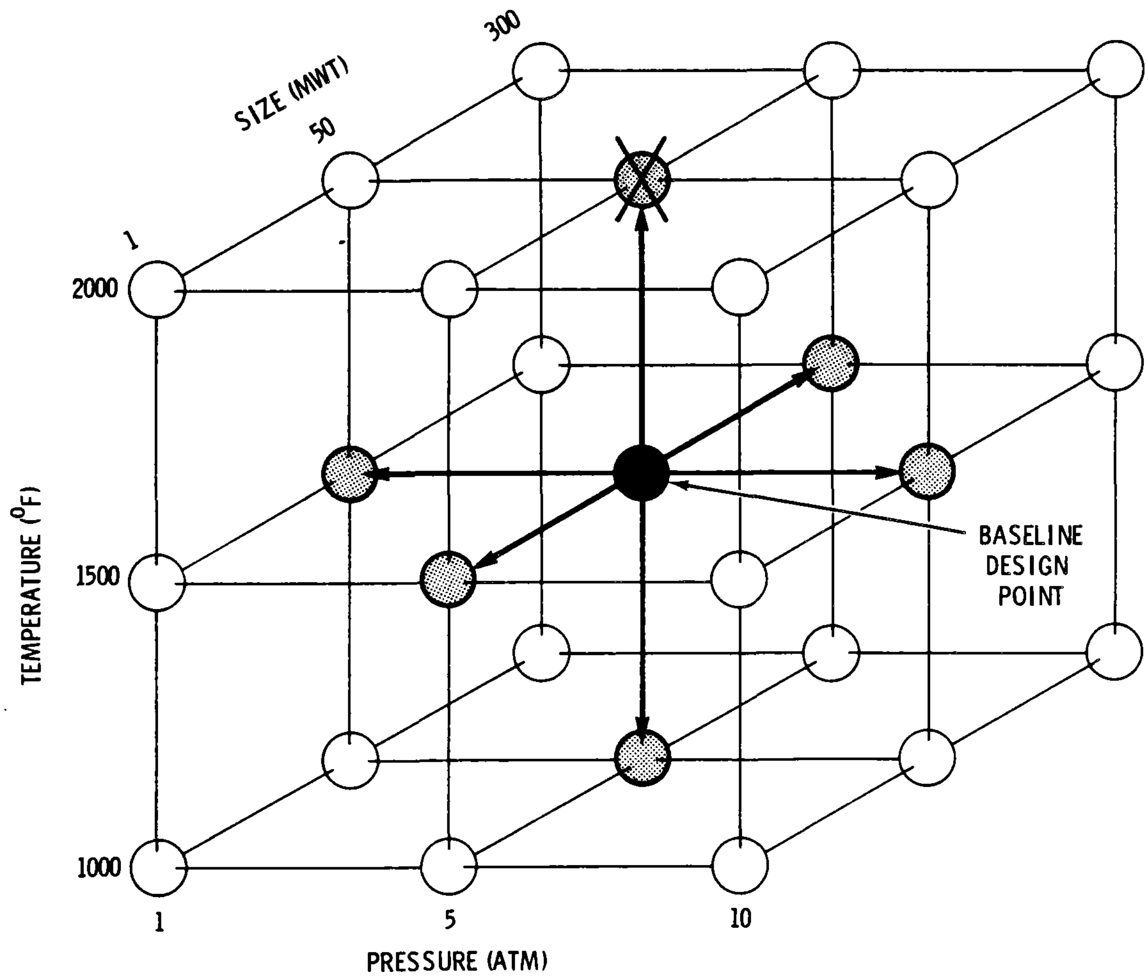

FIGURE 2.1. Selection of Design Points

With this method design points were selected for each of the seven receivers, as listed in Table 2.1. Note that these are the possible design points that were selected for further analysis. In some cases a selected design point, while it may have been possible, was deemed impracticable during the conceptual design task and was eliminated from the analysis. These few cases are discussed further in subsections 2.3 through 2.9.

2.2 METHOD AND GROUND RULES

The purpose of the conceptual designs was to facilitate the ensuing performance and cost analyses. The scope of the study precluded an extensive, detailed design effort. Rather, the intention was to produce accurate, uniform designs of sufficient detail that receiver performance and cost could be suitably estimated. Where possible conceptual designs were based on designs suggested by the proponent and modified to reflect changes in operating conditions. To ensure uniform designs and to limit the design process to a tractable task, several ground rules were adopted.

1. System boundaries. The analysis was concerned only with the receiver heat exchanger, support structure and enclosure, distribution piping, and immediate auxiliary equipment. Receiver tower, riser and downcomer, heliostat field, and storage were not considered. Where the unique features of a particular receiver would have an unusual impact on one of the plant components not analyzed, this fact was noted and is discussed in Section 5.

2. Receiver geometry. A standard geometry was assumed for each receiver based on the proponent's suggestions. This basic geometry was then used for all design points. The limited scope of the study did not permit major changes in configurations between design points. In several cases the basic geometry was used as a module that could be combined with other modules for the 300-MWt case. This practice yielded 300-MWt receivers for some concepts with four cavities of similar appearances but different sizes.

TABLE 2.1. Receiver Design Points

Receiver Concept	Pressure, atm	Temperature, °F	Size, MWt	Base Line Design Point
Metal Tube	1	1500	50	
	5	1000	50	
	5	1500	1	
	5	1500	50	Base Line
	5	1500	300	
	10	1500	50	
Ceramic Tube	1	2000	300	
	5	2000	300	
	10	1500	300	
	10	2000	1	
	10	2000	50	
	10	2000	300	Base Line
Sodium Heat Pipe	1	1500	50	
	5	1000	50	
	5	1500	1	
	5	1500	50	Base Line
	5	1500	300	
	10	1500	50	
Ceramic Matrix	1	1000	300	
	1	1500	300	
	1	2000	1	
	1	2000	50	
	1	2000	300	Base Line
Ceramic Dome	1	2000	50	
	5	1000	50	
	5	1500	50	
	5	2000	1	
	5	2000	50	Base Line
	5	2000	300	
	10	2000	50	
Small Particle	1	1500	50	
	5	1000	50	
	5	1500	1	
	5	1500	50	Base Line
	5	2000	50	
	10	1500	50	
Volumetric	1	1000	300	
	1	1500	300	
	1	2000	1	
	1	2000	50	
	1	2000	300	Base Line

3. Feasibility. Several of the receivers have components that have not been tested in actual operation: ceramic-metal seals, ceramic welding of tubes, carbon particle generators, etc. For the purpose of this study these components were assumed to perform as intended. No attempt was made to estimate development costs for undeveloped components or to analytically assess the feasibility of these components. Qualitative judgments of component feasibility that surfaced during the design and analysis tasks are presented in Section 6.

4. Design optimization. The purpose of the study was to evaluate the receiver concepts advanced by the proponents, not to redesign them. Receiver designs for this study were not extensively optimized and may not represent the lowest-cost configurations possible. Whenever possible, proposed designs were adhered to.

5. Materials. Materials were standardized for all receivers at a given operating temperature. Insulation materials were also standardized. Standard insulation thicknesses at each operating temperature were optimized based on insulation costs, assumed energy costs, (51, 68, and 85/mills/kWh_t at 1000, 1500, and 2000°F) and pay back period (five years).

6. Inlet conditions. The inlet air for atmospheric-pressure receiver designs was assumed to be at ambient conditions. For pressurized receivers the air was assumed to be ambient air pressurized to the desired state in a compressor with an isentropic efficiency of 80%. Receiver inlet conditions are listed in Table 2.2.

7. Power rating. All receivers were sized based on the thermal input added in the receiver itself. This ground rule was required because product pressure determines receiver inlet temperature with higher inlet pressures having higher inlet temperatures. This ground rule means that receiver power rating will not vary with inlet conditions, but it has two interesting effects. First, the mass flow rate and total energy output (energy added in the receiver plus energy added in the compression process) will increase with increasing inlet

TABLE 2.2. Receiver Inlet Conditions and Downcomer Size

Product	Inlet Pressure, atm (kPa)	Inlet Temperature, °F (°C)	Inlet Mass Flow Rate, kg/h-MWt)	Downcomer Inside Diameter, m 1 MWt	50 MWt	300 MWt
1 atm/1000°F Air	1 (101.4)	70 (21)	6,680	.42	3.0	7.3
1 atm/1500°F Air	1 (101.4)	460 (238)	4,220	.39	2.7	6.8
1 atm/2000°F Air	1 (101.4)	690 (366)	3,050	.37	2.6	6.4
5 atm/1000°F Air	5 (507)	70 (21)	11,270	.23	1.6	3.9
5 atm/1500°F Air	5 (507)	460 (23)	5,680	.20	1.4	3.5
5 atm/2000°F Air	5 (507)	690 (366)	3,750	.18	1.3	3.2
10 atm/1000°F Air	10 (1014)	70 (21)	19,340	.23	1.6	4.0
10 atm/1500°F Air	10 (1014)	460 (238)	7,200	.16	1.2	2.8
10 atm/2000°F Air	10 (1014)	690 (366)	4,350	.14	1.0	2.4

pressure. Second, in a low-temperature, high-pressure receiver (1000°F (538°C), 5 atm) almost as much energy is required in the compressor as is added in the receiver.

8. Field layout. Although this study was not concerned with components of the solar thermal plants other than the receiver, some knowledge of other components was necessary to accurately characterize the receiver. Such information included the field layouts, energy distribution from each field quadrant of surround fields, and tower heights. These data were determined for each receiver design by personnel at Sandia using the DELSOL2 central receiver simulation computer program.

2.3 METAL TUBE RECEIVER

The metal tube receiver is a forced-draft, cavity receiver with metal tube heat exchanger panels. The analysis of the metal tube receiver is based on the conceptual design developed by Boeing Engineering and Construction Company under contract to the Department of Energy for the United States Gypsum Plant Solar Retrofit Program (Boeing 1980). The conceptual system is designed to supply solar-heated process air to a gypsum board drying kiln. This receiver heats air, which has been compressed to 3.3 atm, from 440°F (227°C) to 1335°F (724°C). The receiver produces approximately 12 MW of thermal energy at the design point conditions. After exiting the receiver, the air is expanded through a turbine to near-ambient pressure and a temperature of about 900°F (483°C). The turbine provides power to run the air compressor as well as 1 MWe of power for the plant. About 10.5 MWt are provided to the process for drying.

The following sections described the metal tube design, the design points that were selected for analysis, and the final conceptual designs.

2.3.1 Description of Concept

The metal tube receiver consists of a cavity lined with metal tube heat exchanger panels (see Figure 2.2). The aperture is oval and is tilted downward at an angle of 40 degrees from vertical.

The steel receiver shell is supported by external skeletal beams. The shell provides air-tight support for the cavity insulation and protects the cavity from the external environment. The shell is fabricated from 10-gauge steel plate. The external beam structure supports not only the steel shell, but also the heat exchanger panels, the manifold, and the riser and downcomer piping. The external beam configuration allows the beams to remain at ambient temperatures, thereby avoiding thermal stresses.

The riser enters the bottom of each receiver cavity. Externally insulated carbon steel air supply pipes extend radially from the center plenum to the bottom header of each heat exchanger panel. Each panel consists of a number of tubes welded in parallel to an inlet and outlet header. The outlet manifold extends from both sides of the downcomer, which is located outside the receiver structure, 180 degrees opposite the aperture. The manifold pipe is internally insulated to allow the use of carbon steel rather than stainless or Inconel. Pipes penetrate the receiver shell to connect the outlet header of each heat exchanger panel to the exit manifold.

For multicavity receivers, the riser and downcomer are situated between the cavities. Connecting pipes join the riser and downcomer to the inlet and exit manifold of each cavity, respectively. The piping within each cavity is identical to that described previously for a single-cavity receiver.

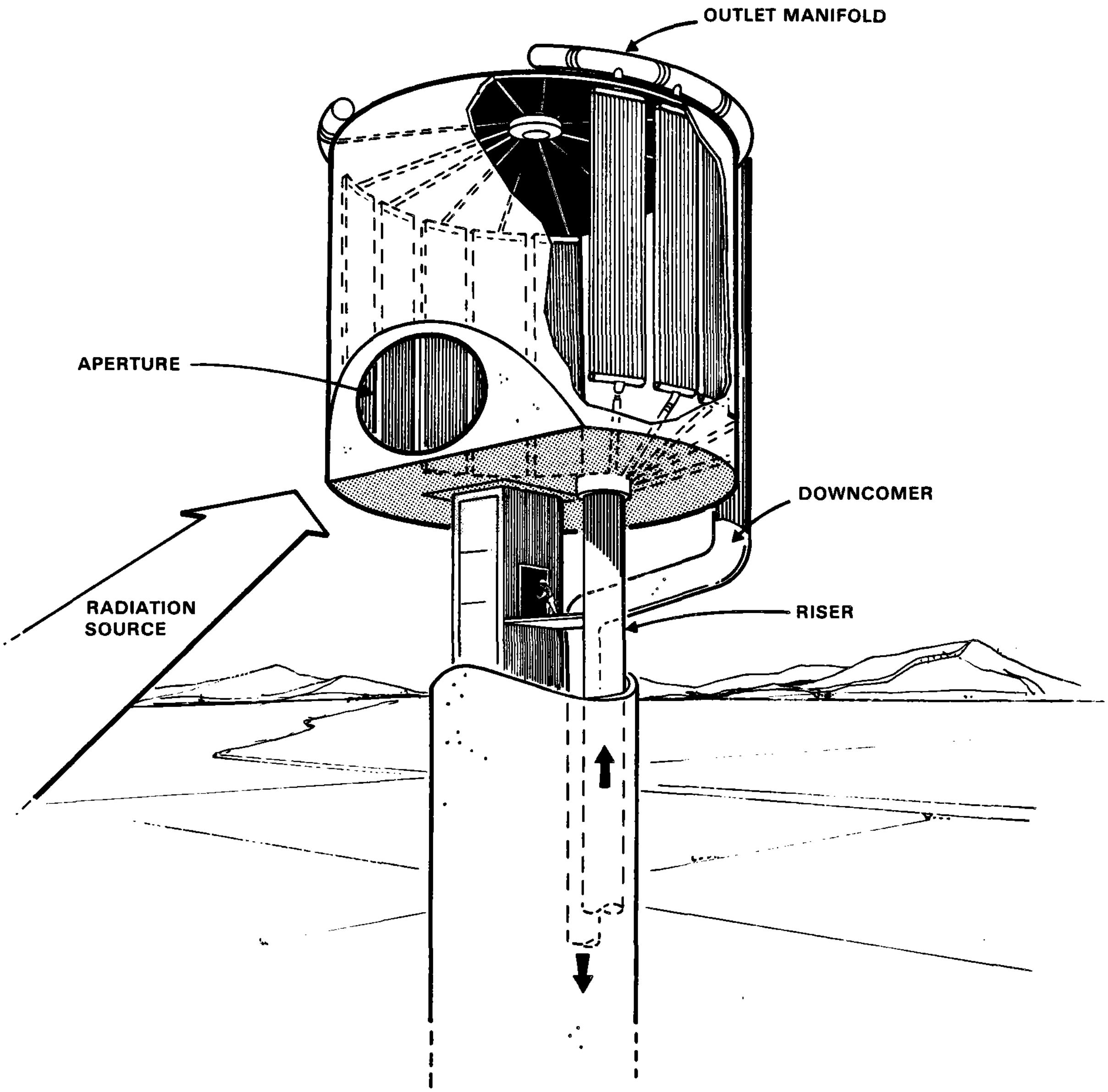

FIGURE 2.2. Metal Tube Receiver

During initial receiver checkout, the mass flow rate is balanced among the panels using pressure loss trimming orifice plates. Once adjusted, these orifice plates remain set during further operation. With this design, no active control system is required within the receiver. A master control valve is used to control the flow to each cavity. Check valves are located in the pipes that connect the exit manifolds to the downcomer for multi-cavity receivers to allow a single cavity to be isolated during plant operation.

During operation, air enters the bottom of the receiver cavity through the riser. Each heat exchanger panel header is fed radially from the center plenum. The air stream is divided into numerous parallel paths as it enters the tube section of the heat exchanger. The air is heated as it flows through the heat exchanger tubes. Air from each tube is recombined for each panel in the exit header. The heated air from the exit headers flows through the exit manifold to the downcomer.

2.3.2 Formulation of Conceptual Designs

This section discusses the design points selected for analysis and the design method used, and presents a brief discussion of the final designs for a metal tube receiver.

The design points initially selected for the purposes of this study are listed in Table 2.3.

The use of metal tubes in this receiver precludes the possibility of a 2000°F (1093°C) product. To achieve this temperature a ceramic material would have to be used. For this reason, the metal tube design analysis was limited to the 1000°F (538°C) and 1500°F (816°C) product temperatures. The base line design point was chosen to be 50 MWt, 5 atm, and 1500°F (816°C). This point was closest to the proponent's design point.

During the conceptual design task, it became apparent that there were some problems associated with designing a receiver for producing a product at 1 atm. It was virtually impossible to reduce the pressure drop across the receiver to

TABLE 2.3. Metal Tube Receiver Design Points

Pressure, atm	Temperature, F	Size, MWt	Special Design Points
1	1500	50	
5	1000	50	
5	1500	1	
5	1500	50	Base Line
5	1500	300	
10	1500	50	
3.3	1335	12	Proponent Design Point

a reasonable level. Tube lengths were successively shortened in an attempt to reduce the pressure drop; however, at a receiver height-to-diameter ratio of almost two, the pressure drop was still 75.84 kPa. Due to the low density of air at atmospheric pressure, a pressure drop of 75.84 kPa results in a very high head loss, making this approach impractical. Going to an even shorter, wider receiver did little to lower the pressure drop and made the overall receiver geometry impractical. For this reason, the 1-atm, 50-MWt, 1500°F (816°C) design point was dropped from further analyses. A more reasonable approach to designing for the 1-atm condition may be to operate the receiver at a higher pressure and then expand the product stream through a turbine to 1 atm. This approach was used for the gypsum plant conceptual study.

The general approach used to design the metal tube receivers was an iterative process whereby an initial tube exit temperature, a fraction of receiver power absorbed by directly and indirectly radiated surfaces, and a tube length was assumed. Then, the mass flow rate, heat transfer area, tube diameter and pressure drop were calculated. The initial tube length assumption was varied until a reasonable receiver height-to-diameter ratio and receiver pressure drop were achieved. Then, as a check, the tube exit temperature was recalculated to make sure that it did not exceed the tube material properties.

A brief summary of the key features for each of the design points appears in Table 2.4. Tubes and headers for the 1500°F (816°C) receiver were fabricated from Inconel 617. At 1000°F (538°C) 316 stainless steel was used. The 300-MWt design consisted of four cavities, but the length and diameter of the tubes were held constant to facilitate fabrication. The diameter of the cavities and number of tubes in the cavities were varied to account for the varied amounts of energy from the north, south, east, and west quadrants. Note two major changes at 1000°F (538°C): the tube material was changed to stainless steel, and fewer, larger-diameter tubes were used. Increasing the operating pressure to 10 atm increased the air density, improving the heat transfer and reducing the number of tube required.

TABLE 2.4. Metal Tube Receiver Designs

Design Points	Receiver Height, m	Receiver Width, m	Number of Tubes	Tube ID, cm	Tube Length, m	Aperture Size, m
5 atm, 1000°F, 50 MWt	21.34	21.34	277	7.62/7.54[a]	12.19	10.05x7.92
5 atm, 1500°F, 1 MWt	4.57	4.57	366	.77/ .68	1.87	1.65x1.34
5 atm, 1500°F, 50 MWt	22.86	22.86	665	3.71/3.43	10.67	10.05x7.92
5 atm, 1500°F, 300 MWt:						
N	24.38	38.40	1024	4.14/3.38	10.67	14.02x11.28
E, W	22.86	32.10	810	4.14/3.38	10.67	12.50x10.05
S	19.81	19.81	488	4.14/3.38	10.67	9.75x7.92
10 atm, 1500°F, 50 MWt	19.81	19.81	559	4.14/3.38	12.13	12.50x7.92

(a) Directly irradiated panels/Indirectly irradiated panels.

2.4 CERAMIC TUBE RECEIVER

Conceptual designs for the ceramic tube air-heating cavity receivers were based on information from the Black and Veatch report (Grosskreutz 1978). In work sponsored by the Electric Power Research Institute (EPRI), the above report describes the development of a conceptual design for a commercial-scale solar electric power plant. The receiver was designed to produce air at 9.5 atm and 1900°F (1038°C) with a capacity of 184 MWt. Power plant turbomachinery was required to operate from either the solar receiver or a fossil fuel combuster, with a turbine inlet temperature of 1800 to 2000°F (982 to 1083°C). Selection and testing of the heat exchanger material were given special attention. The silicon carbide heat exchanger tubes are the most distinguishing feature of the Black and Veatch receiver. Their suitability for use in a solar thermal receiver was discussed in detail by Black and Veatch. The results of the Black and Veatch review indicated that there is reasonable hope that ceramic materials can be successfully used for high-temperature solar applications with a ceramic tube arrangements.

2.4.1 Description of Concept

The ceramic tube receiver incorporates silicon carbide U-tube heat exchangers in an octagon-shaped cavity as shown in Figure 2.3. Black and Veatch modeled the cavity as a right circular cylinder, but the octagonal shape was chosen for ease of construction. One of the eight sides contains the aperture, which has a 0° inclination from vertical. The aperture width covers the one full side of the octagon, while its height is roughly half the full receiver height. All U-tubes are vertically oriented along the other seven sides of the octagon. There are no U-tubes or other heat exchange surfaces above the aperature or on the floor or ceiling. The tubes are set out half of one tube diameter from the back wall with a three-diameter, center-to-center spacing between U-tube legs. Neither end of the U-tubes is directly exposed to the solar flux. The lower ends, which attach to the headers, are beneath the cavity floor. The upper U-bend, attached to a compressive spring, is behind a false ceiling. Below the the cavity floor the inlet and outlet headers run in parallel paths with the outlet header above the inlet header. The outlet header is internally insulated to protect the pressure-bearing surface from the heated exit air.

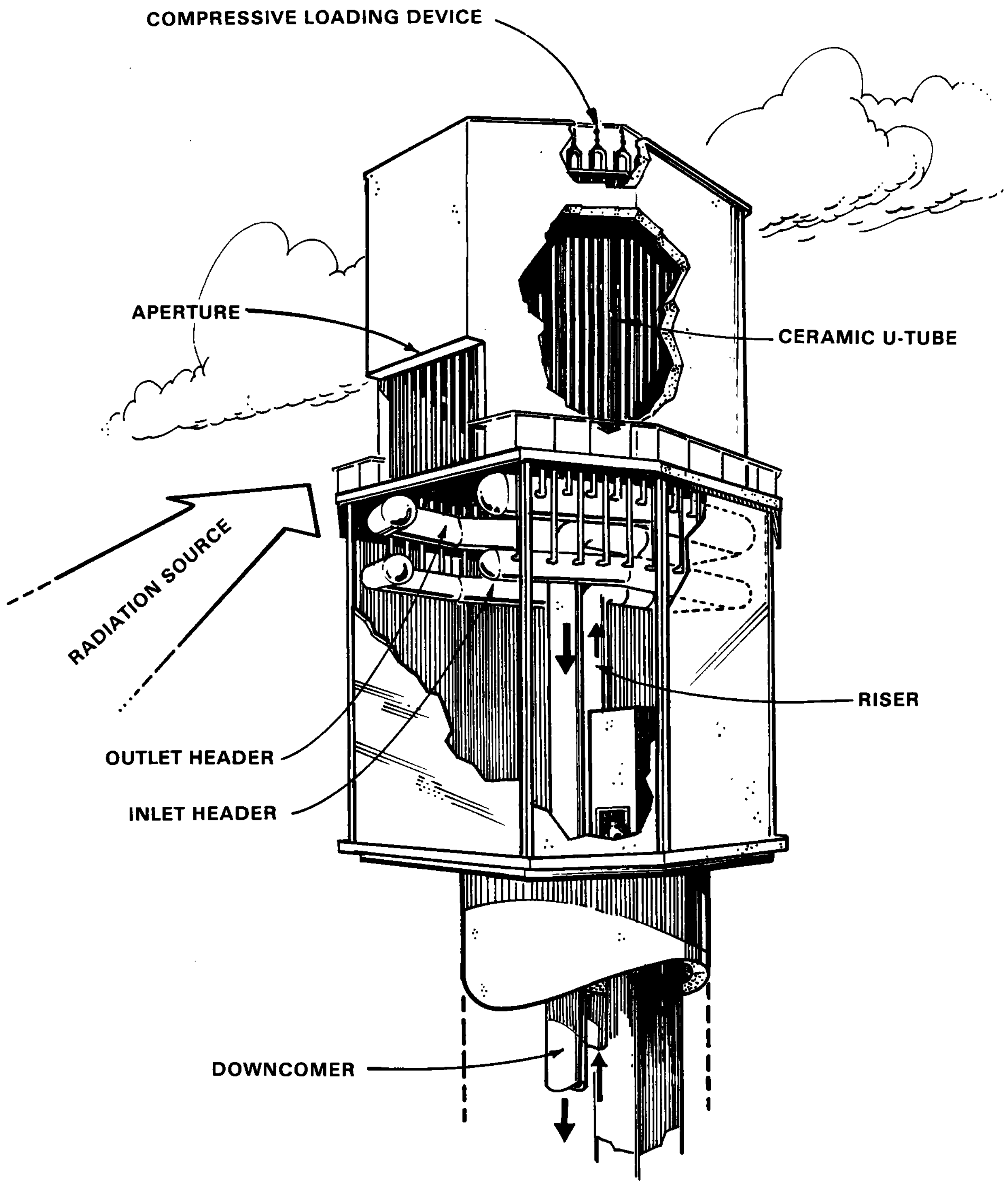

FIGURE 2.3. Ceramic Tube Receiver

Most of the special features associated with the ceramic tube receiver are designed to reduce or eliminate different sources of thermal stress on the silicon carbide heat exchanger. The U-tube allows vertical expansion and lateral bending. The compressive ceiling spring not only allows for vertical expansion, but keeps the U-tube in compression. (Silicon carbide is stronger in compression than tension.) Shielding both ends of the U-tube from direct solar flux serves to dampen the thermal expansion cycles at two critical areas: the U-tube bend and the ceramic-metal joints at the headers. Placing the supply header underneath the return header tends to eliminate differential thermal expansion between U-tube legs since the hot leg is necessarily shorter in this arrangement. Black and Veatch spent considerable effort optimizing placement of the U-tubes on the cavity walls. Their goal was to create uniform circumferential radiation on the U-tubes. One half diameter spacing from the back wall and three-diameter, center-to-center spacing between U-tubes created a fairly uniform flux and minimized circumferential stress.

The internally insulated return headers not only protect the metal pressure-bearing surface but allow the use of cheaper materials as well. Even for the 1500°F (816°C) design point, internal insulation is employed so that carbon steel can replace Inconel as the pressure-bearing material. Although internal insulation requires a larger pipe and more expensive installation, the switch from Inconel to carbon steel still results in a substantial cost saving. Cavity height for all four cavities of multicavity receivers is kept constant because of cost considerations. This should reduce costs in two ways. Construction should be facilitated and the unit cost per U-tube should decline because of economies-of-scale in fabrication.

Air flows into the supply header under the receiver cavity after passing through a control valve. Multicavity receivers have supply manifolds as well, which distribute air to each inlet header from the riser. There is one control valve per cavity. All U-tubes are connected in a parallel flow arrangement. No specific flow distribution device regulates air flow past the control valve because Black and Veatch did not consider unbalanced flow a problem at tube pressure drops in the range of 27.57 kPa. Air flow proceeds directly back to the outlet header (and out the return manifold for multi-cavity receivers) and into the downcomer. An isolation valve, located at the exit of the return header, is included for maintenance purposes.

2.4.2 Formulation of Conceptual Designs

Six design points were initially investigated for the Black and Veatch ceramic tube receiver. A base line design point was identified that roughly corresponded to the operating conditions suggested by Black and Veatch. The six design points and the proponent design point are presented in Table 2.5.

Although the ceramic tube receiver could be operated at temperatures below 2000°F (1093°C), the metal tube receiver more appropriately covers the 1500°F (816°C) range and under. For this reason the ceramic tube receiver was not investigated under 1500°F (816°C).

During the design process the 1 atm design point was eliminated because of excessive pressure drop or unreasonable receiver geometry. At a tube length of 24.38 m, heat transfer considerations required a flow rate of over 121.92 m/s with a resulting pressure drop of 0.5 atm. Even at these unlikely conditions the ratio of diameter to height was nearly 2 to 1. Decreasing the tube length further would not yield a reasonable flow rate and pressure drop without stretching the bounds of reasonable geometric proportionality.

The design procedure began by identifying lateral zones within the receiver where the flux was relatively constant. The flux profile for the Black and Veatch receiver did not vary radically, thus one single average flux

TABLE 2.5. Ceramic Tube Receiver Design Points

Pressure, atm	Temperature, F	Size MWt	Special Design Points
1	2000	300	
5	2000	300	
10	1500	300	
10	2000	1	
10	2000	50	
10	2000	300	Base Line
9	1900	184	Proponent Design Point

value was chosen for design purposes. An exit tube temperature was selected with attention to material temperature limitations. Tube length was arbitrarily fixed, based on geometric proportionality of cavity diameter and height. Receiver power rating and air inlet and outlet temperatures were fixed for each design point. With these parameters fixed, calculation of heat transfer coefficient, tube diameter, pressure drop, and other design variables was straightforward. Adjustments were made to the selected exit tube temperature and tube length as necessary in order to avoid unreasonable designs. Finally, adjustments were made to incorporate standard tube sizes and integer tube numbers per cavity.

All of the conceptual designs appear similar; differences are primarily due to alterations to tube length, tube diameter, number of tubes, and overall dimensions. The 300-MWt receivers each have four cavities and require additional pipe manifolding for air distribuiton and collection. The 1500°F (816°C) receiver requires less insulation than the 2000°F (1093°C) design points. Tube wall thickness is limited to a minimum of 0.635 cm for the silicon carbide tubes because of fabrication considerations. Thus, all heat exchanger U-tubes have 0.635-cm walls. Table 2.6 summarizes the specifications for a few parameters of each design point.

2.5 SODIUM HEAT PIPE RECEIVER

The sodium heat pipe central solar receiver is based on a conceptual design for a central solar receiver gas turbine plant that utilizes a high-temperature heat pipe receiver. The technical work was performed by Dynatherm Corporation as a prime contractor to DOE with Foster Wheeler Development Corporation as a subcontractor to Dynatherm.

The heat pipe receiver is ideally suited for heating gases to high temperatures. Heat pipes are essentially loss-free "thermal diffusers" that accept a high solar flux and transform it to a lower flux more suitable for transfering heat to air. This reduces receiver heating surface, thereby reducing receiver heat losses. Dynatherm's suggested operating conditions for their air-heating receiver at a design point of 27 MWt, 1500°F (816°C), and

TABLE 2.6. Ceramic Tube Receiver Designs

Design Points	Receiver Height, m	Receiver Width, m	Number of Tubes	Tube ID, cm	Tube Length, m	Aperture Size, m
5 atm, 2000°F, 300 MWt:						
N	20.91	31.15	126	9.525	34.08	9.54x12.28
E, W	20.91	24.78	99	9.525	34.08	9.54x9.66
S	20.91	15.61	60	9.525	34.08	9.54x5.85
10 atm, 1500°F, 300 MWt:						
N	20.57	30.69	106	14.76	33.8	9.54x12.16
E, W	20.57	24.20	83	14.76	33.8	9.45x9.54
S	20.57	15.18	50	14.76	33.8	9.45x5.76
10 atm, 2000°F, 1 MWt	4.36	4.57	47	2.26	5.06	1.40x1.28
10 atm, 2000°F, 50 MWt	17.80	20.21	104	9.02	28.65	8.02x7.77
10 atm, 2000°F, 300 MWt:						
N	21.52	30.78	141	10.66	35.17	9.78x12.16
E, W	21.52	24.54	111	10.66	35.17	9.88x9.57
S	21.52	15.39	67	10.66	35.17	9.85x5.76

5.8 atm. This design point is based on 30-MWt incident solar radiation to a north-facing cavity receiver, 3 MWt of heat losses, and an air receiver inlet temperature of 839°F (448°C).

2.5.1 Description of Concept

Incident solar radiation from a heliostat field enters the sodium heat pipe cavity receiver through an octagonal aperture as shown in Figure 2.4. The internal energy-absorbing surfaces that form the back of the receiver consist of a number of panels. The panel depth is a function of the air mass flow rate through it, which in turn is proportional to the heat flux impinging upon and being absorbed by the panel. Panel depth is such that each panel has approximately the same pressure drop. The cavity consists of the heat pipe receiving panels, an enclosure, inlet and outlet plenums, insulation, and support structure.

The heat pipes are installed in a 14.76-cm triangular-pitch pattern and are attached to the front and back panel plates so they can be removed from the back of the panel in case of failure. The evaporator surfaces of the heat pipes, which protrude about 1 ft from the front panel plate, absorb the incident solar heat flux. The heat pipes then isothermally transport the energy to the finned condenser section. Compressed air is introduced at the bottom of the panels and is gradually heated by contact with the fins as it passes up through the finned condenser section of the heat pipes. The compressed air also receives some heat from contacting the insulated front panel wall. The isothermal transport of the heat pipes is a continuing process of liquid sodium being vaporized by the incident solar heat flux. The vapor travels from the evaporator to the condenser section where it is cooled as heat is transferred to the air passing up through the receiver panel. The vapor condenses to liquid in this process and returns by capillary pumping to the evaporator section through an appropriately designed wick system.

The protruding evaporator section of the heat pipes provides enough area to keep the heat flux below design limits, and it also shades the front panel wall area between heat pipes from direct exposure to the incident solar heat flux. The inner surfaces of the cavity are faced with 2.54-cm of ceramic fiber

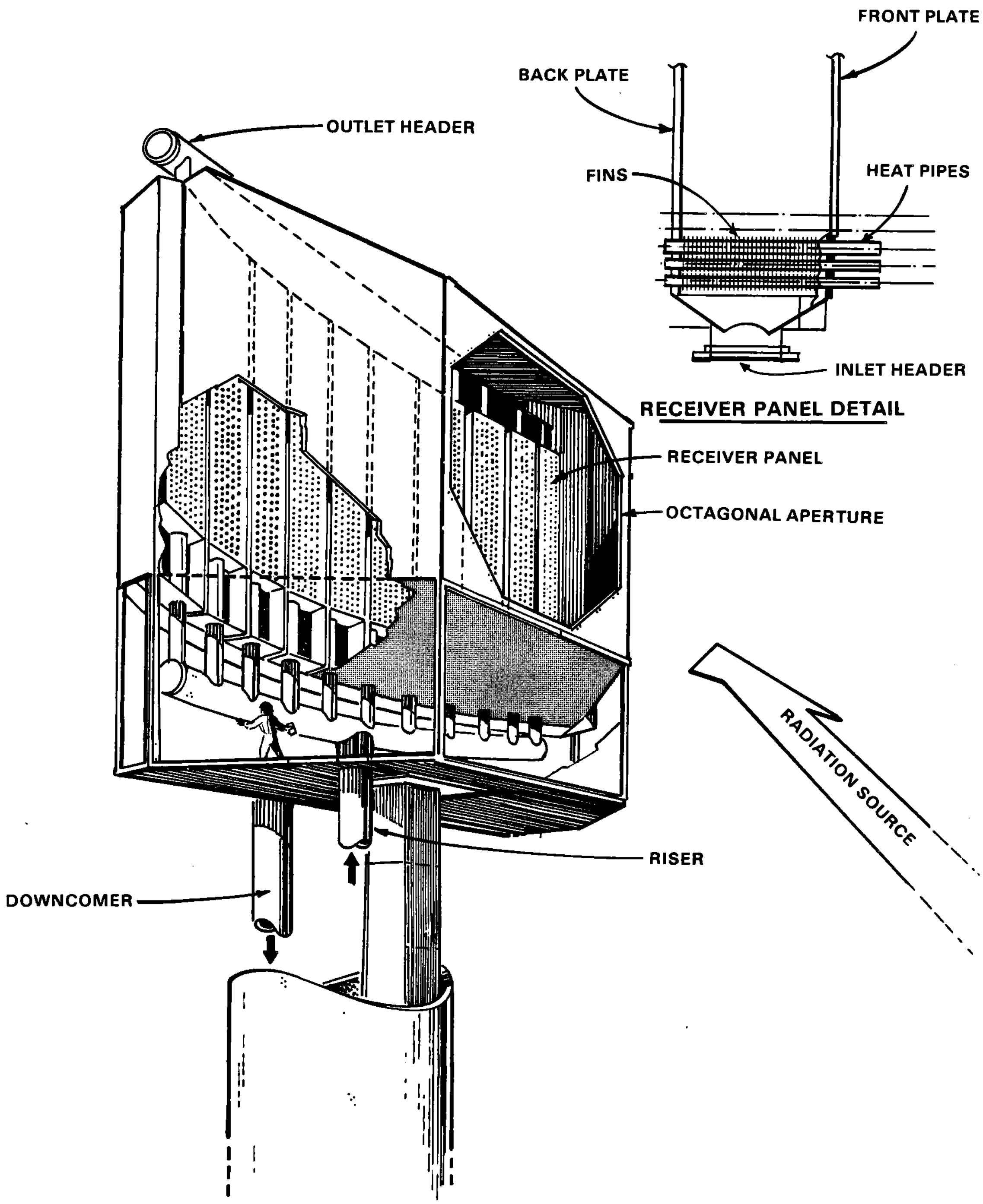

FIGURE 2.4. Sodium Heat Pipe Receiver (50 MWt)

insulation for additional protection. The outer surface of the cavity is encased in fiberglass and calcium silicate insulation and covered by corrugated aluminum siding.

The panel shells consist of a front plate, a rear plate, and stiffened side walls. The heat pipes are welded to both the front and rear walls and act as supports for these 0.635-cm plates. The side walls are tapered I-sections formed by 0.9525-cm-thick flanges (plates) and 0.635-cm-thick webs. The panel inlet and outlet heads consist of a pyramidal shell formed by 0.9525-cm-thick plates, which are supported at five intermediate locations by 0.9525-cm stiffeners. The inlet header, its inlet pipe, and butterfly valve are carbon steel material.

The remaining support structure of the receiver consists of removable insulation walls that form the very back of the receiver behind the rear panel walls. All framing members are carbon steel beams with welded construction. Carbon steel plate 0.635-cm thick is bolted to the framing members to form the inside walls of the cavity.

2.5.2 Formulation of Conceptual Designs

The design points chosen for the sodium heat pipe cavity receiver are shown in Table 2.7, which includes the proponent design point for comparison.

TABLE 2.7. Sodium Heat Pipe Receiver Design Points

Pressure, atm	Temperature, F	Size, MWt	Special Design Points
1	1500	50	
5	1000	50	
5	1500	1	
5	1500	50	Base Line
5	1500	300	
10	1500	50	
5.8	1500	35	Proponent Design Point

Conceptual designs at each of the design points were derived using an iterative procedure. Total panel area for each power rating was determined based on the average panel heat flux proposed by Dynatherm. Mass velocity and heat pipe and fin dimensions were held constant for all designs with the exception of the 1-MWt design. Panel widths were calculated and used to calculate other receiver dimensions. Data for convective heat transfer coefficients for the finned tubes were based on a value quoted by Dynatherm for their average conditions. This base line figure was scaled using results presented by Kays and London (1964) to determine heat transfer coefficients for other operating temperatures and pressures. The receiver designs were iterated until requirements for panel frontal area, total heat transfer area, flow area, and material temperature limitations were simultaneously satisfied.

Table 2.8 highlights a few of the significant features of the sodium heat pipe receiver designs. All 50-MWt designs have the same height, number of panels, panel frontal area, and aperture size. The depth of the panels (and therefore heat pipe condenser length and heat transfer area) is varied to account for changes in air temperature and pressure. As the exit air temperature is lowered or operating pressure is raised, the temperature difference across the receiver becomes smaller and a larger mass flow rate (and therefore a larger cross-sectional flow area) is required. For the 1-atm case the temperature difference becomes larger and the panels can be made shallower. All of the 1500°F (816°C) cases used Inconel 601 for the heat pipes and other hot parts of the receiver. At 1000°F (538°C) 316 stainless steel was used.

The 1-MWt case is something of an anomaly. To keep the peak heat pipe temperatures reasonable the number of panels and panel heat flux had to be reduced from the values suggested by Dynatherm. These changes resulted in a proportionally larger receiver at 1 MWt than for the 50-MWt base line case.

2.6. CERAMIC MATRIX RECEIVER

Sanders Associates have been working since the early 1970s on ERDA and DOE contracts to develop the concept of a 100 MWt central solar receiver for power generation. At least two published reports have summarized this work (Sanders

TABLE 2.8. Sodium Heat Pipe Receiver Designs

Design Points	Receiver Height, m	Receiver Depth, m	Number of Heat Panels	Number of Panels	Panel Height, m	Panel Width, m	Panel Depth, m	Aperture Width,[a] m
5 atm, 1500°F, 50 MWt	14.33	7.62	10458	9	10.06	1.36	.61/.52	7.92
5 atm, 1000°F, 50 MWt	14.33	8.84	10458	9	10.06	1.36	1.68/1.28	7.92
5 atm, 1500°F, 1 MWt								
5 atm, 1500°F, 50 MWt	14.33	7.92	10458	9	10.06	1.36	.82/.61	7.92
5 atm, 1500°F, 300 MWt:								
N	16.76	10.67	20232	9	14.33	1.92	1.22/.91	10.97
E, W	15.54	9.14	16164	9	13.41	1.59	1.10/.85	9.14
S	12.80	7.32	9171	9	9.75	1.24	.79/.61	7.62
10 atm, 1500°F, 50 MWt	14.33	8.23	10458	9	10.06	1.36	1.09/.82	7.92

(a) Aperture width is the distance from one side of the octagonal aperture to the opposite side across the aperture.

1978; Sanders 1979). The latest report describes the design and testing of a 1/4-MWt prototype receiver and briefly outlines the concept of a commerical size (100-MWt) power plant.

The Sanders concept uses a novel ceramic matrix as the primary absorbing surface and is designed to produce 2000°F (1093°C) air. Since the entire concept includes an open-cycle Brayton engine for generating electricity, the inlet air temperature for the design point is 1200°F (649°C). Checker stoves are proposed to be used as storage between the collection cycle and the generation cycle. The high inlet air tempertures required using a closed loop through the receiver. The aperture is open to the atmosphere, forcing the receiver to always operate at atmospheric pressure.

2.6.1 Description of Concept

The ceramic matrix receiver is basically a cylindrical cavity with conical ends. The shape allows for effective distribution of the radiation around the cavity walls. Figure 2.5 shows an artist's conception of the receiver as air enters the receiver from the outer surface of the cylindrical wall. The air is heated while passing through the thin honeycomb ceramic to the interior of the cavity. Having the cooler air on the external side of the cavity facilitates cooling the support structure of the receiver, thus allowing cheaper materials to be used.

A computer analysis done by Sanders showed that the addition of a terminal concentrator increased the capture rate by about 10% and allowed the use of a slightly smaller aperture. The aperture is tilted 14° from horizontal to the north to increase the capture rate without significantly increasing the convective losses.

Air is supplied to the receiver through a closed ducting system. The closed system allows the aperture of the receiver to be open without exchanging air across its boundary. As illustrated in Figure 2.5 the air is fed into an annulus between the ceramic matrix and the terminal concentrator. The annulus facilitates uniform distribution around the cylinder. The air then flows up and through the absorber and out the top of the receiver. Some type of storage

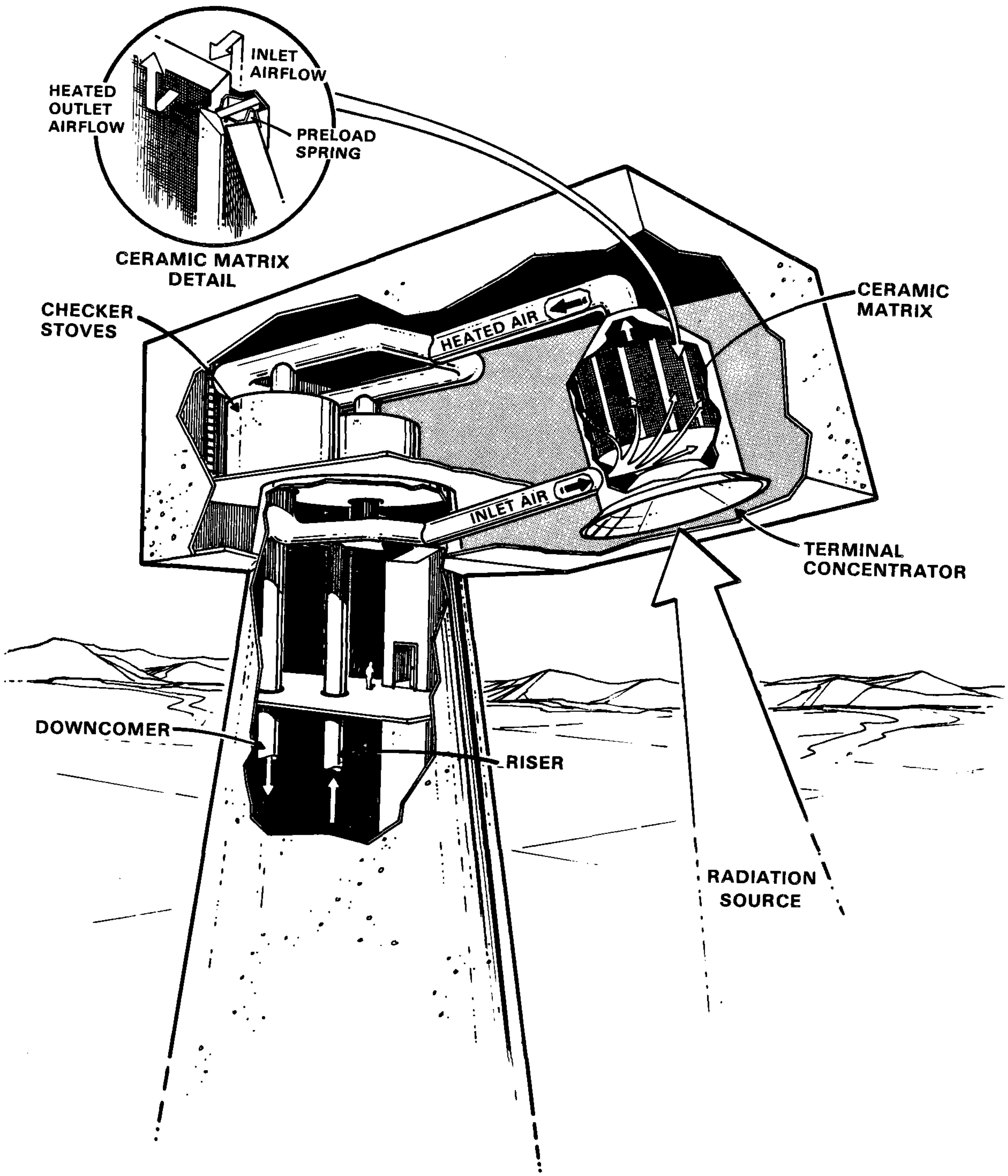

FIGURE 2.5. Ceramic Matrix Receiver (50 MWt)

must be provided in order to transfer the heat to another air loop that transports the heat to the user. For continuous operation multiple storage modules are necessary with appropriate valves and control systems.

2.6.2 Formulation of Conceptual Designs

The open aperture of the ceramic matrix receiver requires the receiver to operate at atmospheric pressure. As discussed in the previous section it is possible to provide a pressurized product with the receiver by using the checker stoves. However, this study was concerned only with the receiver, so the operating pressure was limited to atmospheric pressure. With this constraint five design points were selected as indicated in Table 2.9. Table 2.9 includes the proponent design point where the design is assumed not to include a checkered stove.

The crucial part of the Sanders design is the ceramic matrix which lines the inside of the cylindrical cavity. The matrix is made of thousands of small passages each with a hydraulic diameter of 0.254 cm. The depth of the matrix is 4.44 cm. The free flow area is 60% of the total surface area thus allowing for very low air velocities through the matrix and corresponding low Reynolds numbers (~20). At these low flows the heat transfer is due primarily to conduction from the matrix walls to the air instead of convection. This results in a heat transfer coefficient that is independent of air flow rate and thus constant over a wide range of operating conditions.

TABLE 2.9. Ceramic Matrix Receiver Design Points

Pressure, atm	Temperature, F	Size, MWt	Special Design Points
1	1000	300	
1	1500	300	
1	2000	1	
1	2000	50	
1	2000	300	Base Line
1	2000	300	Proponent Design Point

The main advantage of the ceramic matrix design is the ability of the cylindrical absorbing matrix to withstand much higher fluxes than a typical cavity receiver. The design method focused on estimating the maximum flux allowable on the cavity surface without the cavity temperature being excessive. A standard heat transfer computer code was used to do an energy balance on the heat transfer matrix, estimating the temperature distribution for various incident radiation fluxes. Thus, calculations were made for fluxes of 280 kW/m^2, 350 kW/m^2, and 420 kW/m^2. The maximum surface temperature of the matrix was predicted to be 2150°F (1177°C), 2200°F (1209°C) and 2300°F (1260°C), respectively.

Although higher fluxes could possibly be used, an average flux of 300 kW/m^2 was chosen for the 300-MWt design points. This was very near the 280 kW/m^2 used by the Sanders proposed design. For the smaller receivers at 1 MWt and 50 MWt, smaller average fluxes were used since the chance for poor distribution causing excessive surface temperatures is increased.

For the 300-MWt design points all major dimensions were taken from the Sanders 300-MWt proposed design. For the 1-MW and 50-MWt design points the major dimensions were roughly scaled down from the 300-MWt design. The apertures for these two cases were made slightly larger than would be obtained by scaling the Sanders design. Table 2.10 lists the significant design information for each of the five design points.

2.7 CERAMIC DOME RECEIVER

The ceramic dome receiver consists of an insulated cavity housing a number of solar heated ceramic domes. The dome assemblies are the key feature of the receiver and are the building blocks from which the required heat transfer area is obtained. The domes assemblies are airtight and positioned with the concave side facing the receiver. Air is transferred to the rear of the dome assembly, and heated as it passes over the dome's convex side by impingement heat transfer. After passing through several domes to achieve the desired temperature rise, the air enters the outlet header and is carried to the downcomer.

TABLE 2.10. Ceramic Matrix Receiver Designs

Design Points	Receiver Height, m	Receiver Width, m	Matrix Height, m	Matrix Diameter, m	Aperture Diameter, m	Terminal Concentrator Inlet Diameter, m
1 atm, 1000°F, 300 MWt	17.5	32.0	12.5	25.3	11.9	36.6
1 atm, 1500°F, 300 MWt	17.5	29.9	12.5	25.3	11.9	36.6
1 atm, 2000°F, 1 MWt	1.5	2.4	1.2	1.8	1.2	3.0
1 atm, 2000°F, 50 MWt	10.6	11.9	7.6	10.1	7.6	18.0
1 atm, 2000°F, 300 MWt	17.5	29.0	12.5	25.3	11.9	36.6

The ceramic dome receiver has been proposed by Dr. P. T. Jarvinen of the Massachussetts Institute of Technology's Lincoln Laboratory. The design originally proposed by MIT was aimed at producing hot air that could be effectively used in an open-cycle gas turbine for the production of electricity. The design conditions chosen by MIT called for an outlet temperature of 1800°F (982°C) and an operating pressure of 4 atm. A nominal power rating for the receiver was not specified by MIT. Because of the modular nature of the ceramic dome heat transfer assemblies, the power rating of the receiver can be scaled up or down over a wide range by varying the number of domes in the receiver.

2.7.1 Description of Concept

The ceramic dome receiver described in this report was developed using guidelines discussed by MIT, but it is not based upon a specific design proposed by MIT. The ceramic dome receiver concept was developed by MIT in a generalized way without detailed design of the cavity configuration, flow scheme, or dome assembly. Hence many of the specific design details discussed herein were developed by PNL.

As previously mentioned, the key characteristic of the MIT receiver is the ceramic dome heat transfer assembly. The ceramic dome concept was developed because of the many potential advantages it may offer. The use of ceramics as a material of construction, as opposed to metals, allows the possibility of high outlet fluid temperatures. Where more conventional heat exchanger tubes resist pressure stresses by tensile forces, ceramic domes carry pressure loads in compression. This is an advantage in that ceramic materials can sustain loads between 5 to 20 times greater (depending on the ceramic) in compression than in tension. Another potential advantage of the dome concept is that dome connecting piping, manifolds, and air seals need not be exposed to the high flux conditions in the receiver cavity, and so can be of simpler design, Finally, the use of impingement heat transfer can result in very high heat transfer coefficients, which may be a factor of 3 to 6 times greater than for air flowing through tubes.

The basic configuration of the receiver is quite simple, as shown in Figure 2.6. The receiver structure consists of a steel frame that supports the ceramic domes. The dome units are mounted flush to each other on the cavity

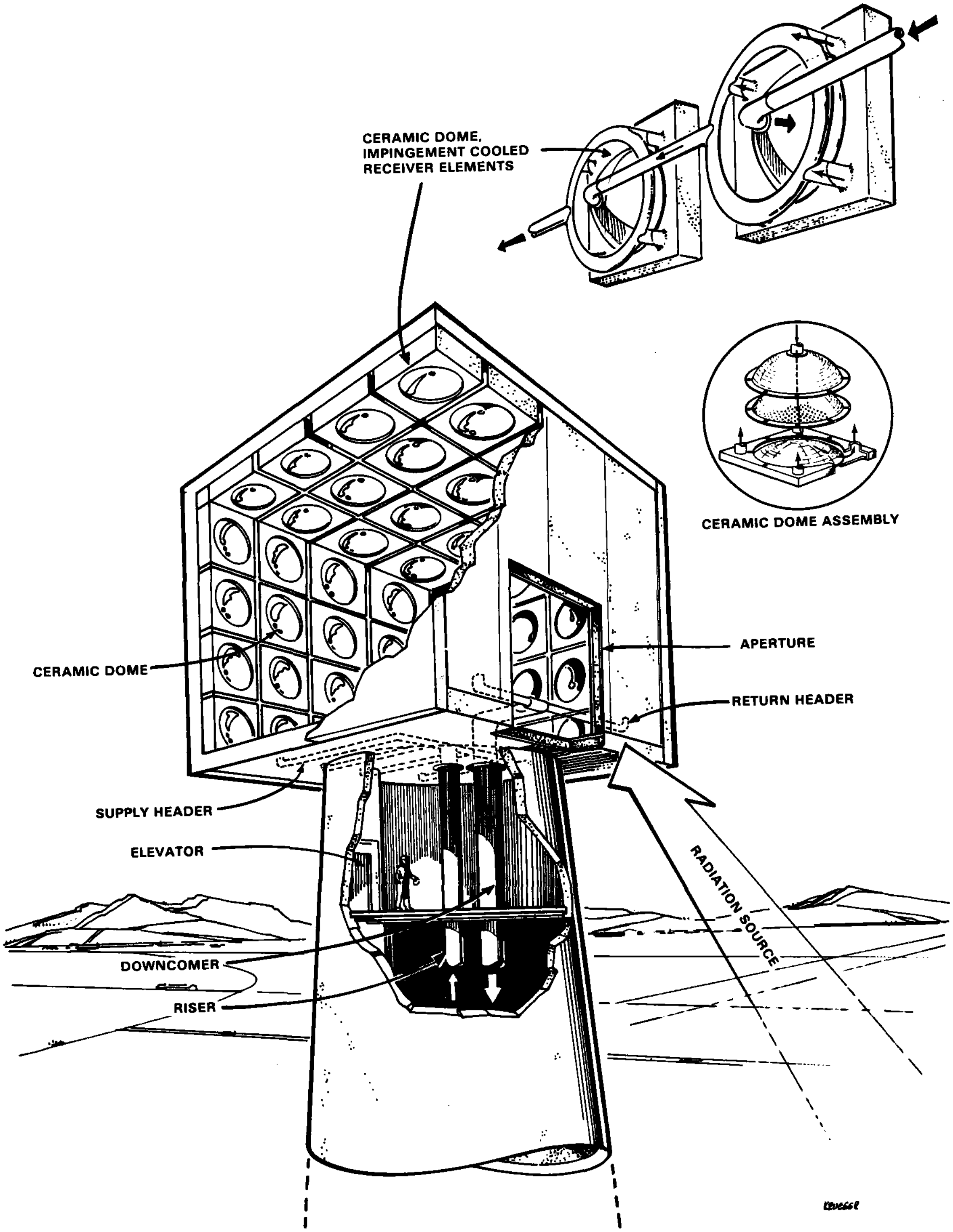

FIGURE 2.6. Ceramic Dome Receiver (50 MWt)

sides, and in some cases the ceiling. For most design configurations, a large portion of the receiver interior walls are made up of the dome units. The receiver cavity area that is not covered by domes is insulated with alumina silica insulation. An access space of several feet is allowed between the cavity interior wall and the exterior wall of the receiver. This space accommodates headers and connecting piping, and allows maintenance access. The receiver is insulated both behind the cavity interior wall and on the inside of the exterior wall. The cavity interior wall is sufficiently insulated to maintain a temperature of no more than several hundred degrees Fahrenheit in the access space.

The ceramic dome assembly consists of an air plenum, and impingement jet air diffuser, a ceramic dome, a dome enclosure, and inlet/outlet ducting. In operation, air enters the air plenum and passes through the impingement jet air diffuser, which distributes air to all parts of the ceramic dome. The ceramic dome is surrounded by a stainless steel enclosure, with the receiver side of the steel enclosure protected by a silicon carbide front plate. After being heated by contact with the ceramic dome, the air leaves the unit via one of the four heated-air outlets. The air ducting for individual domes is illustrated in the inset of Figure 2.6. A single air inlet admits cool air in the center of the air plenum. The four air outlets, located at corners of the dome enclosure, are connected with a circular duct that combines the hot air flow into a single stream, and conducts it to the next dome or an outlet header.

Air enters the receiver through the riser, and is transfered to the dome assemblies through the inlet header behind the rear cavity wall. To provide maximum cooling to the domes on the rear cavity wall, the air first flows through these domes, each of which is a parallel flow path. After exiting the rear wall domes, the air flows through several domes on the cavity side walls or ceiling to reach the desired air outlet temperature. An expansion joint would be included in the connecting pipe between each dome assembly. One control valve would be used to control the flow of air to each cavity.

2.7.2 Formulation of Conceptual Designs

The design conditions of 1800°F (982°C) and 5 atm proposed by MIT were used to select a base design point of 2000°F (1093°C), 5 atm, and 50 MW. As described in Section 2.2, this resulted in seven design points being chosen for analysis as indicated in Table 2.11. A proponent design point was not included because the proponents have not developed a design in sufficient detail to allow the identification of a design point.

Because of problems in using comparable dome designs for all design points, which are discussed more fully later, a feasible 1-MWt design was not identified, resulting in the elimination of this design point.

The approach used to design the ceramic dome receiver was to maintain to the greatest extent possible similar domes for all design points. A common dome diameter (2 meters) and radius of curvature were used in all designs. Receiver flux, mass flow rate, dome wall thickness, impingement jet hole diameter and hole spacing, and the number of domes connected in series were varied to minimize the number of domes required at each temperature and pressure. For a given temperature and pressure, identical domes designs were used for all power levels. Rather than using a fixed receiver geometry, receiver dimensions were varied to accomodate the different dome quantities that were required at alternative design points.

The basic dome design using a 2-m-dia dome proved to be impractical for the 1-MWt receiver. The low flow rates required for the 1-MWt output resulted in poor heat transfer coefficients. The use of smaller domes was investigated for the 1-MWt design but resulted in an unworkably small receiver aperture.

TABLE 2.11. Ceramic Dome Receiver Design Points

Pressure, atm	Temperature, F	Size, MWt	Special Design Points
1	2000	50	
5	1000	50	
5	1500	50	
5	2000	1	
5	2000	50	Base Line
5	2000	300	
10	2000	50	

While it would be possible to develop a 1-MW design based on this receiver concept, it would require dome designs and design approaches considerably different than for the other design points. Because of these problems, the 1-MWt design was dropped from consideration.

Basic correlations and design equations used in the design of the ceramic domes were taken from Jarvinen (1977). Domes were laid out with several domes in series to achieve the required temperature rise. Following the basic layout discussed by Jarvinen, the first dome of each line was mounted on the rear wall of the receiver, where it was exposed to the highest insolation. Subsequent domes were mounted on the receiver side walls and ceiling.

The inlet and exit air temperatures, pressure drop, and dome surface temperature were calculated for each of the domes in series. Fluid properties for the previous dome were used as an initial guess to estimate a bulk average fluid temperature for the dome. Fluid properties at the estimated bulk temperature of the dome were then obtained, and the calculations repeated until sufficient convergence had been obtained.

Domes were designed to minimize the number of domes required to achieve a given temperature rise, while at the same time maintaining a low cavity temperature and receiver pressure drop. Because these are contradictory goals, a number of tradeoffs were required in the designs. Guide lines used in making the tradeoffs were to keep the pressure drop below 5% of the receiver working pressure and to keep the dome surface temperature less than 700°F above the air temperature exiting in the receiver.

A summary of the key design features of the ceramic dome receivers appears in Table 2.12. All 50 MWt receivers required approximately the same number of domes, ranging from 45 to 55. The base line design (5 atm, 2000°F, 50 MWt) required 55 domes. Reducing the outlet temperature or increasing the operating pressure, both of which decrease the temperature rise across the receiver, reduced the required number of domes for the 50-MWt designs. Dome wall thickness was reduced somewhat at 1-atm and increased for the 10-atm design.

TABLE 2.12. Ceramic Dome Receiver Designs

Design Points	Receiver Dimensions (HxWxL), m	Aperture Size (HxW), m	Number of Domes in Series	Total Number of Domes	Dome Thickness, mm
1 atm, 2000°F, 50 MWt	107x10.7x13.7	6.4x6.4	4	64	3.35
5 atm, 1000°F, 50 MWt	10.7x10.7x9.4	4.9x4.9	3	48	7.92
5 atm, 1500°F, 50 MWt	8.8x8.8x9.4	4.9x4.9	5	45	7.92
5 atm, 2000°F, 50 MWt	10.7x8.8x9.4	8.2x6.4	5	55	7.92
5 atm, 2000°F, 300 MWt:					
N	12.8x10.7x13.7	4.9x4.9	5	100	7.92
E, W	10.7x10.7x13.7	8.2x8.2	5	80	7.92
S	10.7x8.8x11.6	8.2x6.4	5	60	7.92
10 atm, 2000°F, 50 MWt	10.7x8.8x9.4	8.2x6.4	5	50	10.97

2.8 SMALL PARTICLE RECEIVER

The small particle heat exchanger receiver is a cavity receiver characterized by the use of small, submicrometer-size carbon particles that act as the heat exchange medium by absorbing the incident solar radiation. At the desired receiver temperature, the carbon particles oxidize and enter the process stream as carbon dioxide.

The proponent and inventor of the concept is Dr. Arlon Hunt of the Lawrence Berkeley Laboratories (LBL). Dr. Hunt published his first paper describing the concept in June 1978. Since then he has made preliminary calculations of receiver performance and has assembled a laboratory test apparatus. He is currently developing a 30-kW prototype of the receiver for testing at the Georgia Tech Solar Test facility.

Dr. Hunt and his associates at LBL have been very helpful during the study in providing us with information through reports and conversations. Personal contacts were made early in the project to facilitate the exchange of information, to clarify the concept, and allow us to be apprised of new developments in the design philosophy.

Conceptual work at LBL has centered around a small cavity receiver operating at high temperatures and high solar concentration ratios. The receiver described in previous LBL reports has been a 4 MWt receiver with a design solar concentration ratio of 2000:1 at the window and an output air temperature of 1000°C. This design was applied to the production of electricity through an open-cycle gas turbine. Though high flux ratios are desired for high efficiency, window material considerations limit the maximum flux. Manufacturing limits on currently available Corning Vycor Glass 7913 dictated the size of the aperture and hence the power rating of LBL's conceptual receiver.

2.8.1 Description of Concept

The small particle receiver is simply a hollow cavity that permits exposure of the carbon particles to direct solar flux as shown in Figure 2.7. The carbon particles are mixed into the air stream via the carbon particle generator, which is located at the base of the tower (upstream of the compressor) for

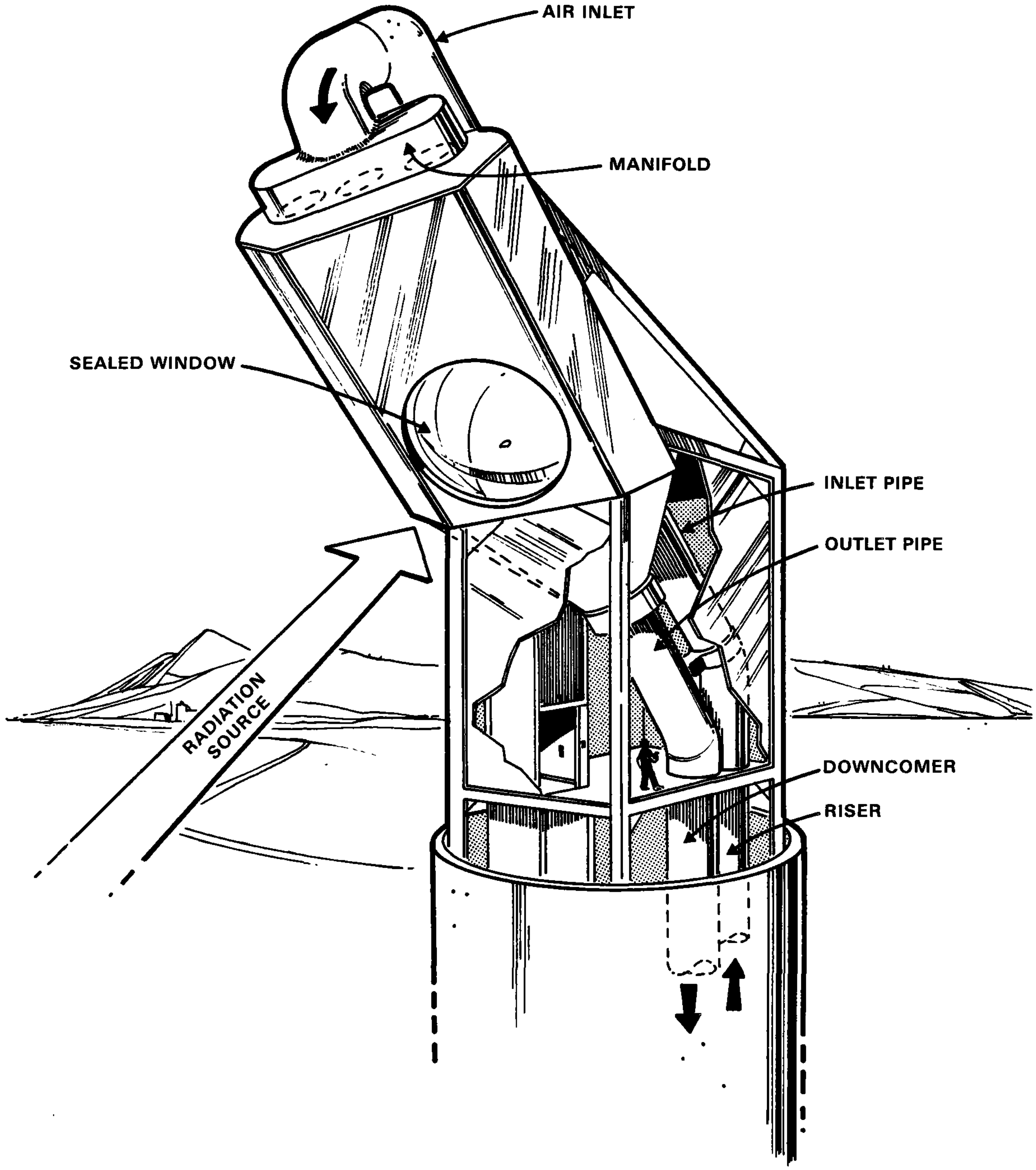

FIGURE 2.7. Small Particle Receiver (50 MWt)

pressurized operation or on the tower for atmospheric operation. The entrained particles pass through the inlet manifold at the top of the receiver and are dispersed into the cavity via the manifold flow distributors. In the cavity, the particles absorb the incoming solar radiation and, as the particles pass into the downcomer, oxidize to form carbon dioxide. A window is placed at the aperture of the receiver to contain the particles and to permit pressurized operation.

The simple receiver design permits a minimum number of components, with none that require precision machining. These components include the insulation, receiver shell, window, window seal, inlet manifold, inlet flow distributors, a pressure relief valve, an opacity meter, temperature sensors, a cavity lining [at 1000°F (538°C)], the receiver support structure, and the carbon particle generator.

The carbon particles forming the active heat exchange medium in this design are produced with an average particle diameter an order of magnitude smaller than the peak wavelength of solar radiation (0.52 μm). With the particle diameter much smaller than the characteristic absorption length of incident light, the entire volume of the particle participates in the absorption. The high surface-to-volume ratio of the particles also enhances efficient heat transfer to the process air. Rayleigh theory for small particles was used to predict the carbon mass loading requirements for the design conditions.

Preliminary experimental work by Dr. Hunt indicates that the actual mass loading requirements may be much lower than that predicted by Rayleigh theory. The size and the nonspherical shape of the carbon allotropes place the particles in a region ill-defined by theory. Experiments indicate that the mass extinction coefficient of the particles is approximately 4 times greater than predicted. This would reduce the required mass loading to 1/4 the anticipated value.

Varying the size and allotrope of the carbon particles allows a broad range of air temperatures: approximately 600°F (315°C) to 3600°F (1982°C).

However, the particle upper temperature bound appears to be considerably lower because of material limitations of the window. This limit currently restricts the maximum cavity operating temperature to approximately 2000°F (1093°C).

These carbon particles can be produced by a number of methods among which are arc evaporation, pyrolysis of organic resins, and thermal decomposition of hydrocarbons. Because the properties of the carbon particles are highly dependent upon the precise method of production, the ultimate selection will have to be determined through laboratory testing. The method that will be used by Dr. Hunt in the test receiver will be production via the pyrolysis of acetylene in an inert gas, argon. Preliminary experiments at LBL indicate that an argon-to-acetylene ratio of 7:1 will be necessary to attain the desired dispersion of carbon particles. At lower ratios, the particles tend to agglomerate. At the 7:1 mixture, particle agglomeration is negligible several seconds after formation and suspension into the air stream.

The small particle receiver concept possesses several advantages over conventional cavity receivers. The cavity temperature is effectively the temperature of the carbon particles, which is very close to the gas temperature, hence reradiation losses are lower. The receiver design is inherently simple, lightweight, easy to construct, and the pressure drop is very low.

An interesting feature of this design is the proportional relationship between the power rating and the carbon mass loading rate and cavity depth. At constant inlet and outlet temperatures, gas specific heat, and gas density, increasing either the cavity depth or carbon loading rate will proportionally increase the rated receiver power. For example, doubling the receiver depth, hence doubling the flow area, will allow twice as much gas to be heated with the same carbon loading. This is possible because the solar flux heats the particles and the particles in turn heat the air.

2.8.2 Formulation of Conceptual Designs

The reference design point was selected as one near that of LBL's conceptual receiver. The reference design outlet temperature is 1500°F (816°C), the operating pressure is 5 atm, and the power rating is 50 MWt. The 50-MWt power rating is notably larger than LBL's 4-MWt receiver, but the larger rating is still possible with a single-cavity, single-aperture geometry, and the larger size is suspected to be better suited for a field of low-cost, production heliostats. Using this as the base line point, the initial set of design conditions were selected as listed in Table 2.13. A proponent design point is not included in Table 2.13 because the proponents have not developed a concept design of sufficient detail to allow the selection of a design point.

TABLE 2.13. Small Particle Receiver Design Points

Pressure, atm	Temperature, F	Size, MWt	Special Design Points
1	1500	50	
5	1000	50	
5	1500	1	
5	1500	50	Base Line
5	2000	50	
10	1500	50	

A 300-MWt case was not considered because of window size limitations, the necessity to change the receiver geometry to a circumferential scalloped window arrangement, and recommendation by Dr. Hunt.

Fused silica, Corning 7940, has been chosen as the window material for all designs. Fused silica with an anti-reflective coating provides attractive optical properties such as low reflectivity and high solar transmissivity. Fused silica also has a low coefficient of expansion and a high tolerance to thermal shock.

The principal design requirement was that the incident flux pass through the particle stream to a desired depth before impinging on a receiver wall. This feature determined the angle of the cavity side walls away from the window and the height of the rear cavity wall. In addition, the rear wall must be maintained below an acceptable temperature. Using the 2000:1 solar concentration ratio at the aperture as recommended by Dr. Hunt, the above considerations led to the selection of a 95% one-way absorption of solar flux.

Because the geometry is dictated by the heliostat field shape, the design is essentially constant at a given power rating. Though the 1-MWt receiver is much smaller than the reference 50-MWt design, the basic geometry is the same in both instances. In designing the 1-MWt receiver, the window size was not reduced to the level of accepting a 2000:1 concentration ratio. To achieve this flux, the window diameter would be reduced to approximately 0.80 m, which is impractically small. The window was therefore resized to 2.0 m. Further, in downsizing, the characteristic length used in Beer's equation to determine absorption was reduced from 1 m, which was used in LBL reports, to 1/2 m to enable a more compact design.

Flow distributors at the inlet manifold were deemed necessary to ensure dispersion of the carbon particles throughout the cavity. Similarly, the exit duct is tapered to protect against zones of recirculation that would form in ducting through a floor perpendicular to the particle flow.

At the higher temperatures, 1500°F (816°C) and 2000°F (1093°C), the inner lining for the cavity is provided by the insulation. At 1000°F (538°C) the fiberglass insulation is protected from the flow of hot gas by a sheet of aluminum.

Table 2.14 summarizes key features of the small particle receiver designs. All 50-MWt receivers have the same dimensions; carbon particle loading is adjusted to achieve the desired temperature rise in the receiver. The 1-MWt design is proportionately larger than other designs because of optical properties of the heliostat field.

TABLE 2.14. Small Particle Receiver Designs

Design Points	Receiver height, m	Receiver width, m	Receiver depth, m	Aperature diameter, m	Carbon Mass loading rate, Kg/hr
1 atm, 1500°F 50 MWt	15.5	12.8	4.3	6.0	52.4
5 atm, 1000°F, 50 MWt	15.5	12.8	4.3	6.0	18.6
5 atm, 1500°F, 1 MWt	5.8	5.5	2.7	2.0	.52
5 atm, 1500°F, 50 MWt	15.5	12.8	4.3	6.0	14.2
5 atm, 2000°F, 50 MWt	15.5	12.8	4.3	6.0	11.2
10 atm, 1500°F, 50 MWt	15.5	12.8	4.3	6.0	8.9

2.9 VOLUMETRIC RECEIVER

The volumetric air-heating receiver concept was developed at the Pacific Northwest Laboratory (PNL) as part of PNL's involvement in solar thermal power generation. Earlier comparisons of generic solar thermal systems conducted by PNL identified problem areas associated with producing high-temperature air. The development of the volumetric receiver was in response to these problems. This concept has not been analyzed in the same detail as several of the other air-heating receiver concepts. A preliminary analysis of the concept was conducted at PNL and the results were sufficiently encouraging to have the concept included in this comparison study.

The volumetric receiver was originally developed as a receiver to produce high-temperature air for process heat applications. Further analysis showed that with the addition of two checker stove heat exchangers, the concept could be used to produce hot air at pressures above atmospheric pressure. Similarly, with the addition of a boiler and superheater the receiver can be used to generate steam for a Rankine cycle power plant.

2.9.1 Description of Concept

The volumetric receiver is cylindrically shaped and is similar in appearance to an external receiver, but the design of the receiver produces performance characteristics similar to a cavity receiver. The concept consists of an array of fin-shaped pins arranged in concentric cylindrical rows around an inlet manifold. Solar radiation from the heliostat field, focused on the receiver, is absorbed on the pins. Air is drawn through the pin array by means of an induced draft fan and is heated by direct contact with the pins. The fin-shaped pins have a large surface area relative to the area exposed to solar radiation so good convective heat transfer can be expected between the pins and the air. The geometry of the pin array will cause the incident radiation to be absorbed over a large number of pin surfaces so that it appears that the radiation is being absorbed in a volume rather than on one external surface. This arrangement means that a very high flux can be tolerated on the external surface of the receiver because the flux is actually absorbed on a large number of surfaces in the interior. The receiver is divided into zones, each of which consists of one row of pins. The two exterior zones reflect incident radiation

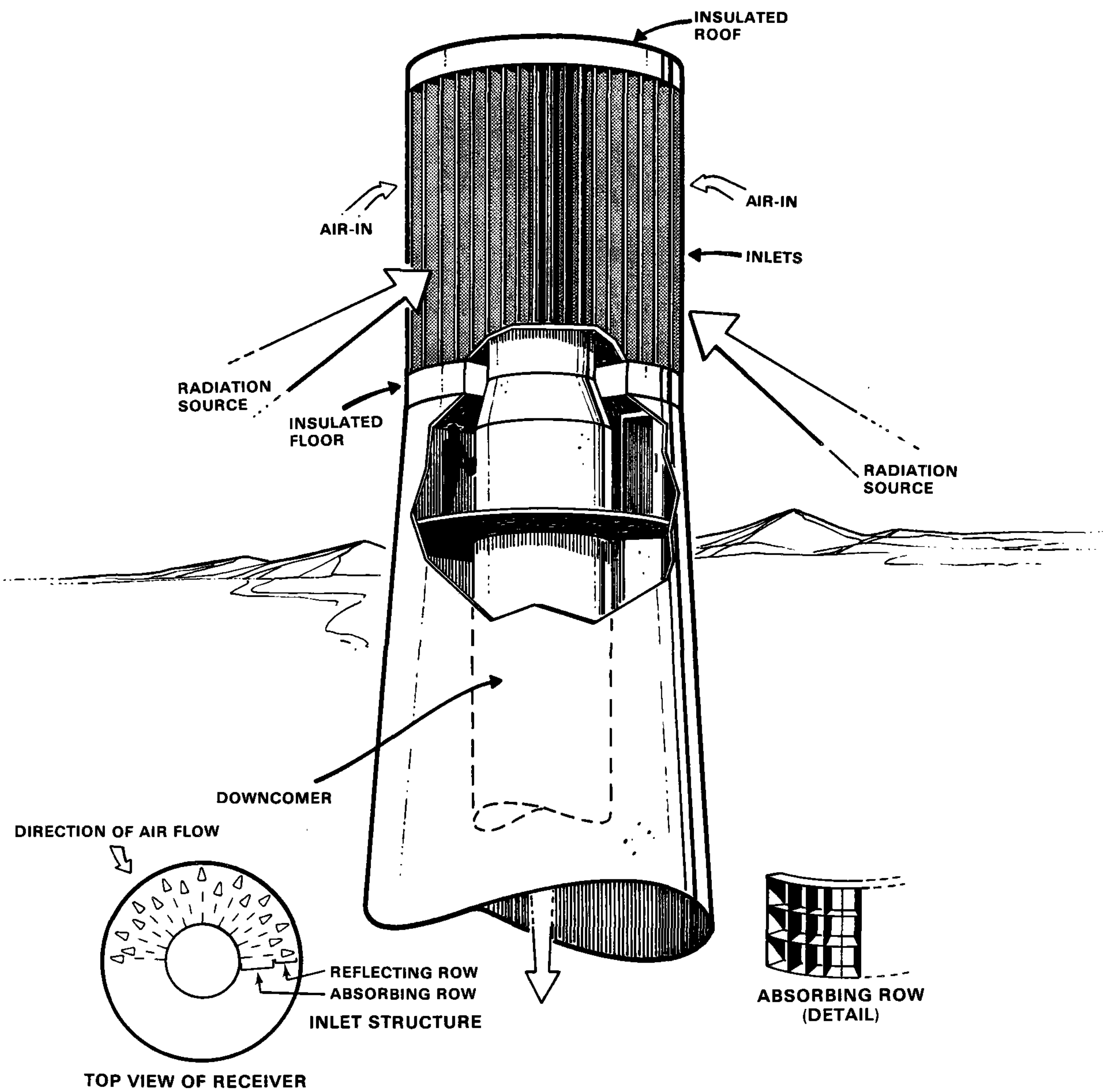

FIGURE 2.8. Volumetric Receiver (50 MWt)

into the receiver and block reradiation and reflection from the interior of the receiver. The intermediate zones are absorber zones, each of which is designed to absorb a fraction of the incident radiation. The interior zone is the inlet manifold, which absorbs all incident radiation that has not been absorbed in the other zones. The volumetric receiver is shown in Figure 2.8.

The two reflecting zones consist of wedge-shaped pins that have specular reflecting surfaces on the surfaces exposed to incident radiation. The incident radiation is reflected into the receiver. The interior surfaces of the reflecting rows have absorbing surfaces that absorb reflected or reradiated energy from the interior absorber zones. The two reflecting zones dramatically reduce reflection and reradiation losses, and due to the low operating temperature of the reflecting zones, these pins can be fabricated from carbon steel and can provide the structural support for the receiver roof.

The absorber zones consist of fin-shaped pins. The pins are located in vertical and circumferential rows around the receiver. The length of the fin is determined by the required heat transfer area for heat transfer between the pins and the air. The amount of energy absorbed in one row is determined by the cross-sectional area perpendicular to the direction of incident radiation and by the absorptivity of the pins. In this study all absorber pins were assumed to have the same absorptivity, but by varying the absorptivity between rows, the amount of energy absorbed in any one row can be tailored to meet other criteria, such as heat transfer constraints. The absorbing pins can be fabricated from either metals or ceramic material, depending on zone operating temperature.

The interior zone consists of the inlet manifold, which both absorbs any incident radiation that passes through the absorber zones and distributes air flow in the receiver to prevent hot spots and recirculation. Depending on operating temperature, the inlet manifold can be fabricated from either carbon steel, alloys, or ceramics.

Air is moved through the receiver by an induced draft fan. The heated air from the receiver is used to charge a multiple-vessel pebble bed or checker stove storage. Process heat is provided by a forced draft fan that blows air through storage to produce heated air. This arrangement both shields the induced draft fan from high temperature and provides storage. By using the checker stove, the product loop can be operated at pressures above atmospheric. For lower temperature applications hot air can be supplied directly from the induced draft fan.

2.9.2 Formulation of Conceptual Design

The formulation of the conceptual design includes the selection of design points and the development of a design methodology. The selection of the design points was straightforward and will be briefly discussed, but the unique design of the volumetric receiver required the development of an unusual design methodology, which will be discussed in some detail.

Conceptual designs were developed for the five design points given in Table 2.15. A proponent design point did not exist; therefore no information related to a proponent design point is included in Table 2.15. The design points include product temperatures from 1000°F (538°C) to 2000°F (1093°C) and sizes from 1 MWt to 300 MWt. Product pressures were limited to 1 atm. With a multiple-vessel checker stove higher product pressures could be provided. However, this study was concerned only with the receiver itself, which alone cannot produce pressurized air. The volumetric receiver concept appears to be suitable for a wide range of product temperatures with appropriate selection of absorber pin material. The concept can also be used over a wide range of sizes, but at a size of 1 MWt the receiver is larger than optimum because of optical characteristics of the heliostat field. This effect produces a less efficient design at very small sizes.

The design methodology consisted of developing one geometric arrangement for the receiver and then scaling the design to compensate for size variations. At a given size, the dimensions of the receiver did not change with temperature, only absorber pin material was changed.

TABLE 2.15. Volumetric Receiver Design Points

Pressure, atm	Temperature, F	Size, MWt	
1	1000	300	
1	1500	300	
1	2000	1	
1	2000	50	
1	2000	300	Base Line

The receiver diameter is determined by the inlet manifold diameter, number of zones, and the length of the pin in a given zone. In order to keep the receivers geometrically similar, all receiver designs consist of the same number of zones. The number of zones was determined by an analysis of reflection and reradiation losses as a function of the number of absorber zones for the 300-MWt, 1000°F (538°C) design. It appears that losses decline rapidly for the receivers consisting of few zones, but for receivers with 15 to 20 zones there is an insignificant decline in losses. For this study a receiver consisting of 2 reflecting zones and 14 absorbing zones was chosen.

One result of the absorber zone optimization was the calculation of absorbed flux for each reflecting and absorbing zone. This distribution was assumed to be constant for all temperatures and power ratings, as long as the number of zones and the ratio of row lengths were not varied.

The length of the absorber row is determined by the heat transfer requirements of the row. A short row would have a reduced heat transfer area but an increased heat transfer coefficient because of entry length effects. A long row has more area but a lower heat transfer coefficient and results in a heavier and larger receiver. Several absorber row designs were completed for the 300-MWt, 1000°F (538°C) design case, and the design giving the best combination of heat transfer characteristics and absorber pin weight was chosen. This design used absorber pin lengths of 0.5 ft (0.15 m) and reflecting pin lengths of 0.75 ft (0.26 m) and 0.68 ft (0.21 m) for the first and second rows.

While the geometry of the receiver remained constant, regardless of operating temperature, the selection of absorber zone material did depend on the temperature of each zone. Zonal temperatures were calculated by determining the amount of energy absorbed in the zone and the convective heat transfer coefficient between the pins in the zone and the air. The absorbed flux was calculated as part of the absorber zone optimization study described above. The convective heat transfer coefficient was calculated by modeling air flow through the pin matrix as internal laminar flow in a smooth tube with the appropriate hydraulic diameter. The air experienced low flow velocities and large temperature differences between the pins and the air, which resulted in a natural convection heat transfer coefficient approximately equal to the forced convection component. In order to account for natural convection a correction factor was calculated, and the forced convection component increased appropriately. After calculating zonal temperature for each zone in a given receiver, design materials were selected for each zone. In all cases the reflecting zones were at a temperature low enough to allow the use of carbon steel.

A summary of the key elements of the volumetric receiver designs appears in Table 2.16. At 300 MWt the receivers are all the same size; only materials change. At 2000°F (1093°C) the absorber pins are ceramic material; at 1500°F (816°C) they are 316 stainless steel and Inconel 601; and at 1000°F they are carbon steel and 316 stainless steel. The 1-MWt design is proportionately larger than the other sizes because of optical characteristics of the heliostat field.

TABLE 2.16. Volumetric Receiver Designs

	Receiver Height, m	Receiver Diameter, m	Number of Vertical Absorber pins	Absorber Pin Size cm	Absorber Pin Length, m
1 atm, 1000°F, 300 MWt	10.4	8.2	7825	15.2x.152	9.1
1 atm, 1500°F, 300 MWt	10.4	8.2	7825	15.2x.152	9.1
1 atm, 2000°F, 1 MWt	3.0	14.4	808	15.2x.152	1.5
1 atm, 2000°F, 50 MWt	6.7	4.9	4527	10.2x.152	5.5
1 atm, 2000°F, 300 MWt	10.4	8.2	7825	15.2x.152	9.1

2.10 SUMMARY OF DESIGNS

Conceptual designs were developed for each of the seven concepts at several design points, leading to a total of 38 individual designs. Performance and cost estimates were developed for each of the 38 designs. Results of these analyses appear in Section 5.

This study was concerned only with the receivers themselves. No attempt was made to characterize the heliostat field or receiver towers. However, it is possible to make some rough judgments of the relative impact of each receiver design on the rest of the central receiver system.

Table 2.17 presents weights for each of the seven receiver concepts at 50 MWt. All of the results are not exactly comparable; the data are for several different operating pressure and temperatures. However, they do provide a good, approximate idea of the receiver masses and therefore the tower strength requirements. A few general conclusions can be drawn from Table 2.17. Ceramic receivers tend to weigh less than metal receivers. Receivers with high allowable heat fluxes tend to be smaller, and weigh less, than receivers with lower heat fluxes. The one exception to both of these trends is the ceramic dome receiver. Although it has a high heat flux and ceramic heat transfer surfaces, it is quite heavy. This is because of the metal enclosures for the ceramic domes and the considerable piping required to connect the domes. The small particle and volumetric receivers are very light. In both cases they absorb radiation in a volume, rather than on a surface, making them quite compact, and therefore very light.

TABLE 2.17. Receiver Masses

Design Concept	Receiver Mass (1000 Kg) 1 MWt	50 MWt	300 MWt
Metal Tube (5 atm, 1500°F)	15	467	3003
Ceramic tube (10 atm, 2000°F)	5	163	771
Sodium heat pipe (5 atm, 1500°F)	17	145	1225
Ceramix matrix (1 atm, 2000°F)	4	136	816
Ceramic dome (5 atm, 2000°F)	-	344	2495
Small particle (5 atm, 1500°F)	5	59	-
Volumetric (a atm, 2000°F)	4	109	635

Receiver cross-sectional area (because of wind loading) and tower height have very significant effects on tower cost. Receiver sizes were determined during the conceptual design phase. Tower heights were estimated by the DELSOL computer simulations performed at Sandia. Figure 2.9 depicts the receiver sizes and tower heights for each concept at 50 MWt (and the pressure and temperatures indicated in Table 2.17). Tower heights are strongly dependent on the receiver configuration. The ceramix matrix receiver, with its down-facing aperture required the highest tower. The volumetric receiver, which appears as an external receiver to the field, used a low tower. The size of the receiver is determined by the configuration of the heat transfer surface and the allowable heat flux.

The primary effect of the receiver designs on the field is the amount of heliostat surface required for a given power rating. This is determined by the receiver efficiencies, which will be presented in Section 5. In addition, the amount of land covered by the heliostats is also sometimes of interest. Figure 2.10 gives an idea of the field layouts that would be required for each of the 50-MWt receivers. These field designs, which were predicted by the DELSOL simulation runs, have not been extensively optimized but do provide a rough idea of the relative field requirements. As expected, short towers require spread out fields while receivers with taller towers can use more compact layouts.

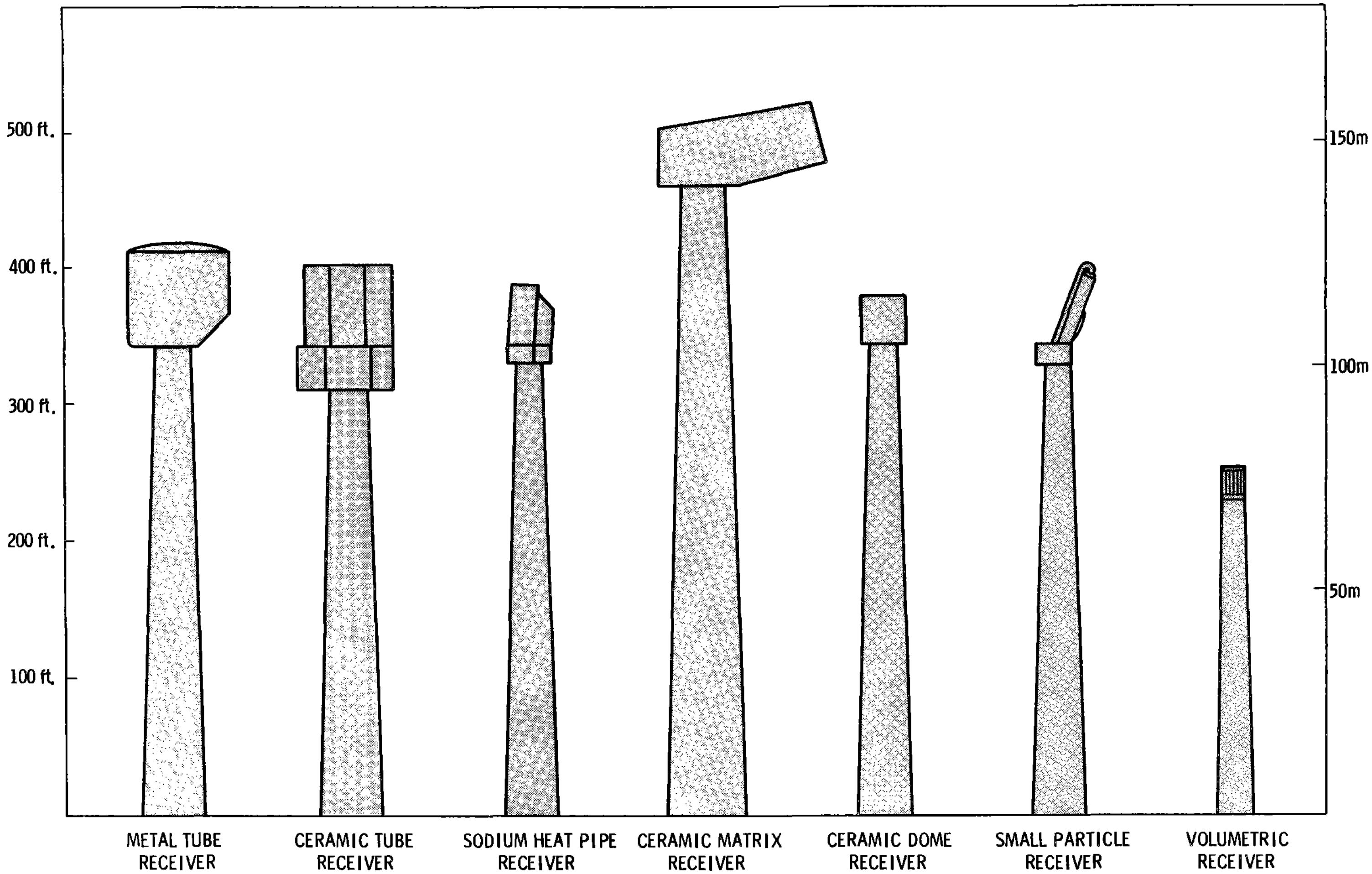

FIGURE 2.9. Comparison of 50-MWt Receiver and Tower Designs

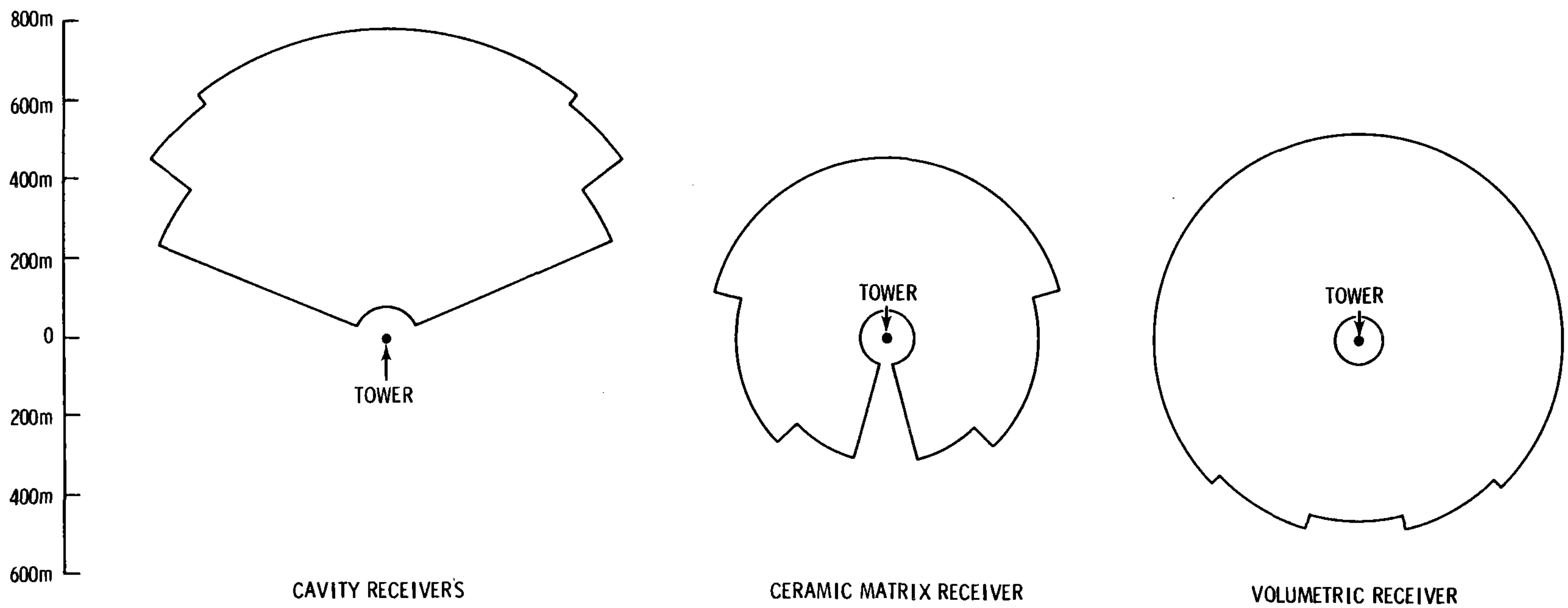

FIGURE 2.10. Comparison of Field Layouts Required for 50-MWt Receivers

3.0 PERFORMANCE ANALYSIS

Each of the receiver designs developed during the conceptual design task was analyzed to assess its performance characteristics. This section discusses the method, ground rules, and models used in the performance evaluation. The results of the performance analysis appear in Section 5.

3.1 METHOD AND GROUND RULES

From a performance standpoint the receiver should produce the desired product with minimum losses. Therefore, the measure of a receiver's performance is receiver efficiency. Receiver losses consist of three components: optical losses associated with spillage and reflection; thermal losses associated with conduction, convection and reradiation; and auxiliary power requirements, which consist of auxiliary power required to overcome the pressure losses associated with moving a fluid through the receiver. In this study, optical and thermal losses will be combined into one efficiency. Auxiliary power will be reported separately because auxiliary power is a high grade energy source such as electricity, and cannot be directly compared to thermal and optical energy losses.

Average annual spillage losses were provided by Sandia Livermore using the DELSOL computer code. Inputs for DELSOL were based on the receiver designs developed at PNL. In the case of the ceramic matrix concept the impact of the secondary concentrator on spillage was not determined by DELSOL. The secondary concentrator was modeled as increasing the capture rate by 10%. DELSOL was not used to optimize receiver aperatures.

Thermal losses were determined by developing a model that described the analytic method for calculating thermal losses. Three thermal loss models were developed because two of the receiver concepts differed sufficiently from the typical cavity design to require a separate model.

Auxiliary power requirements consist of the work necessary to overcome the pressure drop across the receiver. Pressure drops were calculated using standard techniques such as Fanning friction calculations.

In all cases simplified analytical procedures were used, particularly for the thermal analysis. Funding and time constraints limited the depth of the analysis, particularly when 41 designs were considered. In the following sections many of the simplified analytical procedures will be discussed, but the major simplifying assumptions will be discussed here:

- Flux distribution - Flux distributions across the receiver surfaces were not determined. A detailed analysis of flux distribution would have allowed a more accurate calculation of receiver operating temperature in addition to identification of potential hot spots.
- Reflection loss analysis - Reflection losses were calculated by determining view factors for receiver designs that had been reduced to relatively simple geometric shapes. A more accurate view factor analysis, ray tracing, or a Monte Carlo analysis would have provided a more accurate estimate of reflection losses.
- Convective loss analysis - Forced convective losses for the cavity receivers were calculated by modeling the cavity aperature as a flat plate with cross flow.
- Aperature area optimization - The aperature areas of the seven receiver designs were not optimized as part of this study. Where possible, proponent-supplied information was used to pick aperature size. For a given concept, aperature sizes were scaled assuming aperature average energy flux would remain constant. Where proponent-supplied information was not available, other methods were used. The aperature area of the ceramic dome receiver was optimized by trading off thermal losses vs spillage. A similar analysis could not be used on the small particle receiver because the concept required a minimum flux concentration to operate. Any increase in aperature areas above those given in this report result in flux concentrations below the minimum value. This prevented the optimization of the aperature area. The aperature area of the volumetric design was not optimized and the performance of this concept would benefit from an optimization study of aperature. For all concepts, it was found that scaling aperature area based on receiver size from large sizes (300 MWt) to small sizes (MWt) can produce designs with excessive losses.

Although a simplified analysis was used, it was consistently applied to all designs so that results from a detailed analysis are not compared with the results of a less rigorous analysis.

Several ground rules were established as part of the performance analysis. These were used to maintain consistancy during the performance calculation. The ground rules included:

- Ambient temperature was assumed to be 70°F (21°C) for reradiation, conduction, and convection. Sky temperature was assumed to be the same as ambient temperatures.
- Convective losses were calculated for wind speeds ranging from 0 m/s to 10 m/s.
- All absorbing surfaces were assumed to have an emissivity of 0.85. Selective surfaces were not considered.
- All specular reflecting surfaces were assumed to have a reflectivity of 0.9.
- Pressure drops were calculated between the receiver inlet and exit. The risers and downcomers were not included in the pressure drop calculations.

3.2 PERFORMANCE MODELS

In the performance analysis, the receiver designs were separated into three categories with different characteristics, and a model of energy losses and work requirements was developed for each category. Five cavity receiver concepts were in one category. Although the small particle receiver is a cavity receiver, it had a separate energy loss model in a second category because of the cover glass included in the design. The third category contained the volumetric receiver, which also required a separate performance model. The performance models are discussed below. A nomenclature section including definitions of symbols used here appears after the report references.

3.2.1 Cavity Receiver Performance Model

The five cavity receiver concepts have similar geometric configurations and energy loss mechanisms. Therefore, the metal tube receiver, ceramic tube receiver, sodium heat pipe receiver, ceramic matrix receiver, and the ceramic dome receivers were included in one performance model. The loss mechanisms identified for the cavity receiver group are shown in Figure 3.1. The method of calculating losses associated with each loss mechanism is given below.

3.2.1.1 Conduction losses

Conduction losses consist of thermal energy that is lost through the insulated surfaces of the receiver by conduction. This thermal energy is ultimately lost by convection to the environment. Conduction losses were calculated using Equation (3.1), where the numbered subscripts refer to the various components of the insulation system.

$$Q = \frac{A\ (T_W - T_\infty)}{\frac{L_1}{k_1} + \frac{L_2}{k_2} + \frac{L_3}{k_3}} \tag{3.1}$$

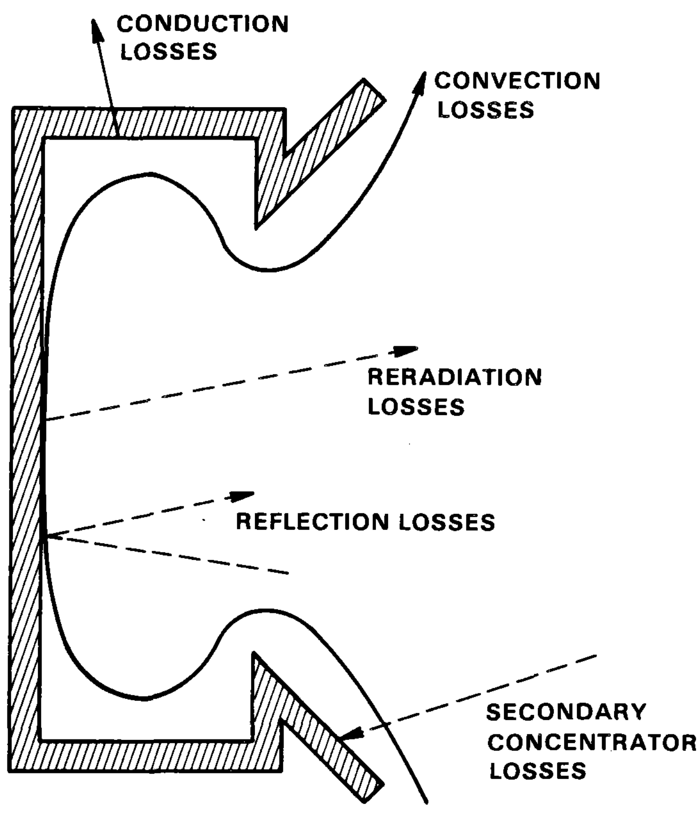

FIGURE 3.1. Cavity Loss Mechanisms

where A = exterior area of receiver (m^2)

T_w = cavity temperature (K)

T_∞ = ambient temperature (K)

L = thickness of insulation (m^2)

k = thermal conductivity (kWt/m•K).

The exterior receiver temperature was assumed to be at ambient air temperature so that all resistance to heat flow was assumed to be caused by the insulating material.

3.2.1.2 Reflective losses

Reflective losses consist of incident radiation from the collector field that is reflected out of the cavity rather than being absorbed on a cavity surface. Reflection losses are given by Equation (3.2).

$$Q_{reflection} = Q_{aperture} \, (1-\varepsilon_{eff}) \qquad (3.2)$$

where $Q_{aperture}$ = energy incident on aperture (kWt)

ε_{eff} = effective emissivity

The $Q_{aperture}$ is the sum of the receiver power rating, and the conduction, convection and reradiation losses. The ε_{eff} is the effective emissivity of the receiver, which includes the effect of material emissivity and the impact of the cavity shape on emissivity. Effective emissivity is calculated by assuming an ambient temperature of 0°K and calculating the radiation losses, Q_R, from the cavity when the cavity is at an assumed temperature of T_w. Effective emissivity is calculated using Equation (3.3).

$$\varepsilon_{eff} = Q_R/\sigma T_w^{\,4} \qquad (3.3)$$

Q_R in Equation (3.3) was calculated assuming a diffuse gray model, which produces a set of simultaneous equations with one equation for each receiver surface and one for the environment. These equations are either solved for surface temperature or energy flux required by the surface to maintain thermal equilibrium. In the second case all surface temperatures were specified and the equations were solved for energy fluxes where the energy flux on the surface representing the environment is Q_R. The solution of the diffuse gray model equations requires knowledge of the various view factors which were calculated for simplified receiver geometries using computer programs available at PNL. σ given in Equation (3.3) is the Stefan Boltzmann constant. Details of the diffuse gray model are given by Seigel and Howell (1972).

3.2.1.3 Reradiation Losses

Reradiation losses consist of energy that is radiated out of the cavity because the cavity is above ambient temperature. Reradiation losses are given by Equation (3.4).

$$Q_{reradiation} = A_a \sigma \varepsilon_{eff} (T_w^4 - T_\infty^4) \tag{3.4}$$

where A_a = aperture area (m^2)

ε_{eff} = effective emissivity.

3.2.1.4 Secondary Concentrator Losses

Secondary concentrator losses consist of energy that is aborbed on a secondary concentrator rather than reflected into the receiver, but detailed optical calculations of secondary concentrator performance were beyond the scope of this study. The impact of the secondary concentrator included in the ceramic matrix design was modeled as increasing the energy flux entering the receiver by 10%.

3.2.1.5 Convection Losses

Convection losses consist of energy that is transferred from the cavity interior walls to the surrounding air by convection. The hot air then exits the cavity through the aperture and is lost to the environment. Convective losses are assumed to consist of two components, natural convection and forced convection. Natural convection was calculated using the simplified convective loss model proposed by Abrams and Greif (1981). Forced convection was calculated assuming that the aperture can be modeled as a flat plate at the cavity temperature. The wind direction was assumed to be parallel to the aperture.

The average Nussett number for flow parellel to a flat plate is given in Equation (3.5), (Gebhart 1971).

$$Nu = 0.037\ (Re)^{.8}\ (Pr)^{1/3} \qquad (3.5)$$

where Reynolds Number is based on aperture width

The combined convective heat transfer coefficient was calculated using $h = \sqrt{h^2_{fc} + h^2_{nc}}$

3.2.1.6 Cavity Temperature

All loss mechanisms depend on the cavity interior wall temperture, which was calculated from information from the design studies. The ceramic matrix receiver was assumed to be at a constant temperature that was calculated as part of the design study. The other four cavity concepts were assumed to have temperatures varying inside the cavity, and temperature profiles for the absorber sections were provided by the design studies. For conduction and convection loss calculations those receivers were assumed to be at one temperature that was the weighted average of the temperature profile. For reradiation a weighted average of the temperatures raised to the fourth power was used.

3.2.2 Small Particle Receiver Performance Model

The small particle receiver is a cavity receiver, but the addition of a cover glass added several new loss mechanisms that required the development of a separate performance model. The loss mechanisms identified for the small particle receiver are shown on Figure 3.2. The method of calculating each loss mechanism is given below.

3.2.2.1 Conduction Losses

The method of calculating conduction losses is described in Section 3.2.1.

3.2.2.2 Reflection Losses

There are two possible sources of reflection losses; the receiver interior and the cover glass. For this study it was assumed that the small particle cloud behaved as a black body with no reflection. The reflection of the cover glass is given by Equation (3.6).

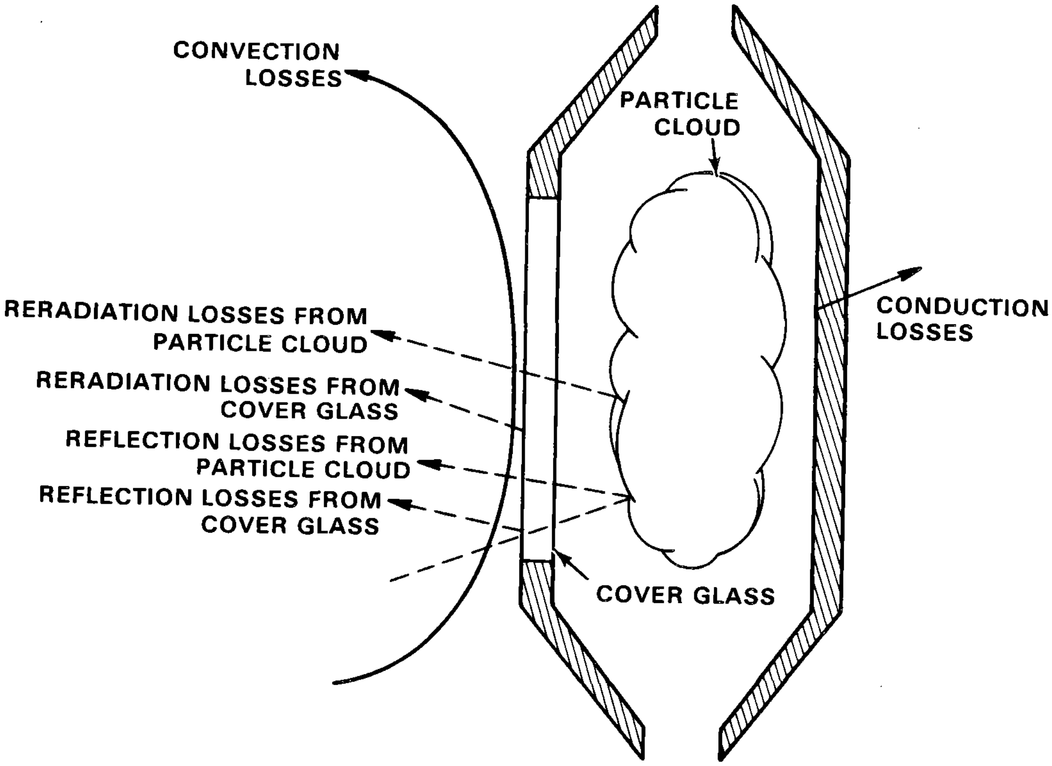

FIGURE 3.2. Small Particle Receiver Loss Mechanisms

$$Q_{reflection} = \int_{0}^{\phi} \rho(\phi)\ Q_{aperture}\ d\phi \qquad (3.6)$$

where $\rho(\phi)$ = reflectivity as a function of incident angle.

In order to simplify the calculations, the concentrator field was divided into zones and one average reflectivity was associated with each zone, so that Equation (3.6) was modeled as

$$Q_{reflection} = \sum_{1}^{n} \rho_n\ Q_{aperture\ n} \qquad (3.7)$$

The reflectivity was determined by contacting vendors of cover glass material and anti-reflection coatings. Vendors indicated that for design points at

2000°F (1093°C) anti-reflection coatings are not feasible. For design points at 1500°F (816°C) and below, anti-reflection coatings can be used. Based on vendor contacts an anti-reflection coating would reduce reflectivity to 0.036 for incident angles less than 45°. For angles greater than 45° the vendor suggested the reflectivity of normal glass should be used. For cases without anti-reflection coating, the reflectivity was calculated using an index of refraction of 1.45332 for the quartz window.

3.2.2.3 Reradiation Losses

There are two possible sources of reradiation losses; the receiver interior and the cover glass. Reradiation from the cover glass was calculated using Equation (3.4) where ϵ_{eff} is the emissivity of the quartz cover glass that was taken from vendor-supplied information. Reradiation from the interior consists of energy that is radiated from the particle cloud and passes through the cover glass rather than being absorbed and is given by Equation (3.8).

$$Q_{reradiation} = A_a \sigma \epsilon_{eff} \tau (T_c^4 - T_\infty^4) \qquad (3.8)$$

where ϵ_{eff} = effective emissivity of particle cloud, which is assumed to be 1.00

τ = transmissivity of cover glass to thermal radiation from a black body at the particle cloud temperture

T_c = temperature of particle cloud

3.2.2.4 Convection Losses

Convection losses were assumed to consist of two components; natural convection and forced convection. Convection losses only occur from the cover glass. The natural convection component is calculated using the Bayley correlation given in Equation (3.9).

$$Nu = 0.10(Gr\ Pr)^{.333} \qquad (3.9)$$

where Gr = Grashof number evaluated at film temperature

Pr = Prandtl number evaluated at film temperature

Nu = Nusselt number based on cover glass height.

Forced convection will be calculated assuming that the cover glass can be modeled as a flat plate at the temperature of the cover glass. Wind direction is assumed to be parallel to the cover glass.

The average Nusselt number for flow parallel to a flat plate is given in Equation (3.10) (Gebhart 1971).

$$Nu = 0.037\ (Re)^{.8}\ (Pr)^{1/3} \tag{3.10}$$

where Reynolds Number is based on cover glass width.

The combined convective heat transfer coefficient was calculated using:

$$h = \sqrt{h_{fc}^2 + h_{nc}^2} \tag{3.11}$$

3.2.2.5 Cover Glass and Cavity Temperature

All loss mechanisms depend on either cover glass temperature or cavity temperature. The cavity temperature is assumed to be the same as product temperature because there is very little temperature difference between the small particles and the product. The cover glass temperature was calculated by conducting a heat balance on the cover glass. The equilibrium cover glass temperature produced cover glass losses that equal the amount of heat being added to the cover glass.

3.2.3 Volumetric Receiver Performance Model

The volumetric receiver absorbs incident radiation on a series of concentric surfaces and draws air past the absorber surfaces with an induced draft fan. While this concept has the same loss mechanisms as the cavity receivers, the methods of calculating receiver temperature and the magnitude of the various loss mechanisms is fundamentally different. The methods for calculating the different receiver losses is described below. The loss mechanisms are shown in Figure 3.3.

3.2.3.1 Conduction Losses

The method of calculating conduction losses is described in Section 3.2.1.

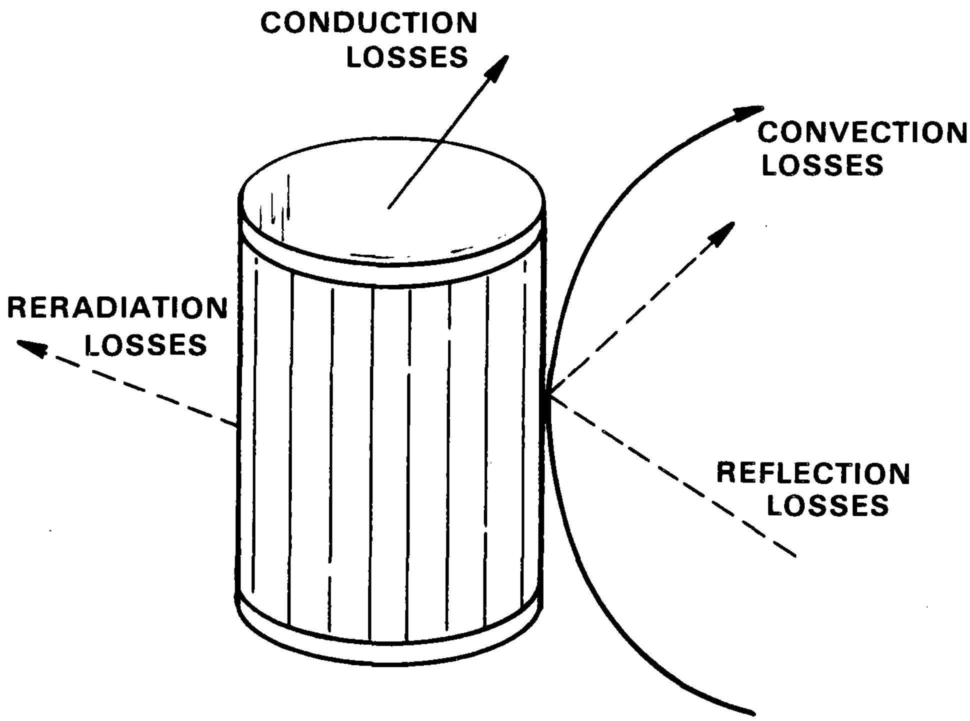

FIGURE 3.3. Volumetric Receiver Loss Mechanisms

3.2.3.2 Reflection Losses

Reflection losses were calculated by assuming that the volumetric receiver could be modeled as a series of concentric cylindrical zones, each with a specified absorptivity, reflectivity, and transmissivity. For two adjacent zones with specified optical properties the following equations were developed (see Figure 3.4).

Energy Absorber on Surface One

$$Q\alpha_1 + \sum_{1}^{\infty} Q(\rho_2)^j(\rho_1')^{j-1}\alpha_1' \tag{3.12}$$

Energy Absorbed on Surface Two

$$Q\tau_1\alpha_2 \sum_{0}^{\infty} (\rho_1')^j(\rho_2)^j \tag{3.13}$$

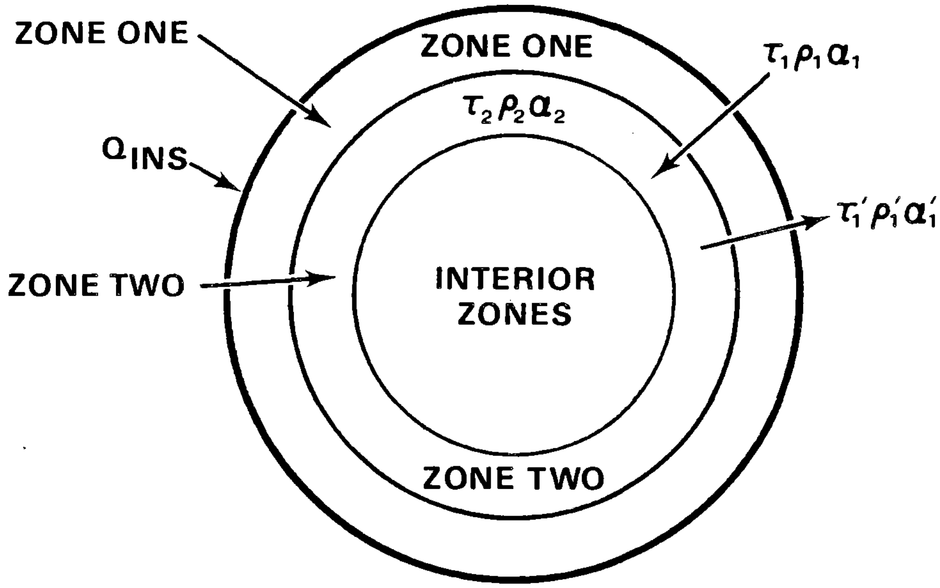

FIGURE 3.4. Receiver Model for Radiation Analysis

Energy Transmitted Through Surface 1 and Surface 2

$$Q\tau_1\tau_2 \sum_1^{\infty} (\rho_1')^j(\rho_2)^j \tag{3.14}$$

Energy Reflected and Lost

$$Q\rho_1 + \sum_1^{\infty} Q\tau_1\tau_1' (\rho_2')^j(\rho_1')^{j-1} \tag{3.15}$$

The reflecting zones are modeled as having one set of optical properties for incoming radiation and a second set for outgoing radiation; therefore, two values for optical properties are included for zone 1. The analysis started with the outermost two zones. The reflectivity and transmissivity for the two zones were calculated using Equations (3.14) and (3.15). The two zones were then modeled as one zone, with the optical properties of the combined two zones. The process was repeated using the next interior zone as the second zone in the analysis. The procedure was repeated until all zones were analyzed. At that point the total reflection losses are given by Equation (3.15) applied to the last interior zone. Equations (3.12) through (3.15) were evaluated by calculating the first four terms of the series. Evaluating additional terms had negligable effect on the results.

The transmissivity of an absorber zone was assumed to be equal to the fraction of the area of a right circular cylinder which consists of pin material. The right circular cylinder is modeled as having a radius equal to the zone radius. Zone absorptivity was given by Equation (3.16).

$$\alpha_n = \varepsilon(1-p_n) \tag{3.16}$$

where ε is material emissivity

p_n is fraction of area consisting of pins for row n.

A preliminary analysis of the reflecting zones indicated that for incoming radiation the transmissivity of the combined reflecting zones would be 0.9, while the transmissivity for outgoing radiation would be 0.167. This effect is due to the geometric arrangement of the wedge-shaped pins in the zones and not to any special surface treatment. The rows of wedge-shaped pins behave as a secondary concentrator because the throat area is smaller than the aperture area between two individual pins.

3.2.3.3 Reradiation Losses

The total receiver reradiation losses are the sum of reradiation losses from each reflecting and absorbing zone. The total receiver reradiation losses are given by Equation (3.17).

$$Q_{reradiation} = \sum_{1}^{n} A \, \sigma \, \varepsilon \, F_{n-\infty} \left(T_n^4 - T_\infty^4\right) \tag{3.17}$$

where n = zone number

A_n = frontal area of zone n

ε_n = emissivity of zone n

$F_{n-\infty}$ = view factor from zone n to the environment

T_n = temperature of zone n.

3.2.3.4 Convection Losses

The receiver was modeled as a right circular cylinder for convective loss calculations. The natural convection component was calculated using the correlation suggested by Clausing for external receivers, which is given in Equation (3.18). For convective loss calculations the cylinder was assumed to be at the temperature of the external reflecting zone.

$$Nu = g\ (Ra)\ f\ (T_w/T_\infty) \tag{3.18}$$

where $f(T_w/T_\infty) = -.303 + 1.604\ (T_w/T_\infty) - .330\ (T_w/T_\infty)^2$

$g(Ra_f) = .10((Gr)(Pr))^{1/3}$

Nu is calculated based on cylinder height

Pr, Gr, and k are calculated at film temperature.

Forced convection is calculated by modeling the receiver as a cylinder in cross flow and using the McAdams correlation. At high wind speeds the McAdams correlation was extrapolated beyond its suggested limits. The McAdams correlation is given in Equation (3.19) (Welty, Wicks, and Wilson 1969).

$$Nu_D = B(Re)^n \tag{3.19}$$

where $B = .0239$

$n = .805$

Nu_D is calculated based on receiver diameter.

Forced and free convection are combined using Equation (3.11).

3.2.3.5 Pin Temperature

Reradiation and convective losses depend on reflecting zone and absorbing zone pin temperature. This was calculated based on the energy absorbed in a given zone, the air zonal inlet and zonal exit temperature, and the heat transfer coefficient between the pins and the air.

The energy absorbed in a given zone can be calculated using Equations (3.12) and (3.13). The air temperatures are calculated by conducting an energy balance on the air. The convective heat transfer coefficient was calculated assuming laminar flow through a tube given by Equation (3.20) (Welty, Wicks, and Wilson 1969).

$$Nu_L = 1.86 \left(Re\ Pr\ \frac{D}{L_n}\right)^{1/3} \left(\frac{\mu_b}{\mu_w}\right)^{.14} \qquad (3.20)$$

where μ_b = viscosity calculated at bulb temperature

μ_w = viscosity calculated at wall temperature

D = hydraulic diameter of flow channel in absorber zone

L_n = depth of absorber zone.

Preliminary calculations indicated that natural convection would also be important and in many cases would exceed forced convection as the primary means of heat transfer between the pins and the air. In order to account for the effect of natural convection the forced convection heat transfer coefficient was corrected using a correction factor suggested by General Electric (1974) and given in Equation (3.21).

$$C_c = 1 + .015 \left[\frac{D^3 \rho^2 g\ \Delta T}{\mu^2\ T}\right]^{.333} \qquad (3.21)$$

where D = diameter (ft)

ρ = density (lbm/ft^2)

g = acceleration due to gravity (ft/sec)

ΔT = temperature difference between the pin and the air (°R)

μ = viscosity of air (lbm/ft/sec)

T = absolute temperature (°R).

3.2.4 Calculation of Receiver Auxiliary Power Requirements

The primary demand for auxiliary power in all receiver designs was the compressor or fan power needed to overcome the pressure drop across the receivers. Other auxiliary power requirements such as power for instruments and control valves were assumed to be negligible.

Pressure drops were calculated for all design points associated with each receiver. The pressure drop across the receiver includes all receiver components from the receiver inlet to the receiver outlet. The risers and downcomers were not included. Pressure drop calculations for the metal tube, ceramic tube, and small particle receivers did not present any unusual problems. Pressure drops were calculated using Fanning friction factors and equivalent lengths for fittings. The pressure drops across the finned tube sections of the heat pipes in the sodium heat pipe design and in the absorber pin array of the volumetric receiver were calculated using correlations from Kays and London (1964). The ceramic matrix design involved estimating the pressure drop across the receiver matrix. Due to the very low Reynolds number in the matrix flow paths, the pressure drop across the matrix was assumed to be negligible. The calculation of the pressure drop in the ceramic dome design was based on correlations developed by the design proponent.

3.2.5 Nighttime Cool Down

Nighttime cool down represents thermal losses that occur when the receiver is not in service, such as during night and other periods of reduced insolation. The receivers will lose heat to the environment that must be replaced before the receiver can be brought into service. It may be possible to replace a fraction of the night losses with early morning insolation where the amount of insolation is insufficient to justify operating the plant but could be used to raise the receiver to operating temperature. Because of the difficulty in determining the fraction of nighttime cool down that is truly a thermal loss, it was decided to report nighttime cool down separately.

Nighttime cool down was considered for several reasons. First, it was speculated that nighttime cool down would be a significant loss. Secondly, it appeared that the impact would not be the same for all designs. In particular, the impact of measures for reducing nighttime cool down could be assessed because the ceramic tube receiver includes a door that covers the aperture and eliminates reradiation and convection losses.

The calculation of nighttime cool down involved several simplifying assumptions. First, the receiver was modeled as having one composite specific heat that was calculated based on the gross material inventory calculated during the cost analysis. Second, heat losses from the receiver were modeled as Newtonian cooling where internal resistance to heat flow is assumed to be negligible. Receiver temperatures were calculated as a function of time for a 12 hour cooling period and an ambient temperature of 70°F (21°C). The receivers were assumed to lose thermal energy by conduction, convection, and reradiation. In the case of the ceramic tube receiver with an aperture door, convection and reradiation were assumed to be eliminated.

Due to the inclusion of radiation heat transfer, the heat balance on the receiver produces a nonlinear, first-order differential equation that was solved numerically.

4.0 COST ANALYSIS

The receiver cost analysis consists of capital cost estimates for each receiver at each of the design points analyzed. The capital costs are total installed costs, which include manufacturing and fabrication costs, transportation costs, field assembly and installation charges, and indirect costs. All costs are reported in mid-year 1981 dollars, and do not include allowances for interest or escalation during construction.

Capital cost estimates given in this report are not intended to replace or substitute for more detailed receiver cost estimates, but rather to allow for reasonable comparisons to be made between the alternative receiver concepts. The uncertainties in the cost estimates in this report can be attributed to two primary sources. First, the estimates are based on conceptual designs, which by necessity contain limited design detail. This factor contributes to the cost estimates uncertainty that would be present in any conceptual design study. Second, many of the concepts use advanced components for which detailed cost and/or fabrication information is not available. This creates uncertainty in the cost data base used. An additional consideration in the interpretation of the cost estimates is that the conceptual designs have not been optimized. Design optimization could result in lower costs for any of the concepts.

4.1 METHOD AND GROUND RULES

The goal of the cost estimating task was to generate comparable cost estimates for all the receiver concepts. To ensure comparability, independent estimates were developed for each concept, rather than simply scaling contractor cost data. By independently estimating capital costs, it was possible to standardize the items included in each receiver cost, the costing methodologies employed, unit costs, and ground rules and assumptions used.

Basically, the method used to estimate receiver costs was to break down each receiver design into a number of components, characterize the type and number of the components for each of the design points, and assess the total installed cost for each of the components using a standardized cost data base. The approach used in characterizing receiver component costs varied somewhat among the different receiver components. For example, the receiver structural costs required a somewhat different estimating approach than the heat exchanger costs. A more detailed description of the approaches used for each receiver cost component is given in Section 4.2.

Ground rules and assumptions used in the cost estimating task were aimed at establishing a reasonable framework within which receiver costs could be compared. In general, the receivers are compared on the basis of future conditions that allow the postulation of advanced manufacturing technologies and reasonably high receiver production rates. This type of comparison effectively compares what ultimate costs each receiver might reach, but does not account for development costs or the likelihood of ever reaching the ultimate cost. It should be pointed out that the receivers in this report are all in different stages of development, and all represent different levels of technological risk. Because these factors are not accounted for in the capital cost estimates, the receiver cost estimates reported herein are not valid for near-term applications. Major assumptions and ground rules are summarized in Table 4.1.

4.2 COST ESTIMATING APPROACH

Receiver capital cost estimates are reported for five cost centers: structural costs, heat exchangers costs, auxiliary costs, installation costs, and indirect costs. The approaches used to estimate costs for each of these cost centers varied depending on the amount of design detail available, the type and quantity of cost information available, and the overall magnitude of the component costs. The approaches used were intended to represent a compromise between too much detail and too little. More detailed costing approaches would not have been commensurate with the level of design, while more general approaches would not have yielded adequately distinguishing estimates. Approaches used to estimate costs for each cost center are described in the following sections.

TABLE 4.1. Receiver Cost Estimating Assumptions and Ground Rules

- All costs are reported in mid-year 1981 price levels.
- Receiver costs are installed costs that include the manufacturer's selling cost, transportion charges, field fabrication and assembly costs, field installation costs, and field indirect costs.
- Receiver cost estimates do not include R&D costs, costs associated with commercializing the solar industry, or contingency costs.
- Receiver costs are reported as "overnight" construction costs. Allowances for escalation and interest during construction are not included.
- Cost estimates assume a commerical, mature solar industry that could be developed within the time frame of the mid 1990's.
- All receiver components specified in designs are assumed to be feasible for commercial manufacturing within the time frame assumed for the study.
- The receiver cost estimates include only components above the tower platform. The only exception to this rule is the particle generator for the small particle receiver, which is included in the cost estimates, although located on the ground.
- A single contractor is assumed to be handle all aspects of receiver installation.

4.2.1 Structural Costs

The receiver structure cost account includes the purchase cost of the materials, the cost of transporting the materials to the construction site, and the cost of field assembly of the receiver structural components. These components include the sheathing material, the shell frame assembly, and the shell insulation. For the small particle receiver, the costs associated with the window are also included.

The receiver structure cost was estimated by aggregating the individual estimates for receiver materials, material transport, and field assembly. The total material cost was determined using a materials take-off approach. With this approach, the quantity of a given material is determined from the conceptual design data, and then the quantity is multiplied by the unit price to obtain the total material cost for that component. Materials transport costs were estimated based on the weight of the material to be shipped to the construction site. Field assembly costs include the costs of construction activities that are likely to take place at ground level. For the 1-MWt receivers, field assembly was assumed to include constructing the entire receiver. For the 50- and 300-MWt receivers, the field assembly tasks would primarily involve materials handling (unloading) and construction of the receiver frame assembly to which the shell material is attached. Most of the construction of receivers at these power levels was assumed to occur at the top of the tower; costs of construction activities at the top of the tower are included in the field installation account.

The metal tube, ceramic matrix, small particle, and volumetric receivers use carbon steel plate as a shell material. The ceramic tube and ceramic dome receivers use aluminum, and the sodium heat pipe design has a carbon steel inner shell and an aluminum outer shell. Carbon steel has the advantage of being cheaper than aluminum, but aluminum is much lighter weight, which is an advantage in the construction process. Current prices for both of these materials were obtained from vendors quotes. Prices reflect the quantity of the material purchased.

For the volumetric receiver, the outer reflecting rows and the downcomer are assumed to act as support for the receiver roof. The roof, in turn, supports the absorbing rows. For this receiver the structure cost was simply estimated from the calculated weight of the reflecting rows and the unit price of the material. For all other receivers, in the absence of more detailed designs, the quantity of structural steel beams needed to support the receiver shell, piping, heat exchange system and insulation, was estimated as a percentage of the total receiver weight. Ratios of beam weight to total receiver weight were derived from design information developed by receiver proponents (Boeing 1980, Foster Wheeler 1978, Weber 1980). Comparison of ratios derived from the various designs indicated that a range of 6 to 10% of total receiver weight was typical for the beam weight of receivers 50 MWt and larger. the typical percentages for receivers smaller than 50 MWt were found to be about twice this range. Midrange values of 8% for 50- and 300-MWt receivers and 16% for 1-MWt receivers were used to estimate beam weight for each design. The estimated beam weight was then multiplied by the unit cost obtained from vendors for steel beams to obtain the capital cost of the structural steel.

At a given product temperature, all the receivers used the same thicknesses of insulation for the shell. Again, a materials take-off approach was used along with unit prices from vendors to estimate the total receiver insulating material cost.

Field assembly costs for all power levels include the cost of material handling for the shell material, structural steel, and the insulation. Also included are the cost of erecting and plumbing, temporary bolting, and riveting the structural steel frame assembly at ground level. In addition, for the 1-MWt design points, the costs of cutting, erecting and plumbing, and temporarily bolting and riveting the shell material to the frame assembly and the costs of installing the shell insulation are also included in the field assembly tasks. Cost estimates for field assembly tasks are based on estimates of the number of man-hours needed to complete the tasks outlined above (Winslow 1972, Page 1976). Man-hour estimates are typically in terms of hours per ton of steel erected, hours per linear foot of weld, or hours per square foot of insulation installed.

The cost of the receiver insulation dominates other structure costs for the metal tube, ceramic tube, ceramic dome, ceramic matrix, and sodium heat pipe concepts (with the exception of the 1000°F (538°C) heat pipe receiver). With the 1000°F (538°C) sodium heat pipe design, the cost of the double shell exceeds the cost of the fiberglass insulation. The dominant structural cost item for the small particle receiver is the cost of the aperture window. The other structural cost components are almost negligible compared to this cost. The structure costs of the volumetric receiver are lower at any given design point than any of the other concepts. This can be attributed to the fact that: 1) the overall dimensions of the receiver are smaller at a given capacity than any of the cavity receivers, 2) the receiver is an external receiver, requiring no air-tight shell, and 3) only the ceiling and floor are insulated resulting in significantly lower insulating costs than for other concepts.

4.2.2 Heat Exchanger Costs

The heat exchanger equipment typically is the single most distinguishing part of a central receiver design and often accounts for the majority of the cost. The heat exchanger category includes the heat-absorbing or air-heating surfaces, any inlet or outlet piping required, plus associated apparatus. Fabrication and pre-assembly are included along with materials in this cost category. Fabrication and pre-assembly include all shop tasks for the heat exchanger plus field tasks that occur at ground level. The lifting and assembly tasks that occur at the top of the tower are included in Field Installation Costs. Inlet and outlet piping is included to the point where riser and downcomer are running parallel in a vertical orientation within the top of the tower.

The heat exchanger costing task began by identifying the components for each concept. These components are listed in Table 4.2. Identification included recording the specific dimensions and material and quantity requirement for each component at each design point. Unit costs were developed for all required materials based on vendor, contractor, cost manual, and PNL data (see discussion of unit cost development in Appendix A). These unit costs were applied to each component to arrive at a materials cost for each design point.

Fabrication and preassembly tasks were identified for each of the design points. For most of the concepts, there are three general operations to consider: shop fabrication of the heat absorbing surfaces, field preassembly of the headers and manifolds, and insulation installation. Shop fabrication was chosen for those tasks that required numerously repeated operations. Field fabrication was chosen for more one-of-a-kind tasks and preassembly operations prior to top-of-the-tower installation. Specific activities include handling and erecting, cutting, drilling, welding, and riveting.

Much of the heat exchanger fabrication begins with pipe and/or plate as the raw materials. Exceptions are complex components such as the sodium heat pipes and most of the silicon carbide products. The small particle concept is distinguished by its lack of a fixed heat absorbing surface. Its particle generator has been included in this cost category, which has little other cost because of the concept's minimal manifolding system.

TABLE 4.2. Receiver Heat Exchanger Components

Design Concept	Heat Exchanger Components
Metal tube	riser manifold, riser connecting pipe, supply pipe, expansion joints, heat exchanger tubes, inlet and outlet headers, return pipes, outlet manifold, downcomer connecting pipe, downcomer manifold, and pipe insulation for all but tubes and headers.
Ceramic tube	U-tubes, compressive springs, supply headers, return headers, riser manifold, downcomer manifold, isolation valve, and insulation for all but U-tubes and compression springs.
Sodium heat pipe	heat pipes, heat pipe panels, inlet panel headers, outlet panel headers, inlet manifold, outlet manifold, expansion joints, downcomer connecting pipe, and insulation for all but the heat pipes.
Ceramic matrix	insulation gasket, clamp, preload spring, stanchion, end clamp, radiation shield, flat absorbing panels, corrugated absorbing panels, inlet header, outlet header, and insulation for both headers.
Ceramic dome	dome, dome enclosure, impingement jet, air plenum, air inlet pipe, air exit pipe, ring manifold, supply headers, return headers, dome connecting pipe, and insulation for all but dome and impingement jet.
Small particle	riser manifold, downcomer manifold, inlet manifold, manifold flow distributor, port flow distributor, carbon particle generator, and insulation for all manifolds.
Volumetric	vertical absorbing pins, horizontal absorbing pins, outlet manifold, and insulation for outlet manifold.

Labor hours were estimated based on several construction man-hour manuals. Fully burdened labor rates were developed based on data in Means (1981b) and other sources for both shop and field activities (see discussion of unit cost development in Appendix A). These labor rates were then applied to the man-hour requirements to give a cost for fabrication and preassembly. The sum of materials, fabrication, and pre-assembly costs equals heat exchanger costs.

4.2.3 Auxiliary Costs

Items in the cost account for receiver auxiliaries included receiver instrumentation, lightning protection, and a light duty crane. Other accessories such as stairways, access platforms, elevators, aircraft warning lighting and access lighting were assumed to be part of the tower cost. Cost information was derived from contractor reports and vendor data. The methodology for determining the cost of auxiliaries for the various concepts is discussed in the following paragraphs.

Limited information was available on instrumentation for all concepts except the metal tube receiver. A contractor's report detailed the requirements for a metal tube receiver used to supply power to a gypsum plant (Boeing 1980). Based on this information, instrumentation requirements were estimated by PNL for the remaining concepts. Because of the long distances from the elevated receivers to the master control room on the ground, hardware and installation expense for the wiring was usually the most important element of instrumentation costs. The number of sensors and the tower height generally increased directly with capacity for a given receiver concept. As a result, capacity had the most dramatic effect on instrumentation costs. The only exceptions are the small particle and volumetric receiver concepts where the number of sensors remains constant for all capacities. The effect of increasing the capacity is lessened because tower height is the only variable influencing cost. In addition, the small particle receiver uses an opacity meter. The opacity meter is a substantial part of the instrumentation cost for this concept. For this reason, at low power ratings instrumentation costs for the small particle receiver are higher than for other concepts. As capacity increases, the instrumentation cost for the small particle receiver compares much more favorably to the other concepts.

Control equipment requirements were estimated by PNL. For the metal tube, sodium heat pipe, ceramic dome, and volumetric concepts, orifice plates control air inlet flow. Control valves are also used for all multicavitied concepts to allow for isolation and shutdown of specific cavities. The ceramic tube receiver used valves to control air inlet flow at all capacities. The only control requirements for the small particle concept is a pressure relief valve. No control items within the scope of this study were required by the ceramic matrix concept. Equipment costs were determined from a contractor's report (Arizona Public Service Co. 1980) and an estimator's manual (Page 1963).

Costs for lightning protection depend primarily on the height of the receiver. Data from Lightning Eliminations Associates, Sante Fe, California, indicate that the installation costs for a complete lightning protection system would vary from $20,000 to $80,000 for tower heights from 60.96 m to 304.8 m. This agrees with published estimates (Boeing 1978; Stearns-Roger 1979). Based on this information, lightning protection costs for the receivers in our study were estimated as follows:

Receiver Specification	Lightning Protection Installed Cost
1 MWt	$15,000
50 MWt	$40,000
300 Mwt	$55,000

The costs for a light-duty service crane (15 ton) is about $150,000 (Black and Veatch 1978). A service crane is included for repair work on the 50-MWt and 300-MWt receivers. For the 1-MWt receivers, a service crane is not necessary unless tower height is excessive.

4.2.4 Field Installation Costs

Field installation costs were defined to include the cost of all construction activities that occur at the top of the tower. For the 1-MWt design points, some of the receiver preassembly tasks at ground level are also included as field installation costs, along with the cost of lifting the preassembled receiver to the top of the tower, securing the structure to the tower, and making the necessary piping connections. Those preassembly tasks included in the field installation account for the 1-MWt receivers are installation of preassembled heat exchanger components and internal receiver piping. For the 50- and 300-MWt receiver design points, field installation involves lifting the frame assembly and securing it to the top of the tower, installing the shell material and the shell insulation, installing the preassembled heat exchanger components and piping, and making the necessary piping connections. Installing the shell covering includes the costs of cutting, erecting and plumbing, temporary bolting, and riveting the plate to the frame assembly. Installing insulation involves tack welding anchoring pins to the inner receiver walls and then applying the specified layers of insulation over these pins.

The type of construction activity required to install heat exchanger components varies widely between receiver concepts. Installation of metal tube and heat pipe heat exchanger panels primarily involves suspending the panels from the receiver support structure and welding the pipe connections. The ceramic tube design will require numerous ceramic-to-metal welds to connect the heat exchanger U-tubes to the inlet and outlet headers. Included as part of the installation of the heat exchanger is the installation of the spring assembly, which keeps each tube in compression. Installation of the ceramic domes in the ceramic dome receiver will involve fastening each dome to the space frame and making numerous pipe welds to connect the flow paths between the domes. For the ceramic matrix design, the matrix support stanchions will first be bolted to the receiver support frame; then matrix installation will simply involve stacking each matrix section in the stanchion assembly. The field installation of the absorbing pins in the volumetric receiver will be done on a modular basis, with modules consisting of sections with six to eight feet arc lengths and heights of six to eight feet. Metal pins will be tack welded to the ceiling of the receiver and ceramic pins can be notched and stacked. The installation of the particle generator for the small particle receiver is expected to be simply a matter of making the necessary pipe connections.

As with field assembly costs, cost estimates for field installation are based on man-hour estimates for particular construction tasks (Winslow 1972; Page 1976). The field installation tasks vary markedly between the receiver designs, and therefore the costs vary as well. A significant portion of the field installation cost can be attributed to the weight of a given component since this directly affects the cost of lifting that component to the top of the receiver. In addition, the power level is a primary driving factor in the lifting costs in that the tower height increases with power level. The height of the tower has a major impact on the set up and operating costs of the crane used to raise the preassembled receiver or the receiver materials to the top of the tower.

Since the heat exchanger components for each concept are preassembled as much as possible at ground level, the cost of field installing this the heat exchanger is reduced. The cost of installing insulation dominates the cost of other field installation tasks for all concepts except the volumetric concept. For the volumetric receiver, installation of the absorbing pins dominates other field installation costs. The overall costs of field installation for the volumetric receiver are significantly lower than those of other concepts at the same design points. This is due to the simplicity of the design and the fact that it does not have the external wall and insulation system required by the cavity receivers.

4.2.5 Indirect Costs

In addition to direct costs for the material and labor used to construct the receiver, a number of indirect costs exist. These costs are necessary for completion of the project but cannot easily be directly charged to any one component of the project. Examples of indirect costs are project engineering and design, contractors fee, and home office overheads. For many projects, indirect costs can make up a substantial fraction of the total project cost.

A number of indirect costs can be closely related to direct labor hours. For the purposes of this report, these costs have been included in the fully burdened labor rate described in Appendix A, and so are not reported with other indirect costs. The indirect costs that have been included in the fully burdened labor rate are contractors home office expense, tools and minor equipment, field office and temporary construction facilities, and contractor's profit.

The costs included in the indirect cost center are engineering and design, field payroll, engineering and management travel and living expenses, and receiver startup. While all of these items have been accounted for in order to be inclusive, the costs associated with engineering and design far outweigh the total of all other items in the indirect cost category.

While contractor reports were reviewed for information on indirect costs, the primary sources used in the developing cost data were from published cost data on indirect costs for conventional construction activities (Peters and Timmerhaus 1968; Guthrie 1974; Hackney 1965; Vatavuk and Neveril 1980).

Indirect costs were estimated as a percentage of the direct capital cost. Because small projects tend to have a greater portion of their total cost composed of indirect costs, the percentages used to estimate indirect costs varied with the direct capital cost for the receiver. The percentages used to calculate indirect costs are shown in Figure 4.1 as a function of the receiver direct capital cost. The trend in the estimating percentage as direct cost varies is similar to that discussed by Hackney (1965).

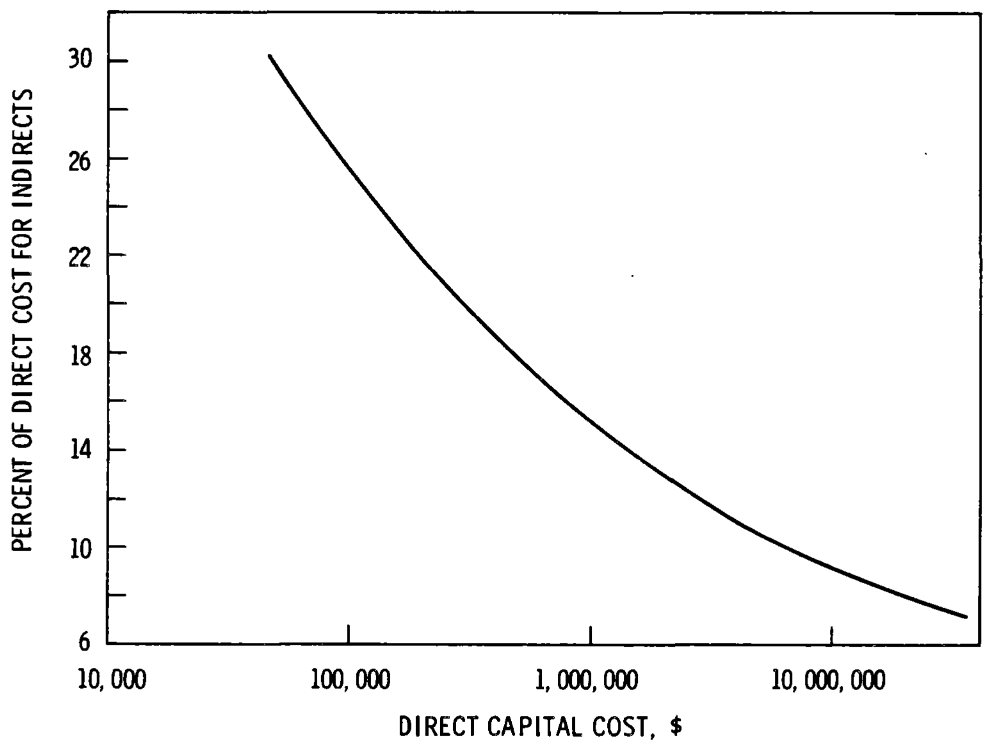

FIGURE 4.1. Indirect Costs

5.0 RESULTS

This section presents the results of the performance (Section 5.1) and cost (Section 5.2) analyses. Some detailed conclusions dealing with these two topics are contained in the following two sections. More general conclusions appear in Section 6.0.

5.1 PERFORMANCE RESULTS

The results of the performance study are presented in the following sections. Each receiver concept is discussed in a separate section, and then all receiver designs are compared in the final section. The performance results are presented on two tables for each receiver concept. The first table presents the components of thermal losses while the second table presents a variety of losses including spillage, auxiliary power, and nighttime cool down. One composite loss including all losses was not calculated because of the difficulty in combining auxiliary power and nighttime cool down with the spillage and thermal losses. Thermal losses were determined for a range of wind speeds, but they proved to be insensitive to increases in wind speed with one exception: the volumetric receiver did show significant increase in thermal loss with increasing wind speed. In order to reduce the amount of data presented in this report, thermal losses are presented at a wind speed of 5 m/s. When % losses are reported, the percentage was calculated by dividing the lost power by the rated output of the receiver.

5.1.1 Metal Tube Receiver

The results of the performance analysis for the metal tube receiver are shown in Tables 5.1 and 5.2. The thermal losses are between 7.5% and 13.8% with reradiation losses being the dominate loss mechanisms. Spillage losses are about 11% with the exception of the 1-MWt design, which had spillage losses of about 36.0%. In the case of the 1-MWt design a large aperture should be considered to reduce spillage (with an accompanying increase in thermal losses). This concept experiences substantial nighttime cool down losses and an aperature door should be considered for use at night to reduce receiver cooling. Because of materials limitations this concept is only suitable for product temperatures below 1500°F (816°C).

TABLE 5.1. Thermal Loss Components for the Metal Tube Receiver

Design Point	Thermal Loss Components and Values					
	Cavity Temperature, K	Reradiation Losses, MWt/%	Conduction Losses, MWt/%	Convection[a] Losses, MWt/%	Reflection Losses, MWt/%	Total Losses, MWt/%
1 MWt, 1500°F, 5 atm	962	.08/8.2	0.01/0.9	.03/3.7	0.01/1.2	.14/14.0
50 MWt, 1000°F, 5 atm	823	1.6/3.2	0.1/0.3	1.5/3.0	0.6/1.1	3.8/7.6
50 MWt, 1500°F, 5 atm	962	3.0/6.1	0.2/0.5	1.8/3.7	0.6/1.2	5.6/11.5
50 MWt, 1500°F, 10 atm	1026	4.0/7.9	0.2/0.4	2.0/4.0	0.6/1.2	6.8/13.5
300 MWt, 1500°F, 5 atm	962	18.3/6.1	1.4/0.5	11.5/3.8	3.4/1.1	34.6/11.5

(a) Based on a wind speed of 5 m/s.

TABLE 5.2. Summary of Loss Components for Metal Tube Receiver

Design Point	Loss Components and Values: Total Thermal Losses, %	Spillage Losses, %	Auxiliary Power, kWe	Nighttime Cool Down, MWt
1 MWt, 1500°F, 5 atm	14.0	36.0	94	0.95
50 MWt, 1000°F, 5 atm	7.6	11.1	697	20.4
50 MWt, 1500°F, 5 atm	11.5	11.1	603	35.4
50 MWt, 1500°F, 10 atm	13.5	11.1	386	34.9
300 MWt, 1500°F, 5 atm	11.5	13.9	4017	215.6

5.1.2 Ceramic Tube Receiver

The results of performance analyses for the ceramic tube receiver are shown in Tables 5.3 and 5.4. Thermal losses for this concept are quite high primarily because of the high cavity temperature. Spillage losses are sufficiently high to prevent decrease in aperture area as a remedy for the high thermal losses. The spillage losses are particularly high for the 1-MWt case because of the small aperture associated with the small power rating. Without the addition of an aperture door this concept experiences substantial nighttime cool down. The inclusion of a door effectively eliminates the problem.

5.1.3 Sodium Heat Pipe Receiver

The results of the performance analysis for the sodium heat pipe receiver are shown in Tables 5.5 and 5.6. The thermal losses for this concept are relatively low, primarily because of the low cavity temperature. The heat pipe design is an effective method of heating the product with a very small temperature difference between the product and the wall. This reduced temperature difference results in a lower wall temperature when compared to designs with less effective heat transfer. The spillage losses are higher than the metal tube design, and some increase in aperture area may be justified because spillage losses are greater than total thermal losses. This concept experiences substantial nighttime cool down that may justify the addition of an aperture door. While nighttime cool down losses are substantial this concept has lower nighttime losses then other cavity designs. The reduction in night time cool

TABLE 5.3. Thermal Loss Components for Ceramic Tube Receiver

Design Point	Thermal Loss Components and Values					
	Cavity Temperature, K	Reradiation Losses, MWt/%	Conduction Losses, MWt/%	Convection[(a)] Losses, MWt/%	Reflection Losses, MWt/%	Total Losses, MWt/%
1 MWt, 2000°F, 10 atm	1276	0.268/26.8	0.002/0.2	0.42/4.2	0.011/1.1	0.337/33.7
50 MWt, 2000°F, 10 atm	1276	5.4/18.5	0.2/0.6	1.1/3.7	0.3/1.1	7.0/23.9
300 MWt, 1500°F, 10 atm	1137	33.2/11.0	1.2/0.4	9.7/3.2	2.9/1.0	47.0/15.6
300 MWt, 2000°F, 5 atm	1211	43.3/14.5	1.6/0.5	10.3/3.5	3.0/1.0	58.2/19.5
300 MWt, 2000°F, 10 atm	1276	54.5/18.2	1.7/0.6	11.1/3.7	3.1/1.0	70.4/23.5

(a) Based on a wind speed of 5 m/s.

TABLE 5.4. Summary of Loss Components for Ceramic Tube Receiver

Design Point	Loss Components and Values: Total Thermal Losses, %	Spillage Losses, %	Auxiliary Power, (kWe)	Nighttime Cool Down, (MWt)
1 MWt, 2000°F, 10 atm	33.7	32.1	2	1.0
50 MWt, 2000°F, 10 atm	23.9	14.9	208	33.4
300 MWt, 1500°F, 10 atm	15.6	16.5	2129	126.0
300 MWt, 2000°F, 5 atm	19.5	16.5	1255	98.7
300 MWt, 2000°F, 10 atm	23.5	16.5	1406	164.0

down losses is caused by the reduced mass of the sodium heat pipe receiver, which cools relatively quickly while other designs stay at elevated temperatures longer with the resulting increased losses. Because of materials limitations this concept is only suitable for product temperatures below 1500°F.

5.1.4 Ceramic Matrix Receiver

The results of the performance analysis of the ceramic matrix receiver are shown in Tables 5.7 and 5.8. Thermal losses are very low for the 300-MWt receiver. The low level of losses is caused by the small aperture area of the concept. The lower-power-rating receivers have more severe losses because of relatively larger apertures. The side effect of a small aperture is very large spillage losses at all sizes. In order to reduce the spillage losses associated with a small aperture the design includes a secondary concentrator, but the secondary concentrator is reported by the proponent to increase capture rate by 10%.

5.1.5 Ceramic Dome Receiver

The results of the performance analysis for the ceramic dome receiver are shown in Tables 5.9 and 5.10. This concept experienced both high spillage losses and high thermal losses. The original concept as described by the proponent has a very large temperature difference between the receiver and the air; coupled with the good heat transfer characteristics of impingement heat transfer, thus means that the area of absorbing surfaces can be small, allowing a compact design. This creates a problem with spillage, however, because an

TABLE 5.5. Thermal Loss Components for the Sodium Heat Pipe Receiver

Design Point	Thermal Loss Components and Values					
	Cavity Temperature, K	Reradiation Losses, MWt/%	Conduction Losses, MWt/%	Convection[(a)] Losses, MWt/%	Reflection Losses, MWt/%	Total Losses, MWt/%
1 MWt, 1500°F, 5 atm	870	0.125/125	0.005/.5	0.066/6.6	.038/3.8	.234/23.4
50 MWt, 1000°F, 5 atm	732	0.8/1.6	>0.1/.1	0.8/1.6	1.7/3.3	3.3/6.6
50 MWt, 1500°F, 1 atm	764	1.0/1.9	>0.1/.1	0.9/1.8	1.7/3.3	3.6/7.1
50 MWt, 1500°F, 5 atm	870	1.6/3.2	>0.1/.1	1.1/2.1	1.7/3.4	4.4/8.8
50 MWt, 1500°F, 10 atm	934	2.7/5.4	>0.1/.1	1.1/2.3	1.8/3.5	5.6/11.3
300 MWt, 1500°F, 5 atm	870	8.9/3.0	0.2/.1	6.1/2.0	10.2/3.4	25.4/8.5

(a) Based on a wind speed of 5 m/s.

TABLE 5.6. Summary of Loss Components for the Sodium Heat Pipe Receiver

Design Point	Loss Components and Values: Total Thermal Losses, %	Spillage Losses, %	Auxiliary Power, (kWe)	Nighttime Cool Down, (MWt)
1 MWt, 1500°F, 5 atm	23.4	12.7	0.8	0.9
50 MWt, 1000°F, 5 atm	6.6	14.4	168	8.7
50 MWt, 1500°F, 1 atm	7.1	14.4	1104	10.7
50 MWt, 1500°F, 5 atm	8.8	14.4	284	12.7
50 MWt, 1500°F, 10 atm	11.3	14.4	52	14.5
300 MWt, 1500°F, 5 atm	8.5	16.5	1704	34.9

aperture properly sized for the small absorbing surfaces is also quite small and produces unacceptable spillage. Increasing aperture size produces excessive thermal losses due to the high wall temperature. The aperture size picked in this study is the result of an optimization where thermal losses were traded-off against and spillage losses. The result produce spillage and thermal losses that are both quite high. It appears that either this concept must be redesigned with a lower temperature difference between the ceramic dome and the product (requiring a larger receiver) or a secondary concentrator must be included. Nighttime cool down is relatively severe, so an aperture door is probably justified.

5.1.6 Small Particle Receiver

The results of the performance analysis for the small particle receiver are shown in Tables 5.11 and 5.12. The thermal losses from this concept are small for the 50-MWt receivers. The normally dominant components of thermal losses, reradiation, and convection are very small. This is caused by the the inclusion of the cover glass in the design, but the increased reflection losses associated with the cover glass tend to offset the reduction in the other components of thermal losses. The major problem with this design is the excessive spillage losses for the 50-MWt design. Unlike other cavity designs the aperture area cannot be increased above the area specified in the 50-MWt design

TABLE 5.7. Thermal Loss Components for the Ceramic Matrix Receiver

Design Point	Thermal Loss Components and Values					
	Cavity Temperature, K	Reradiation Losses, MWt/%	Conduction Losses, MWt/%	Convection[a] Losses, MWt/%	Reflection Losses, MWt/%	Total Losses, MWt/%
1 MWt, 2000°F, 1 atm	1478	.299/29.9	0.001/0.1	0.028/2.8	0.03/3.0	0.358/35.8
50 MWt, 2000°F, 1 atm	1478	11.6/23.3	0.1/0.1	1.4/2.8	1.5/3.0	14.6/29.2
300 MWt, 1000°F, 1 atm	867	2.9/1.1	0.1/0.0	2.5/0.8	7.3/2.4	12.8/4.3
300 MWt, 1500°F, 1 atm	1172	11.8/3.9	0.1/0.1	3.3/1.1	7.6/2.5	22.8/7.6
300 MWt, 2000°F, 1 atm	1478	29.9/9.9	0.2/0.1	3.7/1.2	8.0/2.7	41.8/13.9

(a) Based on a wind speed of 5 m/s.

TABLE 5.8. Summary of Loss Components for the Ceramic Matrix Receiver

	Loss Components and Values			
Design Point	Total Thermal Losses, %	Spillage Losses, %	Auxiliary Power, (kWe)	Nighttime Cool Down, (MWt)
1 MWt, 2000°F, 1 atm	35.8	81.5	5	.4
50 MWt, 2000°F, 1 atm	29.2	32.8	170	16.1
300 MWt, 1000°F, 1 atm	3.6	22.4	1147	40.7
300 MWt, 1500°F, 1 atm	7.6	22.4	977	60.0
300 MWt, 2000°F, 1 atm	13.9	22.4	895	74.0

because fabrication techniques limit cover glass size. With the excessive spillage losses for the concept it appears that an effective secondary concentrator must be included in the design.

5.1.7 Volumetric Receiver

The results of the performance analysis for the volumetric receiver are shown in Tables 5.13 and 5.14. The thermal losses for this concept are very low. The primary cause of the reduced thermal losses is that the surfaces on the exterior of the receiver are the coolest in the receiver, while the high-temperature surfaces are deep in the receiver with little opportunity to lose thermal energy to the environment. An additional cause of the very low reradiation losses is that the the external surfaces are reflecting surfaces with a low emissivity. The aperture area of the design is also smaller then most other concepts. The combined effect is to produce thermal losses far below other concepts. Unlike other designs, the convective losses are relatively sensitive to wind speed. The results in Table 5.13 are for a wind speed of 5 m/s (16.56 ft/s).

Spillage losses are relatively high, but this design has not been optimized, and a substantial increase in receiver size can be expected to produce a relatively small increase in thermal losses. By increasing receiver diameter, spillage can be reduced without a large increase in thermal losses. Any additional design studies on this concept should include the tradeoffs study between combined losses and receiver area.

TABLE 5.9. Thermal Loss Components for the Ceramic Dome Receiver

Design Point	Thermal Loss Components and Values					
	Cavity Temperature, K	Reradiation Losses, MWt/%	Conduction Losses, MWt/%	Convection[a] Losses, MWt/%	Reflection Losses, MWt/%	Total Losses, MWt/%
50 MWt, 1000°F, 5 atm	1100	4.5/9.1	0.1/0.1	1.2/2.4	1.4/2.8	7.2/14.4
50 MWt, 1500°F, 5 atm	1212	6.5/13.0	0.1/0.2	1.3/2.6	1.4/2.9	9.3/18.7
50 MWt, 2000°F, 1 atm	1405	11.6/23.2	0.2/0.4	1.4/2.8	1.6/3.2	14.8/29.6
50 MWt, 2000°F, 5 atm	1403	11.2/22.6	0.1/0.2	1.4/2.8	1.6/3.2	14.3/28.8
50 MWt, 2000°F, 10 atm	1463	12.9/25.8	0.1/0.2	1.5/2.9	1.6/3.2	16.1/32.1
300 MWt, 2000°F, 5 atm	1403	67.7/22.6	0.7/0.2	8.6/2.9	9.4/3.1	86.4/28.8

(a) Based on a wind speed of 5 m/s.

TABLE 5.10. Summary of Loss Components for the Ceramic Dome Receiver

Design Point	Loss Components and Values: Total Thermal Losses, %	Spillage Losses, %	Auxiliary Power, (kWe)	Nighttime Cool Down, (MWt)
50 MWt, 1000°F, 5 atm	14.4	22.5	723	31.3
50 MWt, 1500°F, 5 atm	18.7	22.5	465	33.7
50 MWt, 2000°F, 1 atm	29.6	22.5	120	69.1
50 MWt, 2000°F, 5 atm	28.8	22.5	205	78.0
50 MWt, 2000°F, 10 atm	32.1	22.5	248	54.2
300 MWt, 2000°F, 5 atm	28.8	23.1	1379	335.7

Although this concept would benefit from some method to reduce nighttime cool down, the losses are not particularly severe.

5.1.8 Aperture Area Optimization and Spillage

As discussed in Section 3.1, time and funding constraints prohibited the optimization of aperture area, particularly because 41 separate designs were being considered. Where possible, proponent data was used, and aperture areas were scaled by maintaining a constant average aperature energy flux. where proponent data was not available, other methods were used to select aperture size.

Vendor information was available for the metal tube, ceramic tube, sodium heat pipe, and ceramic matrix designs. The ceramic dome concept aperture area was chosen by trading off thermal losses against spillage. The small particle receiver aperture area was determined by the energy flux concentration required to vaporize the small particles. This set a maximum size on the aperture. Table 5.12 shows that the performance of this concept would improve if a larger aperture was used, but the designs developed for this study already use the largest allowable aperture area. The aperture area of the volumetric concept was chosen without the benefit of any previous optimization study.

Optimization of aperture size would result in lower spillage and thermal losses. The aperture sizing for the metal tube, ceramic tube, sodium heat pipe, and ceramic matrix designs was based on vendor information. Although

TABLE 5.11. Thermal Loss Components for the Small Particle Receiver

	Thermal Loss Components and Values						
Design Point	Cavity Temperature, K	Interior Reradiation Losses, MWt/%	Cover Reradiation Losses, MWt/%	Conduction Losses, MWt/%	Convection[a] Losses, MWt/%	Reflection Losses, MWt/%	Total Losses, MWt/%
1 MWt, 1500°F, 5 atm	1021	.026/2.6	.111/11.1	.03/.3	.029/2.9	.19/5.6	.225/22.5
50 MWt, 1000°F, 5 atm	875	0.1/0.1	0.8/1.5	>0.1/0.1	0.2/0.4	3.3/6.6	12.4/8.7
50 MWt, 1500°F, 1 atm	1022	0.2/0.4	1.5/3.0	>0.1/0.1	0.2/0.5	3.4/6.6	5.3/10.6
50 MWt, 1500°F, 5 atm	1203	0.2/0.4	1.5/3.0	>0.1/0.1	0.2/0.4	3.3/6.6	5.2/10.5
50 MWt, 1500°F, 10 atm	1022	0.2/0.4	1.5/3.0	>0.1/0.1	0.2/0.4	3.3/6.6	5.2/10.5
50 MWt, 2000°F, 5 atm	928	1.4/2.9	2.6/5.2	>0.1/0.1	0.3/1.6	4.5/9.1	8.8/17.9

(a) Based on a wind speed of 5 m/s.

TABLE 5.12. Summary of Loss Components for the Small Particle Receiver

Design Point	Loss Components and Values: Total Thermal Losses, %	Spillage Losses, %	Auxiliary Power, (kWe)	Nighttime Cool Down, (MWt)
1 MWt, 1500°F, 5 atm	22.5	12.0	3	5.4
50 MWt, 1000°F, 5 atm	8.7	34.8	189	4.3
50 MWt, 1500°F, 1 atm	10.6	34.8	69	6.3
50 MWt, 1500°F, 5 atm	10.5	34.8	83	6.3
50 MWt, 1500°F, 10 atm	10.5	34.8	135	6.6
50 MWt, 2000°F, 5 atm	17.9	34.8	63	9.1

scaling vendor-optimized aperture areas may have produced nonoptimum aperture areas, in general, these concepts should have aperture areas approaching the optimum. The ceramic dome receiver was optimized by calculating the combined thermal losses and spillage, and an aperture area was chosen to minimize the combined losses. The small particle receiver aperture could not be optimized because the area was determined by the required flux concentration. The volumetric receiver was not optimized and would benefit from aperture optimization, particularly because the spillage losses were at least four times greater than thermal losses.

The spillage losses reported in this study are average annual spillage and care must be taken in comparing these results with other published results which may be based on one design point. Average annual spillage exceeds 10% for most concepts, the impact of spillage on receiver structural members was beyond the scope of this study, but receiver designs will have to include provisions to prevent damage caused by the radiation flux associated with spillage.

A comparison of all concepts is shown in Table 5.15. The comparison is based on the sum of total thermal losses and spillage losses.

5.1.9 General Comments

Based on the results of the performance analysis the following conclusions can be drawn.

TABLE 5.13. Thermal Loss Components for the Volumetric Receiver

Design Point	Reradiation Losses, MWt/%	Conduction Losses, MWt/%	Convection[a] Losses, MWt/%	Reflection Losses, MWt/%	Total Losses, MWt/%
	Thermal Loss Components and Values				
1 MWt, 2000°F, 1 atm	.023/2.3	0.001/0.1	0.011/1.1	0.012/1.2	0.046/4.6
50 MWt, 2000°F, 1 atm	0.5/0.9	>0.1/0.1	0.2/0.5	0.6/1.2	1.3/2.7
300 MWt, 1000°F, 1 atm	0.4/0.1	>0.1/0.0	0.8/0.3	3.4/1.2	4.7/1.6
300 MWt, 1500°F, 1 atm	0.8/0.3	>0.1/0.0	0.9/0.3	3.4/1.1	5.2/1.7
300 MWt, 2000°F, 1 atm	1.5/0.5	>0.1/0.0	1.1/0.4	3.5/1.2	6.1/2.1

(a) Based on a wind speed of 16.56 ft/s (5 m/s).

TABLE 5.14. Summary of Loss Components for Volumetric Receiver

Design Point	Total Thermal Losses, %	Spillage Losses, %	Auxiliary Power, kWe	Nighttime Cool Down, MWt
1 MWt, 2000°F, 1 atm	4.6	19.3	0.5	0.2
50 MWt, 2000°F, 1 atm	2.7	16.1	131	4.2
300 MWt, 1000°F, 1 atm	1.6	18.8	2232	8.3
300 MWt, 1500°F, 1 atm	1.7	18.8	1883	13.3
300 MWt, 2000°F, 1 atm	2.1	18.8	1715	19.9

- Reradiation is the dominate thermal loss mechanism for all concepts except for the small particle receiver, which includes a cover glass.
- The 1-MWt receivers experience high thermal losses because of the large aperture area relative to the cavity area required to avoid excessive spillage losses. To some extent this was caused by scaling large designs (50 to 300 MWt) down to the 1-MWt power level while trying to maintain approximate geometric similarity. In addition, in order to calculate spillage, collector field characteristics such as heliostat size and arrangement were assumed. These characteristics have a major impact on receiver spillage, but because optimization of these factors was clearly beyond the scope of the study, they were not analyzed in detail. An optimized design at the 1-MWt power level may have substantially improved performance.
- All cavity concepts would benefit from the inclusion of an aperture door to reduce nighttime cool down.
- The areas of greatest uncertainty in this analysis are associated with the calculation of natural and forced convection losses from all receivers, secondary concentrator losses from the ceramic matrix receiver, and reradiation from the volumetric concept. In all cases the calculation of cavity operating temperatures would benefit from a more refined analysis. This is particularly true of the volumetric design where the calculation of zone temperatures depended on a series of assumptions.

TABLE 5.15. Comparison of Concepts Based on Thermal Losses and Spillage

	Losses for the Seven Design Concepts, %						
1 MWt	Metal Tube Receiver	Ceramic Tube Receiver	Sodium Heat Pipe Receiver	Ceramic Matrix Receiver	Ceramic Dome Receiver	Small Particle Receiver	Volumetric Receiver
1000°F, 1 atm							
1000°F, 5 atm							
1000°F, 10 atm							
1500°F, 1 atm							
1500°F, 5 atm	39.8		35.3			32.8	
1500°F, 10 atm							
2000°F, 1 atm				117.3			23.9
2000°F, 5 atm							
2000°F, 10 atm		65.2					
50 MWt							
1000°F, 1 atm							
1000°F, 5 atm	18.6		21.0		36.8	43.4	
1000°F, 10 atm							
1500°F, 1 atm			21.6			45.3	
1500°F, 5 atm	22.5		23.2		41.1	45.3	
1500°F, 10 atm	24.5		25.6			45.3	
2000°F, 1 atm				62.0	51.9		18.8
2000°F, 5 atm					51.5	52.2	
2000°F, 10 atm		38.6			54.5		
300 MWt							
1000°F, 1 atm				26.0			20.4
1000°F, 5 atm							
1000°F, 10 atm							
1500°F, 1 atm				30.0			20.5
1500°F, 5 atm	25.4		24.9				
1500°F, 10 atm		32.0					
2000°F, 1 atm				36.3			20.9
2000°F, 5 atm		35.9					
2000°F, 10 atm		35.8			51.8		

- The volumetric receiver concept has the lowest thermal losses and the lowest combined spillage and thermal losses for a given temperature range.
- The ceramic dome receiver and the small particle receiver have excessive spillage losses and should include secondary concentrators.
- In general, higher product pressure resulted in higher thermal losses because the inlet temperature increases with product pressure. This results in a higher average cavity temperature, which increases thermal losses.

5.2 COST RESULTS

This section reports the costs that were estimated for each receiver concept according to the methodologies described in Section 4.2. Total receiver costs for each concept are tabulated in Table 5.16 by design point to allow cost comparisons between those concepts that were evaluated at similar design points. Some general cost trends have been derived from the overall receiver cost data. These include:

1. The total receiver cost increases with power level for any given product temperature and pressure.
2. All receiver concepts, with the exception of the sodium heat pipe receiver, show economies of scale with respect to power level.
3. The overall cost of the metal tube receiver, the ceramic dome receiver, and the small particle receiver decrease with increasing pressure at a given temperature and power level.
4. The ceramic tube and the sodium heat pipe receiver overall costs increase with increasing pressure at a given temperature and power level.
5. The effect of increasing the temperature is to increase the overall cost of all the concepts with the exception of the sodium heat pipe, the ceramic dome, and the small particle receiver.

The underlying causes of each of these trends will be discussed more fully in subsequent sections.

TABLE 5.16. Summary of Receiver Costs

	Total Receiver Costs, $1000						
1 MWt	Metal Tube Receiver	Ceramic Tube Receiver	Sodium Heat Pipe Receiver	Ceramic Matrix Receiver	Ceramic Dome Receiver	Small Particle Receiver	Volumetric Receiver
1000°F, 1 atm							
1000°F, 5 atm							
1000°F, 10 atm							
1500°F, 1 atm							
1500°F, 5 atm	208		453			394	
1500°F, 10 atm							
2000°F, 1 atm				105			333
2000°F, 5 atm							
2000°F, 10 atm		315					
50 MWt							
1000°F, 1 atm							
1000°F, 5 atm	1,643		12,225		1,776	2,939	
1000°F, 10 atm							
1500°F, 1 atm			8,261			3,197	
1500°F, 5 atm	3,860		9,829		1,711	2,911	
1500°F, 10 atm	3,419		11,882			2,861	
2000°F, 1 atm				2,297	3,286		7,127
2000°F, 5 atm					2,164	2,922	
2000°F, 10 atm		4,064			2,148		
300 MWt							
1000°F, 1 atm				5,464			6,373
1000°F, 5 atm							
1000°F, 10 atm							
1500°F, 1 atm				8,337			10,876
1500°F, 5 atm	21,935		67,921				
1500°F, 10 atm		17,198					
2000°F, 1 atm				10,516			22,922
2000°F, 5 atm		20,713			12,284		
2000°F, 10 atm		21,132					

Tables 5.17 through 5.23 report the component costs by concept for each design point at which that concept was evaluated. The total installed cost of the receiver is shown first in the tables. This total cost is then disaggregated into the following accounts: Receiver Structure, Heat Exchangers, Auxiliaries, Field Installation and Indirect Costs. With the exception of the small particle receiver, the cost of the heat exchanger subsystem dominates the cost of other subsystems. For this receiver, the cost of the structure is dominant primarily because of the high cost of the aperture window. Trends and significant cost features of each of the receiver cost accounts will be discussed in the following sections.

5.2.1 Structural Costs Results

The structural cost account includes the cost of receiver sheathing materials, the receiver support frame, and the insulation. The cost of the insulation is the dominant cost component for all receiver concepts except for the small particle receiver and the volumetric receiver. The dominant cost in the case of the small particle receiver is the cost of the fused silica for the aperture window. The cost of the window is two orders of magnitude higher than the next highest cost component of the small particle receiver structure account. The amount of insulation used in the volumetric receiver is comparatively smaller because it does not have the insulated cavity walls characteristic of the other receivers. For this receiver, the cost of the insulation is less significant than the cost of the structural supports.

In general, structure costs show economies of scale with respect to power level. Only the ceramic dome receiver and the ceramic matrix receiver show slight diseconomies of scale at 300 MWt with respect to the 50-MWt designs at the same pressures and temperatures. It is likely that these slight diseconomies are the result of compounding rounding errors in estimating receiver weights and structure costs. That is, it appears likely that there is no true diseconomy for these designs.

The volumetric receiver and the ceramic matrix receiver show the lowest structural costs at each power level. These receivers are both smaller than the other receiver concepts at a given receiver size. Fewer materials are

TABLE 5.17. Metal Tube Receiver Costs

Design Point	Summary of Cost Components ($1000)					
	Total Cost	Structural Cost	Heat Exchanger Cost	Auxiliary Cost	Installation Cost	Indirect Cost
1 MWt, 1500°F, 5 atm	208	24	102	30	14	38
50 MWt, 1500°F, 5 atm	3,860	436	2,429	321	274	400
50 MWt, 1500°F, 10 atm	3,419	316	2,186	341	213	363
50 MWt, 1000°F, 5 atm	1,643	128	901	281	131	202
300 MWt, 1500°F, 5 atm	21,615	2,615	14,595	1,615	1,523	1,587

TABLE 5.18. Ceramic Tube Receiver Costs

Design Point	Summary of Cost Components ($1000)					
	Total Cost	Structural Cost	Heat Exchanger Cost	Auxiliary Cost	Installation Cost	Indirect Cost
1 MWt, 2000°F, 10 atm	315	25	184	22	30	54
50 MWt, 2000°F, 10 atm	4,064	352	2,783	256	256	417
300 MWt, 2000°F, 10 atm	21,132	2,308	15,423	592	1,268	1,541
300 MWt, 1500°F, 10 atm	17,198	1,614	12,540	652	1,083	1,309
300 MWt, 2000°F, 5 atm	20,713	2,466	14,799	652	1,279	1,517

TABLE 5.19. Sodium Heat Pipe Receiver Costs

Design Point	Summary of Cost Components ($1000)					
	Total Cost	Structural Cost	Heat Exchanger Cost	Auxiliary Cost	Installation Cost	Indirect Cost
1 MWt, 1500°F, 5 atm	453	32	314	22	13	72
50 MWt, 1500°F, 5 atm	9,829	131	8,440	301	117	840
50 MWt, 1500°F, 10 atm	11,882	130	10,367	293	115	977
50 MWt, 1500°F, 1 atm	8,261	134	6,958	301	136	732
50 MWt, 1000°F, 5 atm	12,225	84	10,732	301	109	999
300 MWt, 1500°F, 5 atm	67,921	768	61,423	1,183	674	3,873

TABLE 5.20. Ceramic Matrix Receiver Costs

Design Point	Summary of Cost Components ($1000)					
	Total Cost	Structural Cost	Heat Exchanger Cost	Auxiliary Cost	Installation Cost	Indirect Cost
1 MWt, 2000°F, 1 atm	105	10	41	19	13	22
50 MWt, 2000°F, 1 atm	2,297	163	1,529	240	101	264
300 MWt, 2000°F, 1 atm	10,516	1,133	7,474	478	544	887
300 MWt, 1500°F, 1 atm	8,337	839	5,725	478	557	738
300 MWt, 1000°F, 1 atm	5,464	458	3,579	478	422	527

TABLE 5.21. Ceramic Dome Receiver Costs

	Summary of Cost Components ($1000)					
Design Point	Total Cost	Structural Cost	Heat Exchanger Cost	Auxiliary Cost	Installation Cost	Indirect Cost
50 MWt, 2000°F, 10 atm	2,148	460	926	270	241	151
50 MWt, 2000°F, 5 atm	2,164	461	923	280	248	252
50 MWt, 2000°F, 1 atm	3,286	870	1,263	350	451	352
50 MWt, 1500°F, 5 atm	1,711	280	752	290	180	209
50 MWt, 1000°F, 5 atm	1,776	260	784	350	167	215
300 MWt, 2000°F, 5 atm	12,284	3,392	5,341	905	1,643	1,003

TABLE 5.22. Small Particle Receiver Costs

	Summary of Cost Components ($1000)					
Design Point	Total Cost	Structural Cost	Heat Exchanger Cost	Auxiliary Cost	Installation Cost	Indirect Cost
1 MWt, 1500°F, 5 atm	394	258	31	31	10	64
50 MWt, 1500°F, 10 atm	2,681	2,064	190	233	59	315
50 MWt, 1500°F, 1 atm	3,197	2,061	468	233	73	344
50 MWt, 1000°F, 5 atm	2,939	2,036	283	233	65	322
50 MWt, 1500°F, 5 atm	2,911	2,064	236	233	59	319
50 MWt, 2000°F, 5 atm	2,922	2,088	212	233	69	320

TABLE 5.23. Volumetric Receiver Costs

	Summary of Cost Components ($1000)					
Design Point	Total Cost	Structural Cost	Heat Exchanger Cost	Auxiliary Cost	Installation Cost	Indirect Cost
1 MWt, 2000°F, 1 atm	333	6	236	23	12	56
50 MWt, 2000°F, 1 atm	7,127	65	6,098	233	80	651
300 MWt, 1000°F, 1 atm	6,373	316	4,972	325	164	596
300 MWt, 1500°F, 1 atm	10,876	327	9,070	325	243	911
300 MWt, 2000°F, 1 atm	22,922	336	20,466	325	152	1,643

required to fabricate the shell and to insulate the cavity of these receiver concepts. The small particle receiver has the highest structural costs because of the cost of the aperture window.

5.2.2 Heat Exchanger Cost Results

The heat exchanger is the single most expensive component for all concepts except the small particle receiver. Significant cost trends concerning heat exchangers are discussed below for each concept.

Heat exchanger costs for the small particle receiver are low because there is essentially no heat exchanger hardware. Instead, the carbon particles serve as the heat absorbing surface. The carbon particle generator, included as part of the heat exchanger, accounts for the majority of this concept's heat exchanger cost.

Operating pressure has a major influence on metal tube receiver heat exchanger cost. Higher operating pressures allow smaller flow areas and smaller size piping. At the ranges of pipe size and pressure under consideration, the pipe wall thickness required to support the pipe's weight is typically larger than that required by the pressure differential. Therefore, increased operating pressure results in lower cost piping.

Increased operating pressures do not necessarily reduce heat exchanger costs for ceramic tube receivers. Unlike metal tubes, where cost is directly proportional to size or weight, ceramic tube costs are only directly proportional to length. Tube diameter or wall thickness has very little effect on the cost of ceramic tubes. In general, the largest percentage of ceramic product cost is due to the forming or fabrication process. Raw materials represent only a small portion of the product cost.

Although they have excellent heat transfer characteristics, sodium heat pipes are extremely costly. Their high cost is reflected at all design points where the sodium heat pipe receiver was considered. Design point costs for this receiver also reflect a different trend as a function of operating pressure. Heat pipe receiver costs increased with higher operating pressure in contrast with the pressure effect shown for most other concepts. The heat pipe receiver was designed based on a constant mass velocity rather than absolute velocity. Operating pressure does not affect mass velocity directly as it does absolute velocity. Operating pressure does affect the mass velocity indirectly by changing the inlet condition. Operating pressures of 1, 5, and 10 atm have inlet temperatures of 70°F (21°C), 460°F (238°C), and 690°F (366°C), respectively. At a constant exit temperature, the higher-pressure receiver requires a higher mass flow rate to achieve the same power gain from the heat exchanger. Similarly, the 1000°F (538°C), 5-atm, 50-MWt design point is more costly than the 1500°F (816°C), 5-atm, 50-MWt design point because of the former's lower temperature drop across the heat exchanger.

Cost trends for the ceramic matrix heat exchanger show no suprises. Economies of scale exist between power ratings, and higher-temperature heat exchangers are more costly.

Ceramic dome receiver costs closely track the number of required domes. Increasing operating pressure decreases the number of domes per receiver. This cost reduction trend is lost at 10 atm, however, because of higher unit cost for the domes. The 1000°F (538°C), 5-atm, 50-MWt receiver is more costly than the 1500°F (816°C), 5-atm, 50-MWt receiver because the former employs more domes, even though it uses less costly materials. The 1000°F (538°C) receiver requires more domes because its smaller temperature drop across the heat exchanger requires a larger flow rate to achieve the same power rating.

The cost of the higher-temperature volumetric receiver design points suffer from extremely expensive silicon carbide materials. Fabrication costs were also quite costly for the volumetric design. The densely packed matrix of metallic absorbing rows requires hundreds of thousands of welds. Even with expensive fabrication, though, metal pins are cheaper than ceramic. Notched attachment should be considered for metal pins as well as ceramic pins to further reduce costs.

5.2.3 Auxiliary Cost Results

The cost of auxiliaries are primarily a function of the power level. The power level affects these costs in two ways. First, it determines the number of sensors or instruments required. Secondly, the power level determines the height of the tower, which, in turn, affects the cost of the wiring. The cost of the wiring was found to be one of the most significant components of the instruments cost. Auxiliary costs show economies of scale with respect to power level for all concepts. Auxiliary costs are relatively insensitive to the product conditions.

Although the cost of auxiliaries for the small particle receiver is generally lower than those for other receivers at 50 and 300 MWt, the cost of auxiliaries for this receiver are higher at 1 MWt. This is the result of the relatively large cost of the opacity meter which is independent of capacity.

5.2.4 Field Installation Cost Results

To some extent the field installation costs reflect the relative ease of constructing the various receivers. In general, lower field installation costs indicate that the receiver can either be fabricated mostly at ground level or it can be fabricated in a few modules that can be easily assembled after being raised to the top of the tower.

Both the weight of receiver components and the height of the tower are significant factors affecting field installation costs. The weight of the components affects the size of the load that can be lifted and thereby determines the extent to which the receiver can be assembled on the ground at cheaper labor costs. The height of the tower determines the size of construction crane needed to lift material and also the time required for lifting. Field installation costs increase with receiver capacity both as a result of increased tower height and receiver mass.

In general, the small particle receiver and the volumetric receiver show the lowest field installation costs for a given power level. This is primarily due to the relatively simple design of the small particle structure and to the modular nature of the volumetric receiver. Both benefit from being relatively lightweight. Ceramic dome receiver installation costs are highest at any given power level, both because of the large number of pipe connects that must be made between domes and because of the greater weight of the receiver components. The ceramic tube receiver shows relatively high field installation costs, primarily because of the numerous, expensive ceramic-to-metal welds that must be made to connect the U-tubes to the headers.

5.2.5 Indirect Cost Result

Indirect costs are a function of the direct capital cost, so the only differences in the indirect costs among concepts are due to differences in the direct capital cost.

6.0 CONCLUSIONS AND RECOMMENDATIONS

Based on the performance and cost results presented in Section 5, several conclusions can be formulated concerning the air-heating central receiver concepts. Conclusions concerning individual concepts will be presented first, followed by general conclusions.

- The metal tube receiver was a good performer. Performance and cost results were as good or better than most of the other designs. Most importantly, this concept represents proven, conventional technology that could be built today.
- The ceramic tube receiver was a fair performer. Performance and cost were estimated to be reasonable but not excellent. Although there are still several uncertainties concerning fabrication and durability, the ceramic tube design represents the nearest-term technology for a 2000°F (1093°C) receiver.
- The sodium heat pipe receiver suggested limited potential as an air-heating central receiver. Performance estimates were good, although not better than a couple of others designs, but the predicted costs were extremely high.
- The ceramic matrix receiver showed little promise as an air-heating central receiver. Estimated costs were very low, although they do not include the cost of the checker stoves that would be required for operation. Estimated performance was extremely poor, primarily because of spillage losses. The down-facing cavity causes several problems in a central receiver plant, including high spillage losses, awkward receiver structures, and the necessity of a high tower.
- The ceramic dome receiver suggested limited potential as an air-heating central receiver. Estimated costs were very low, but estimated performance was very poor. Receiver interior temperatures were very high, causing significant reradiation losses. Optimizing aperture size to restrict reradiation losses caused large spillage losses. There is some possibility that the concept could be

reoptimized with lower heat fluxes and surface temperatures to reduce reradiation losses; however, this would enlarge the receiver designs and eliminate the proposed advantage of the impingement-cooled ceramic domes.

- The small particle receiver had very low estimated costs but poor performance at the sizes investigated in this study. The limitations on window size and requirements for high flux make optimizing the size of the receiver a touchy proposition. This concept could show better performance at a different size, perhaps 10 to 30 MWt. Nevertheless, there are significant uncertainties concerning the particle generator and flow distribution system.
- The volumetric receiver showed good potential as a central receiver for heating atmospheric air. Performance estimates were excellent, the best of any of the receivers analyzed, although the cost estimates were somewhat higher than for other receivers at similar conditions. An additional cost for a checker stove at 2000°F (1093°C) to isolate the induced draft fan from high temperatures would be included in a complete design. Because it was the least developed of the concepts analyzed, the volumetric receiver has a high uncertainty about its feasibility but also a large potential for improvements from optimization.
- 1-MWt designs were generally not feasible or at least poor performers for all of the receiver concepts.
- The relative certainty of the receiver costs is directly related to the amount of prior development work that has been performed for a given concept. Where detailed design information was not available, it is possible that the cost of some equipment was not included in the design.
- The choice of design points at which a receiver was evaluated was not necessarily optimal, although this could not be determined until the cost and performance results were available. Tradeoff studies should be performed to optimize operating conditions.

- The complete potential of the receiver concepts cannot be determined until they are evaluated as part of a total central receiver system. Such a study could combine the receiver performance and cost estimates presented here with similar estimates for other system components (heliostats, towers, storage) to determine the levelized energy costs that could be expected for each receiver concept.

Based on these conclusions the following recommendations are offered.

- The metal tube and ceramic tube receiver concepts should be pursued for near-term applications as air-heating central receiver systems.
- The volumetric receiver shows sufficient promise to warrant further development.
- A follow-on study should be performed to assess the potential of the receiver concepts in complete solar thermal power plants.
- Some ceramic components need further development for applications in high-temperature receivers. Particular problems are welding techniques and fabrication. Other ceramic components such as the ceramic matrix may be closer to commercial availability.

6.1 CRITIQUE OF RECEIVER CONCEPTS

Sections 5.1 and 5.2 presented the results of analytical assessments of the receivers' estimated performance and cost. During these assessments a guiding assumption was that the receivers would work as intended. In this section a more qualitative approach is taken in answering this question of the receivers' feasibility and practicality. The comments presented in Table 6.1 are not intended as absolute but merely as impressions concerning the receiver designs that surfaced during the conceptual design, performance analysis, and cost analysis tasks. These impressions address the strengths and weaknesses of the concepts as well as possible ideas for design improvements.

TABLE 6.1. Critique of Receiver Concepts

Receiver Design Concepts	Strengths	Potential Weaknesses	Possible Design Improvements
Metal tube receiver	- Proven technology - Off-the-shelf components, could be built today - Simple control system	- Heavy - Limited to temperatures below 1500°F (816°C); expensive alloys are required at this temperature.	- Use of internal insulation on the exit manifold allows the pipe to be made of carbon steel rather than Inconel. - Could use a lighter weight material for the shell
Ceramic tube receiver	- Forced convection heat transfer is relatively well understood. - Ceramic tubes are available technology. - Most conventional of 2000°F (1093°C) designs	- Adequate ceramic-ceramic and ceramic-metal joining techniques are still under development. - A suitable material for the isolation valve at the outlet of each cavity could not be identified.	- Expansion points may be required in the headers and manifolds.
Sodium heat pipe receiver	- Heat pipes allow high heat fluxes and small receivers. - Nearly isothermal energy transfer in the heat pipes means that metal temperatures will be very near the product temperature.	- Heat pipes require further testing in conditions typical of receiver operation to ensure durability.	- Some method of attaching the heat pipes to the panels other than welding would increase accessibility to defective heat pipes and improve maintenance requirements. - Internally insulated carbon steel walls would be less expensive than externally insulated Inconel walls.
Ceramic matrix receiver		- The downward-facing cavity will require a complicated support structure and probably result in higher tower costs. - Velocities through the matrix are very low (0.3 to 1.5 m/s); portions of matrix could become starved for air flow.	- The roof of the cavity could be finned to enhance heat transfer.

TABLE 6.1. (Cont'd)

Receiver Design Concepts	Strengths	Potential Weaknesses	Possible Design Improvements
Ceramic matrix receiver		- Inside surface of matrix has highest flux and highest air temperature. - The cavity roof receives nearly the same heat flux as the matrix; it's likely to get very hot.	
Ceramic dome receiver	- Excellent heat transfer in the domes allows high heat fluxes and small receivers. - The ceramic dome units can be constructed with no metal exposed to the radiation flux.	- Experimental work is required to verify dome heat transfer and pressure drop characteristics. - Difficult to fabricate large (~2 m) domes - Peak dome temperatures are very high.	- May want to relax heat fluxes on dome surface to reduce ceramic temperatures
Small particle receiver	- Simple, lightweight design - No heat exchangers required - Volumetric heat absorption on particles allows high fluxes and small receivers. - Hollow cavity design minimizes fabrication requirements and pressure drops.	- Necessary to ensure evenly distributed flow of particles; otherwise heat could melt the rear wall. - Receiver size limited by window size - Durability of anti-reflective coatings at high temperatures uncertain - Particle generation techniques uncertain - Feasibility of window fabrication uncertain	- Windowless cavity design may be possible for atmospheric pressure operation. - Circumferential, scalloped window arrangement could be used for large sizes.

TABLE 6.1. (Cont'd)

Receiver Design Concepts	Strengths	Potential Weaknesses	Possible Design Improvements
Small particle receiver		- Necessity to control air flow rate, particle loading, and particle distribution makes controls complicated.	
Volumetric	- Volumetric heat absorption allows high external fluxes and small receivers - Appears optically as an external receiver allowing short towers - Simple design with potential for low cost construction - No pressure stress on ceramic components	- Uncertainty that radiation can actually be distributed to interior pins - Requires accurate control of circumferential air flow distribution to eliminate hot spots - Very high heat fluxes on reflecting pins - Low air, velocities cause poor heat transfer from pine, in most cases flow is in laminar or transition region - Method of fabrication, structural support, and compensation for thermal expansion in absorbing pins uncertain; may not be possible to hang ceramic pins because of poor tensile strength; may not be possible to use reflecting pins for main structural support - Potential for flow induced vibration of pins	- To ensure proper flow distribution the receiver may have to be sectioned into quadrants and flow control orifices placed in the inlet manifold

REFERENCES

Abrams, M., and R. Greif. 1981. A Simple Theory for Predicting the Natural Convection Loss from Side Facing Solar Cavity Receivers. SAND81-8201, Sandia Laboratories, Livermore, California.

Arizona Public Service Company. 1980. Saquaro Power Plant Solar Repowering Project. Vol. III, Appendices. Prepared for the U.S. Department of Energy, San Francisco, California.

Black and Veatch Consulting Engineers. 1978. Solar Thermal Conversion to Electricity Utilizing a Central Receiver, Open Cycle Gas Turbine Design, ER-652. Prepared for Electric Power Research Institute, Palo Alto, California.

Boeing Engineering and Construction Company. 1978. Closed Brayton Cycle Advanced Central Receiver Solar-Electric System. Vol. II, SAN-1726-1. Prepared for the U.S. Department of Energy, San Francisco Operations Office, San Francisco, California.

Boeing Engineering and Construction Company. July 1980. United States Gypsum Plant Solar Retrofit Program Volume 1. DOE/SF 10742-1, Seattle, Washington.

Boeing Engineering and Construction, and the United States Gypsum Company. 1980. United States Gypsum Plant Solar Retrofit. Vol. 2. Prepared for the U.S. Department of Energy, San Francisco, California.

Clausing, A. M. et al. 1981. "An Experimental Investigation of Convective Losses From Solar Receivers." Presented at DOE/SER/SNLL Workshop on Convective Losses from Solar Central Receivers, at Sandia Livermore Laboratory, March 1981.

Gebhart, B. 1971. Heat Transfer. McGraw-Hill, New York, New York.

General Electric. 1974. Heat Transfer Handbook. General Electric.

Guthrie, K. M. 1974. Process Plant Estimating, Evaluation, and Control. Graftsman Book Company of America, Solana Beach, California.

Hackney, J. W. 1965. Control and Management of Capital Projects. John Wiley and Sons, New York, New York.

Kays, W. M. 1966. Convective Heat and Mass Transfer. McGraw Hill, New York.

Kay, W. M., and A. L. London. 1964. Compact Heat Exchangers. McGraw-Hill, New York, New York.

Means, R. S. 1981a. 1981 Labor Rates for the Construction Industry. Robert S. Means Co., Inc., Kingston, Massachussetts.

Means, R. S. 1981b. Means Building Construction Cost Data 1981. Kingston, Massachussetts.

Page, John S. 1963. Estimators Manual for Equipment and Installation Costs. Gulf Publishing Company, Houston, Texas.

Page, John S., and Jim G. Nation. 1976. Estimator's Piping Manhour Manual. Gulf Publishing Company, Houston, Texas.

Peters, M. S., and K. D. Timmerhaus. 1968. Plant Design and Economics for Chemical Engineers. 2nd ed. McGraw-Hill Book Company, New York, New York.

Siegel, R., and J. R. Howell. 1972. Thermal Radiation Heat Transfer. McGraw-Hill, New York, New York.

Stearns-Roger Engineering Company. 1979. Tower Cost Data for Solar Central Receiver Studies. SAND78-8185 V-1. Prepared for Sandia Laboratories.

Vatavuk, W. M., and R. B. Neveril. 1980. "Factors for Estimating Capital and Operationg Costs." Chemical Engineering. 87(2). Page 157-162.

Weber, Eric R. July 1980. Saguaro Power Plant Repowering Project Volume III. DOE/SF 10736-4, Arizona Public Service Company. Phoenix, Arizona.

Welty, J. R., C. E. Wicks and R. E. Wilson. 1969. Fundamentals of Momentum Heat and Mass Transfer. John Wiley and Sons, Inc., New York.

Winslow, Taylor F. 1972. Construction Industry Production Manual. Craftsman Book Company of America. Solana Beach, California.

APPENDIX A

UNIT COST DEVELOPMENT

The cost estimating methodology employed for most of the heat exchanger, structural, and field installation cost categories began by breaking each concept design into material and labor component requirements. Unit costs were then applied to each component to arrive at a total cost for each category. This methodology was chosen as a reasonable approach, given the number of designs and their general development. A more detailed costing approach would not have been commensurate with the level of design detail. A more general approach would not have yielded adequately distinguishing estimates.

"Full" cost recovery labor rates were developed for shop, field, and tower-top activities. For shop activities, "full" cost recovery means that the labor rate includes the total company cost of operation with shop tasks being performed by a subcontractor. The shop labor rate not only allows for the employees' pay and fringes, but also allows for the recovery of all business costs, including capital, O&M, and profit. Based on data from the 1972 Census of Manufacturers and the Monthly Labor Review, July 1981, equations were derived that relate product cost to labor and material requirements. The shop labor represents the value added to the raw materials by the manufacturer plus consumable supplies and other material expenses not included with the raw materials.

The field and tower labor rates are only slightly less inclusive. In addition to employee's pay and fringes, these rates include nearly all other general contractor costs typically defined within contractor's overhead and profit or indirect costs. This includes such items as field supervision, main office expense, tools and equipment, field office, and insurance. Specifically, these labor rates do not include design or engineering costs that are accounted for separately within Indirect Costs. Direct labor costs, including fringes, were based on data given in the 1981 Means and Labor Rates. Means Building Construction Cost Data 1981 provided data concerning the overhead and profit that were added to the base labor rate.

The three labor rates are given in Table A.1. The difference between the tower top and field labor rates reflects the added expense of working in a difficult situation and the general level of skill required. Although the shop rate (which includes an hourly charge plus a percentage of raw materials cost)

TABLE A.1. Receiver Material and Labor Unit Costs

Item	Unit Cost
Tower Top Labor	\$29.00/h
Field Labor	\$26.00/h
Shop Labor	\$25.50/h +0.13 (materials cost)
Aluminum Siding	\$9.90/m^2
Alumina Silica Insulation	\$423.8/m^3
Calcium Silicate Insulation	\$317.8/m^3
Fiberglass Insulation	\$47.7/m^3
Carbon Steel Plate	\$.55/kg
Carbon Steel Structural Shapes	\$.77/kg
Carbon Steel Pipe, D 24 in.	\$.77/kg
Carbon Steel Pipe, D 24 in.	\$.88/kg
Stainless Steel 316 Plate	\$5.51/kg
Stainless Steel 316 Pipe	\$7.72/kg
Inconel 601 Plate	\$11.0/kg
Inconel 601 Pipe	\$19.8/kg
Inconel 617 Plate	\$24.3/kg
Inconel 617 Pipe	\$41.9/kg
Hastelloy X Plate	\$24.3/kg
Hastelloy X Pipe	\$41.9/kg
Silicon Carbide Pipe	\$656/m
Silicon Carbide Domes	\$4000 each
Silicon Carbide Matrix	\$4305/m^2 frontal area
Silicon Carbide Fins, Vertical	\$131.2/m
Silicon Carbide Fins, Horizontal	\$164.0/m

is more expensive than field or tower-top labor, the productivity is much better in the shop. Therefore, the shop completed task is less expensive than the same task completed in the field.

Material unit costs were assembled from a variety of sources, including vendors, cost manuals, cost data bases, other contractor reports, and PNL's own data from related work. All materials are available today at the prices listed in Table A.1, except for the silicon carbide products. Only in the past few years has silicon carbide been seriously considered in high-temperature solar thermal applications. All of the silicon carbide products require development to reach production-level capability. The costs presented in Table A.1 are based on developments that could take place in the next 10 to 15 years. The costs, based on information provided by vendors a median price within the range of sizes of each component. The size and shape of the product is more important than pounds of raw material consumed. For these reasons, a unit cost in \$/kg or m^3 is not appropriate.

APPENDIX B

RECEIVER WEIGHT SUMMARY

APPENDIX B

RECEIVER WEIGHT SUMMARY

This appendix presents the weights of the various receiver concept broken down into component weights. These component weights were used in the cost estimating procedure.

TABLE B.1. Metal Tube Receiver Weight Summary (kg)

Component	1 MW 1500°F 5 atm	50 MW 1500°F 5 atm	50 MW 1500°F 10 atm	50 MW 1000°F 5 atm	300 MW 1500°F 5 atm
Heat Exchanger	454	20,884	20,884	19,976	125,758
Piping	1362	67,646	45,400	71,732	59,020
Shell	2724	64,014	47,670	55,842	389,070
Insulation	10,442	315,984	228,362	155,722	1,906,800
TOTAL	14,982	468,528	342,316	303,272	2,480,648

TABLE B.2. Ceramic Tube Receiver Weight Summary (kg)

Component	1 MW 2000°F 10 atm	50 MW 2000°F 10 atm	300 MW 2000°F 10 atm	300 MW 1500°F 10 atm	300 MW 2000°F 5 atm
U-tubes	454	14,528	84,444	82,628	83,536
Piping	454	20,884	120,764	148,912	202,030
Shell	908	10,896	94,886	90,800	94,432
Insulation	3632	114,862	445,374	729,124	1,125,920
TOTAL	5448	161,170	745,468	1,051,464	1,505,918

TABLE B.3. Sodium Heat Pipe Receiver Weight Summary (kg)

Component	50 MW 1500°F 5 atm	50 MW 1500°F 10 atm	50 MW 1500°F 1 atm	50 MW 1500°F 5 atm	300 MW 1500°F 5 atm	1 MW 1500°F 5 atm
Heat Exchanger[(a)]	34,958	42,676	31,780	56,296	672,374	4,540
Piping	13,166	11,350	50,394	25,878	59,020	454
Shell	31,780	31,780	32,234	32,688	159,808	4,994
Insulation	66,738	66,738	66,738	42,676	349,126	8,172
TOTAL	146,642	152,544	181,146	157,538	1,240,328	18,160

(a) Includes heat pipes, panels, sidewalls, flanges and webs.

TABLE B.4. Ceramic Matrix Receiver Weight Summary (kg)

Component	300 MW 1500°F 1 atm	300 MW 1000°F 1 atm	300 MW 2000°F 1 atm	1 MW 2000°F 1 atm	50 MW 2000°F 1 atm
Heat Exchanger[(a)]	165,256	163,440	93,070	908	21,792
Piping	222,914	300,094	180,692	136	36,774
Shell	103,966	106,236	103,058	545	14,528
Insulation	503,032	439,472	441,742	2270	61,744
TOTAL	995,168	1,009,242	818,562	3859	134,838

(a) Includes ceramic matrix and matrix supports.

TABLE B.5. Ceramic Dome Receiver Weight Summary (kg)

Component	50 MW 2000°F 5 atm	50 MW 2000°F 1 atm	50 MW 2000°F 5 atm	300 MW 2000°F 10 atm	50 MW 1500°F 5 atm	50 MW 1000°F 5 atm
Heat Exchanger[(a)]	111,230	98,064	90,800	660,570	98,972	98,972
Piping	41,768	8,626	9,080	88,984	14,528	31,326
Shell	48,124	27,240	27,240	187,502	21,792	33,596
Insulation	400,882	209,294	208,840	1,555,540	161,170	215,650
TOTAL	602,004	343,224	335,960	2,492,596	296,462	379,544

(a) Includes both domes and dome enclosures.

TABLE B.6. Small Particle Receiver Weight Summary (kg)

Component	50 MW 1000°F 5 atm	50 MW 1500°F 1 atm	50 MW 1500°F 5 atm	50 MW 1500°F 10 atm	50 MW 2000°F 5 atm	1 MW 1500°F 5 atm
Piping	6,356	5,902	3,178	3,632	2,270	90
Shell	23,154	12,712	14,528	16,344	14,528	908
Insulation	35,412	39,952	42,676	42,676	38,590	3,632
TOTAL	64,922	58,566	60,382	62,652	55,388	4,631

TABLE B.7. Volumetric Receiver Weight Summary (kg)

Component	1 MW 2000°F 1 atm	300 MW 1500°F 1 atm	300 MW 2000°F 1 atm	300 MW 1000°F 1 atm	50 MW 2000°F 1 atm
Heat Exchanger	2,724	458,540	239,712	499,400	58,112
Shell	91	1,362	1,362	1,362	454
Insulation	318	14,074	12,712	12,258	4,540
Support Structure	1,362	221,552	221,552	221,552	39,952
TOTAL	4,495	695,528	475,338	734,572	103,058

DISTRIBUTION

No. of
Copies

OFFSITE

A. A. Churm
U.S. Department of Energy
Chicago Patent Group
Argonne, IL 60439

27 DOE Technical Information Center

W. Auer
U.S. Department of Energy
Germantown, MD 20767

G. W. Braun
U.S. Department of Energy
Germantown, MD 20767

C. Mangold
U.S. Department of Energy
Germantown, MD 20767

C. Mc Farland
U.S. Department of Energy
Germantown, MD 20767

S. D. Elliott
U.S. Department of Energy
San Francisco Operations Office
1333 Broadway
Oakland, CA 94612

R. W. Hughey
U.S. Department of Energy
San Francisco Operations Office
1333 Broadway
Oakland, CA 94612

K. Rose
U.S. Department of Energy
San Francisco Operations Office
1333 Broadway
Oakland, CA 94612

No. of
Copies

J. Morley
U.S. Department of Energy
Albuquerque Operations Office
P. O. Box 5400
Albuquerque, NM 87115

G. Pappas
U.S. Department of Energy
Albuquerque Operations Office
P. O. Box 5400
Albuquerque, NM 87115

P. Mathur
Aerospace Corp. D-5, Rm. 1110
2350 E. El Segundo Blvd.
El Segundo, CA 90245

D. Gorman
Arco Power Systems
Suite 306
7061 S. University Blvd.
Littleton, CO 80122

G. Grant
Babcock and Wilcox
1562 Beeson
Alliance, OH 44601

J. R. Darnell
Bechtel National Inc.
Research and Engineering
P. O. Box 3965
San Francisco, CA 94105

J. E. Harder
Black and Veatch
P. O. Box 8405
Kansas City, MO 64114

J. Gintz
Boeing Engineering and
Construction
P. O. Box 3707
Seattle, WA 98124

No. of
Copies

D. Pierson
California Energy Commission
1111 Howe Avenue, M-S70
Sacramento, CA 95825

E. A. Reid, Jr.
Columbia Gas System Service Corp.
1600 Dublin Road
Columbus, OH 43215

J. E. Bigger
Electric Power Research Institute
P.O. Box 10412
Palo Alto, CA 93403

C. Pitman
Energy Laboratory - SPA
4800 Calhoun
University of Houston
Houston, TX 77004

T. Springer
Energy Systems Group
Rockwell International
8900 De Soto Avenue
Canoga Park, CA 91304

George Yenetchi
Exxon Enterprises, Inc.
Solar Thermal Systems
P.O. Box 592
Florham Park, NJ 07932

R. Zoschak
Foster Wheeler Corp.
12 Peach Tree Hill Road
Livingston, NJ 07039

J. J. Jimenez
Gibbs and Hill Inc.
393 Seventh Avenue
New York, NY 10001

A. B. King
Gulf Research and Development
Company
P.O. Drawer 2038
Pittsburgh, PA 15230

No. of
Copies

D. Glenn
Institute of Gas Technology
Suite 218
1825 K. Street N.W.
Washington, D.C. 20036

J. C. Becker
Jet Propulsion Laboratory
4800 Oak Grove Drive
Pasadena, CA 91003

V. C. Truscello
Jet Propulsion Laboratory
4800 Oak Grove Drive
Pasadena, CA 91003

W. C. Dickinson
Lawrence Livermore National
Laboratory
P.O. Box 808
Livermore, CA 94550

T. Heaton
Martin Marietta
P.O. Box 179
Denver, CO 80201

T. Tracey
Martin Marietta
P.O. Box 179
Denver, CO 80201

C. Finch
McDonnell Douglas
5301 Bolsa Avenue
Huntington Beach, CA 92647

L. W. Glover
McDonnell Douglas
5301 Bolsa Avenue
Huntington Beach, CA 92647

J. Meglen
Meridian Corporation
5201 Leesburg Pike
Suite 400
Falls Church, VA 22041

No. of
Copies

J. DeVan
Oak Ridge National Laboratory
P.O. Box Y
Oak Ridge, TN 37830

Jack Gibbons
Office of Technology Assessment
United States Congress
Washington, D.C. 20510

S. Butchock
Solar Energy Report
P.O. Box 1519
Washington, D.C. 20013

B. Butler
Solar Energy Research Institute
1617 Cole Boulevard
Golden, CO 80401

R. J. Copeland
Solar Energy Research Institute
1617 Cole Boulevard
Golden, CO 80401

M. Murphy
Solar Energy Research Institute
1617 Cole Boulevard
Golden, CO 80401

J. P. Thornton
Solar Energy Research Institute
1617 Cole Boulevard
Golden, CO 80401

Solar Energy Research Institute-
TID
Solar Data Bank
1617 Cole Boulevard
Golden, CO 80401

F. B. Smith
Solar Thermal Test Facilities
Users Association
Suite 1204
First National Bank, East
Albuquerque, NM 87108

No. of
Copies

A. F. Hildebrandt
University of Houston
Solar Energy Laboratory
Houston, TX 77004

R. E. McCleary
U.S. Gypsum Company
Dept. 176-2
101 S. Wacker Drive
Chicago, IL 60606

R. W. Devlin
Westinghouse Electric Corp.
P.O. Box 10864
Pittsburgh, PA 15236

37 R. C. Wayne
Thermal Subsystems Division
Sandia National Laboratories
Livermore, CA 94550

ONSITE

DOE Richland Operations Office

H. E. Ransom

42 Pacific Northwest Laboratory

D. R. Brown
M. K. Drost (25)
K. Drumheller
J. A. Fort
B. A. Garret-Price
S. G. Hauser
W. W. Laity
M. A. McLean
T. A. Williams
J. K. Young
Publishing Coordination (2)
Technical Information (5)